




University of
Stavanger

Faculty of Science and Technology

MASTER'S THESIS

Study program/ Specialization: Marine- and Offshore Technology	Spring semester, 2019 Open / Restricted access
Writer: Andreas Borsheim	 (Writer's signature)
Programme coordinator: Prof. Muk Chen Ong Supervisors: Prof. Muk Chen Ong Dr. Guomin Ji	
Thesis title: Pipelaying Simulation for Pipelines with and without Piggyback in Ultra-Deep Water	
Credits (ECTS): 30	
Key words: Pipeline, Piggyback, Pipelaying, SIMLA, Finite Element Method, FEM, Computational Fluid Dynamics, CFD, OpenFOAM, Required Top Tension, Current Angle of Attack, Bending Moment, Lateral Displacement	Pages: 109 + enclosure: 17 Stavanger, June 15, 2019 Date/year

Abstract

Pipelaying operations are pushing the boundaries of installation depth from midwater to ultra-deepwater. Parameters such as combined loading, top tension, and current loading must be investigated appropriately to ensure feasible operations. Until now, current loading effects have not been considered as an important factor for pipelaying operations. However, as modern ultra-deep pipelaying operations reach depths up to 4000 meters, there will be a considerable projected area for current-induced forces to act [1]. In recent years, the application of pipelines with direct electrical heating (DEH) cables has become conventional and is used in oil fields like Skarv, Tyrihans, and Lianzi. Lengths of these installations go up to 44km at depths over 1000 meters [2].

A numerical study has been performed for pipelines with and without piggyback, using the finite element method (FEM) software SIMLA. Pipeline-piggyback configurations have complex hydrodynamic force distributions which are dependent on pipeline inclination and angle of attack of the current. A new approach is developed for pipeline-piggyback-configurations by including body elements in the model to account for current induced hydrodynamic forces. The drag coefficients are defined in the command card “HYDROPRO”, accounting for the variation in the angle of attack of the current. To fully understand the pipeline-flow interaction, a series of two-dimensional numerical simulations was performed for singular pipelines and piggyback-solutions, using the open source Computational Fluid Dynamics (CFD) code OpenFOAM. Hydrodynamic forces are extracted separately for the pipeline and the piggyback cable; and the drag coefficients are obtained for the various angle of attack of the flow. CFD has not been used in combination with pipelaying simulations before. The CFD results give a good insight into the pipe/cable/flow interaction and provide reliable drag coefficients used in pipelaying simulation.

A series of simulations is performed for subsea pipelines of three diameters (20”, 28” and 30”) with and without piggyback. Furthermore, parameter studies are performed for scenarios with and without current loading at different angles of attack. The main findings are as follows:

- A new modelling technique for pipeline-piggyback-configurations is verified for modelling of current induced hydrodynamic forces.
- A new approach combining CFD and FEM to evaluate pipeline lay-ability is applied in the pipelaying simulation for complex configurations.
- Pipeline lateral displacement is significantly increased for a piggyback-configurations.
- Vessel top tension requirement increases when including current loads.

Acknowledgement

I want to extend gratitude and recognition to the following individuals for their support and motivation throughout the completion of this report.

To Dr. Guomin Ji, I would like to offer my sincerest appreciation for always being there to answer questions, spending hours reading dysfunctional codes and correcting the sections time after time. Without his guidance and supervision, this thesis would not have the same quality as it has today.

I want to thank Professor Muk Chen Ong for always pushing and motivating me to work consistently on the thesis, in addition to working behind the scenes to ensure I received proper supervision. I would like to thank Marek Janocha for his help in both writing and performing the CFD-simulations, which were essential for the result-section of the thesis.

Furthermore, I would like to express my gratitude to Vegard Longva for the time spent on debugging the SIMLA-code during my stay in Trondheim. Without his help, the implementation of the HYDROPRO-card in the code would have been a lot harder.

Finally, I would like to thank my co-students at the University of Stavanger for providing a great work environment, and my parents for always backing me up.

Stavanger, Norway

Andreas Borsheim

June, 2019



Table of Contents

Abstract	iii
Acknowledgement.....	v
1 Introduction	1
2 Pipeline Laying Operation	4
2.1 Laying Methods.....	4
2.1.1 S-Lay Method.....	4
2.1.2 J-Lay Method	5
2.1.3 Reeling Method	7
2.1.4 Selected Installation Method.....	8
2.2 Guideline on Laying Operation	8
2.3 Pipeline Systems.....	10
2.4 Flow Assurance	10
2.4.1 Coating	11
2.4.2 Piggyback	11
2.4.3 Hydrate Control.....	12
3 Design Criteria	13
3.1 Classifications.....	13
3.1.1 Loads	13
3.1.2 Limit States	16
3.1.3 Risk classifications.....	17
3.2 Pipeline Material	18
3.2.1 Material Selection	18
3.2.2 Material Grades	19
3.2.3 Characteristic Wall Thickness.....	20
3.3 Pipeline Wall Thickness Design.....	22
3.3.1 Collapse due to External Pressure, Local Buckling	22
3.3.2 Simplified Laying Criteria	26
3.3.3 Combined Loading Criteria.....	26
3.3.4 Collapse Pressure	30

3.3.5	Propagation Buckling due to External Pressure.....	31
3.3.6	On-Bottom Stability	33
3.3.7	Summary of Wall Thickness Design.....	34
3.4	Coating	35
3.5	DEH Cable.....	37
3.6	Strap Material	39
3.7	Current Velocity Profile	41
4	Pipelaying Operation Modelling	48
4.1	SIMLA - Software	48
4.2	Pipelaying Parameters	52
4.3	J-Lay Model.....	54
4.4	Implementation of Drag Coefficients for Pipelaying	58
4.5	Computational Fluid Dynamics (CFD)	64
4.5.1	OpenFOAM.....	64
4.5.2	Governing Equations.....	64
4.5.3	Finite Volume Method	66
4.5.4	k – ω SST Turbulence Model.....	66
4.5.5	Problem definition.....	68
4.6	Assumptions	71
4.7	Analysis Matrix and Main Input Data	72
5	Results and Discussions	74
5.1	Drag Coefficients.....	74
5.1.1	Projected Area	74
5.1.2	CFD - Results	75
5.1.3	Applied Drag Coefficients	79
5.2	Validation of Drag Coefficients Applied Through HYDROPRO.....	82
5.2.1	First Parameter Study	82
5.2.2	Second Parameter Study.....	84
5.3	The Results for Analysis Matrix.....	84
5.3.1	XY – Configuration.....	84

5.3.2	Top Tension.....	89
5.3.3	Sagbend Stress and Strain	99
5.3.4	Pipeline-Configuration in XZ plane.....	103
6	Conclusions and Future Work.....	107
7	References	110
I.	Appendix A	113
II.	Appendix B	118

List of Figures

Figure 2-1 Illustration of S-Lay [9].....	5
Figure 2-2 Illustration of J-Lay [9]	6
Figure 2-3 Illustration of Reeling [10]	7
Figure 2-4. Hydrate region [13]	12
Figure 3-1. Three types of buckle arrestors, [10].....	32
Figure 3-2 Wall thickness design flowchart.....	34
Figure 3-3. DEH cable model	38
Figure 3-4 YoMaHa'07 readings [8]	44
Figure 3-5 Deep water currents, given in cm/s [22].....	44
Figure 3-6 Mean current velocity in gully, given in cm/s [23]	45
Figure 3-7 Velocity along deep water ocean trench [24].....	46
Figure 3-8. Current velocity profile	47
Figure 4-1 Global coordinate system [26].....	49
Figure 4-2 Nodal coordinate system [26].....	49
Figure 4-3 SIMLA module tree [27]	49
Figure 4-4. FlexEdit layout	50
Figure 4-5 SIMPOST layout	51
Figure 4-6 MATRIXPLOT layout	51
Figure 4-7 Pipeline interaction with seabed – XPOST	52
Figure 4-8. Relative position and rotation of elements to the global coordinate system [25]	55
Figure 4-9. Pipe-vessel interaction.....	56
Figure 4-10 J-Lay model	56
Figure 4-11. Pipeline-DEH interaction with vessel	57
Figure 4-12. Stress distribution on pipeline-DEH-vessel-configuration.....	58
Figure 4-13. Pipeline-DEH-configuration with current flow at $\psi = 0^\circ$	59
Figure 4-14 Pipeline-DEH-configuration with current flow at $\psi = 90^\circ$	59
Figure 4-15. Local coordinate systems relative to the global coordinate system [29].....	61
Figure 4-16. Cross section of pipeline-DEH-configuration.	63
Figure 4-17. Pipeline-DEH-configuration inclination relative to current heading	63
Figure 4-18. Structure of simulation case directory	64
Figure 4-19 Sketch of the computational domain and imposed boundary conditions.	69
Figure 4-20 Example of the computational mesh used in the simulations. Whole domain view.	69
Figure 4-21 Detailed view of mesh close to the pipeline-DEH geometry.	70

Figure 4-22 Pipeline-DEH interface meshing details	70
Figure 5-1 Pipeline-DEH-configuration with the projected diameter when exposed to current flows at: $\psi = 0^\circ$, $\psi = 45^\circ$, $\psi = 90^\circ$, $\psi = 135^\circ$, and $\psi = 180^\circ$	74
Figure 5-2 Vorticity contours at $\psi = 180^\circ$	76
Figure 5-3 Vorticity contours at $\psi = 15^\circ$	76
Figure 5-4 Vorticity contours at $\psi = 90^\circ$	77
Figure 5-5 Pressure contours and streamlines at $\psi = 90^\circ$	77
Figure 5-6 Pressure contours and streamlines at $\psi = 180^\circ$	78
Figure 5-7 Pressure contours and streamlines at $\psi = 15^\circ$	78
Figure 5-8 Effect of current heading on single pipe C_D	79
Figure 5-9 Effect of ψ on C_D for 20" pipeline /w piggyback	80
Figure 5-10. Effect of piggyback on pipeline C_D	81
Figure 5-11. XY-configuration at $\psi = 90^\circ$, time = 491s	86
Figure 5-12. Maximum XY-configuration at $\psi = 90^\circ$	87
Figure 5-13 Streamlines and pressure fields at $\psi = 45^\circ$	88
Figure 5-14 Streamlines and pressure fields at $\psi = 135^\circ$	88
Figure 5-15. Effect of current heading on maximum top tension	90
Figure 5-16. Current force components acting on the pipeline-DEH-configuration, at $\psi = 0^\circ$	91
Figure 5-17 Current force components acting on the pipeline-DEH-configuration, at $\psi = 180^\circ$	91
Figure 5-18. Detailed view of the effect of current heading on maximum top tension	92
Figure 5-19. Top tension over time at $\psi = 90^\circ$, 20" /w DEH	93
Figure 5-20. Top tension over time at $\psi = 90^\circ$, 28" /w DEH	93
Figure 5-21. Top tension over time at $\psi = 90^\circ$, 30" /w DEH	94
Figure 5-22. Effect of current heading on top tension for a 20" Pipeline	94
Figure 5-23 Effect of current heading on top tension for a 20" Pipeline /w DEH	95
Figure 5-24 Effect of current heading on top tension for a 28" Pipeline	96
Figure 5-25 Effect of current heading on top tension for a 28" Pipeline /w DEH	96
Figure 5-26 Effect of current heading on top tension for a 30" Pipeline	97
Figure 5-27 Effect of current heading on top tension for a 30" Pipeline /w DEH	97
Figure 5-28 Effect of current on 20" pipeline configuration in the XZ-plane	104
Figure 5-29. Effect of current on 28" pipeline configuration in the XZ-plane	104
Figure 5-30. Effect of current on 30" pipeline configuration in the XZ-plane	105
Figure 5-31. Effect of current on 20" pipeline-DEH-configuration in the XZ-plane	105
Figure 5-32. Effect of current on 28" pipeline-DEH-configuration in the XZ-plane	106

Figure 5-33. Effect of current on 30” pipeline-DEH-configuration in the XZ-plane 106

List of Tables

Table 1-1 Fields where DEH cables are utilized.....	2
Table 2-1 Simplified laying criteria, overbend	9
Table 3-1 Characteristic loads.....	15
Table 3-2 Return period for characteristic environmental loads [12]	15
Table 3-3 Normal links between limit states and scenarios [12]	16
Table 3-4 Location class	17
Table 3-5 Fluid classifications	17
Table 3-6 Safety class classification	18
Table 3-7 Material grades [12].....	19
Table 3-8 Material properties – X65 [15]	19
Table 3-9 Characteristic wall thickness	21
Table 3-10. Wall thickness tolerance	21
Table 3-11. Material resistance factor.....	23
Table 3-12 Safety class resistance factor, γ_{SC}	24
Table 3-13 Material Strength factor, α_U	25
Table 3-14 Maximum fabrication factor, α_{fab}	26
Table 3-15 Condition load effect factors, γ_C	30
Table 3-16 Load effect factor combinations	30
Table 3-17 Summary of applied constants in wall thickness design.....	35
Table 3-18. Corrosion resistant coat (3LPP).....	36
Table 3-19. Insulation and corrosion resistant coat (Alternative 1).....	36
Table 3-20. Insulation and corrosion resistant coat (Alternative 2).....	36
Table 3-21. HDPE Properties.....	37
Table 3-22. Copper C11000 Properties.....	37
Table 3-23. DEH material properties	39
Table 3-24. High tensile carbon steel material properties.....	40
Table 3-25. Selected current velocity profile	47
Table 4-1 Standard coefficients.....	67
Table 4-2. Analysis matrix	72
Table 5-1 CFD simulation parameters	75
Table 5-2 Effect of DEH cable on pipe drag coefficients	81
Table 5-3 Pipeline properties	83

Table 5-4 First parameter study simulation results	83
Table 5-5 Second parameter study simulation results.....	84
Table 5-6 Pipeline drift from surface to seabed	85
Table 5-7. Effect of DEH and ψ on pipeline drift.	88
Table 5-8. Effect of current heading on required top tension	89
Table 5-9 Effect of DEH cable and current heading on top tension	92
Table 5-10 Effect of current on top tension requirement	98
Table 5-11. Stress and strain in sagbend, no current.....	100
Table 5-12. Effect of current on stress and strain in sagbend	100
Table 5-13. Effect of current on sagbend stress	102
Table 5-14. Pipeline configuration and design moment	103
Table I-1. Input parameters for calculation of pipeline wall thickness.....	113

1 Introduction

Subsea pipelines are the most common way to transport oil and gas to- and from offshore installations. As the global standard of living is at an all-time high, and the industry keeps pushing production boundaries; deepwater and ultra-deepwater pipelines will continue to increase in demand.

Fields have been developed and are being planned for water depths up to 4000 meters [3]. An example of this is the proposed Stones field in the US Gulf of Mexico where a gas pipeline is to be installed, supporting the deepest production facility in the world at approximately 2900 meters below sea level [4]. Another example is a proposed gas pipeline from Oman to India, stretching 1100km reaching depths at nearly 3500 meters as an alternative to the existing Iran-Pakistan-India pipeline [20].

Studies have been carried out to investigate the feasibility of pipelaying operations regarding vessel capacity, routing, pipeline properties, and laying conditions. However, none have investigated the effect of current loads on the pipeline lay-ability. When moving towards deeper waters, there will be a significant projected area for current-induced forces to act. Therefore, it is of interest to see how currents loads affect deepwater pipelaying operations.

The application of Direct Electrical Heating (DEH) solutions has steadily increased from its introduction in 2000 at the Asgard-field, which was a collaboration between SINTEF, Statoil and Nexans [5]. DEH is developed as a method to avoid wax and hydrate formation in subsea pipelines. Electrical current is sent from a power source through the DEH cable and returned through the pipeline, where the electrical resistance within the pipeline results in generated heat [6]. Notable projects using pipeline-DEH-configurations are listed in the table below [2].

Table 1-1 Fields where DEH cables are utilized

<i>Field</i>	<i>Installation Year</i>	<i>Pipe Diameter (inches)</i>	<i>Pipeline length (km)</i>	<i>Depth (m)</i>
Maria	2017	14	26	300
Lianzi	2015	12	43	1070
Skuld	2012	14	14.2	380
		12	11.5	
Skarv	2010	12	15	375
Morvin	2009	10.5	20.7	360
Tyrihans	2007	18	44	285

Installation procedure, power requirement, and mechanical properties are considered to be among the main challenges with DEH configurations; listed below are some common problems and requirements which must be met.

- Strapping is a standard method used to fasten the DEH cable to a pipeline using high tensile carbon steel. The coating compression can be significant for strapping designs due to the water pressure experienced in ultra-deep waters. This can result in loss of the strap functionality, leading to problems such as realignment of the cable relative to the pipeline.
- Power requirements are approximately 50-150 KW per km pipeline [6].
- The required level of the current power supply is typically 1000 – 1500 A.
- The deepest installed DEH cable is at 1070 meters. SINTEF Energy has tested and verified DEH cable-functionality for hydrostatic pressures up to 500 bar, but DEH cables have not been used in ultra-deep waters before.

Few studies have investigated the effect of attaching a piggyback-cable to a pipeline [7]. The impact of current loads on a pipeline-DEH-configuration has not been investigated previously, and there is little literature related to the topic. Studies concerning pipelaying operations either include hydrodynamic current loading as a minor environmental load or neglect the effect of current loads altogether.

Recent CFD studies investigating the effect of two cylinders in proximity, shows that the interaction between two cylinders significantly changes the drag and lift force on the pipelines [8]. It is expected that the pipeline-DEH-configuration will experience higher drag forces compared

to a single pipeline configuration under equal current- velocity and angle of attack. In the present report, the impact of current loading on pipeline configurations both with and without piggyback-cable is investigated.

2 Pipeline Laying Operation

From the first offshore pipelaying vessel being developed in the 1940s and 1950s for operation in the shallow shores near the Gulf of Mexico, the development of lay barge systems has grown significantly. The first pipeline in the North Sea was installed in 1968, with the operations subjected to substantial downtime and mechanical breakdowns, high costs, and low production rates. The first operation in the “Forties Pipeline System” required two lay vessels for two seasons to install a 170km long pipeline [1]. In comparison, the modern method of S-Lay has an average lay rate up to 5km/day per vessel. This section will investigate the most feasible pipelaying method for the present study and identify pipeline systems and key-parameters concerning flow assurance.

2.1 Laying Methods

Four standard methods of pipelaying exist:

- S-Lay
- J-Lay
- Reeled Lay
- Towed Installation

The applied installation method relies on parameters such as water depth, pipeline- diameter, weight, and material. Furthermore, vessel capacity, seabed topography, and vessel availability will all affect the applied pipelaying operation. This section investigates the three most common laying techniques; S-Lay, J-Lay and Reeled Lay, discussing positive and negative features of the respective methods.

2.1.1 S-Lay Method

Initially developed in the '40s and '50s for shallow pipelaying operations in the Gulf of Mexico, S-laying is the most commonly used technique for pipelaying, and over 75% of installed deepwater pipelines in the Gulf of Mexico used this method. The pipelaying vessel moves forward while releasing the pipe at the stern supported by a stinger. The pipeline is suspended in water

until it reaches the touchdown point at the seabed. After reaching the seabed, the pipeline lays to rest, and the configuration forms a characteristic S-shape, as shown in Figure 2-1.

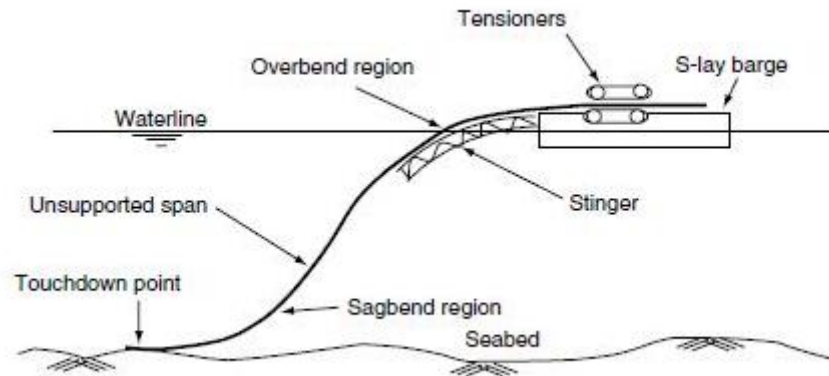


Figure 2-1 Illustration of S-Lay [9]

Applied top tension, submerged pipeline weight, and the stinger geometry determine the sagbend shape. Maximum allowable strains are kept at 0.20%-0.25%, which is around the yield strength of the material [1]. The tensioner capacity dictates the depths of which a vessel can operate. Steep S-Lay method is introduced for deepwater operations, increasing the departure angle, resulting in strains generally around 0.35% (up to 0.5%). The advantage of Steep S-Lay relative to traditional S-Lay is the reduction of pipeline span from vessel to touchdown.

2.1.2 J-Lay Method

The S-Lay configuration encounters difficulties in ultra-deep waters. Due to the pipeline leaving the S-Laying vessel at its stern in an almost horizontal position, and in the transition over to the stinger it forms an overbend (convex upward) configuration, as shown in Figure 2-1. When it leaves the stinger, the pipe forms a convex downward shape, called the sagbend. Applied top tension from the lay-vessel supports the pipeline weight. This tension has to be large enough and to make the pipe slope in the unsupported span region to match the stinger slope, if not the pipe at the end of the stinger will kink. Larger top tension results in a smaller slope in the overbend region. The top tension also has to be large enough to maintain the curvature at the sagbend region at acceptable limits.

Modern lay vessels meet these conditions easily in shallow and intermediate waters, by either changing the top tension or stinger length. Large stingers are undesirable as they are significantly

affected by environmental loads such as waves and currents. While high top tensions might cause structural damage to the pipe and makes it harder to control the operation with the DP/Mooring system [1].

The J-Lay method forms a “J-shape” from a horizontal position at the seabed and vertical on the vessel, as shown in Figure 2-2. It has several advantages compared to S-Lay, such as lower top tension requirement, no stinger, shorter pipe-span and a smaller region exposed to wave loads. Furthermore, the touchdown point will be closer to the vessel, thus simplifying the control parameter of following the planned route.

There are also significant disadvantages of using the J-Lay method; operations such as all welding, coating, and testing must be performed in the J-Lay tower, reducing the production rate significantly. As the pipeline and operations are shifted upwards in the J-Lay tower, the vessel will have a lower stability. Furthermore, if the operation consists of both ultra-deep and shallow water areas the J-Lay tower has to be changed to a less steep angle to reduce the sagbend curvature at shallow water areas

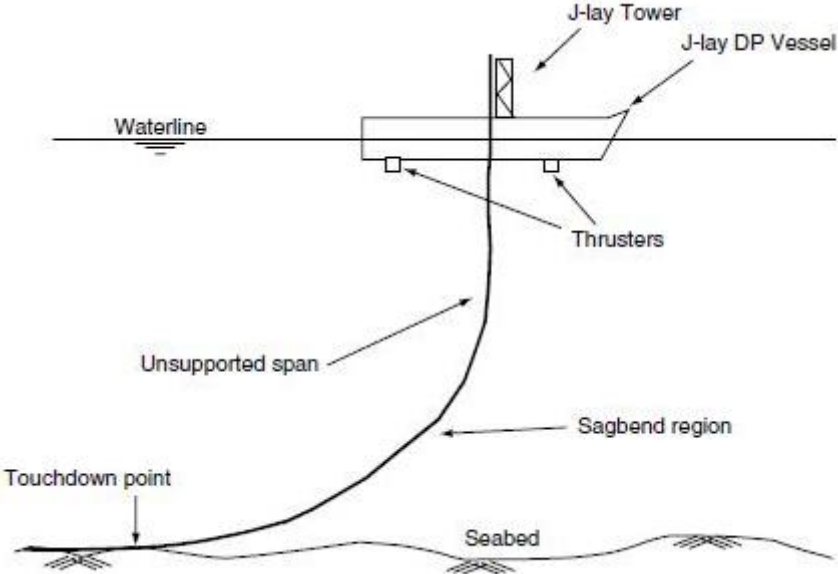


Figure 2-2 Illustration of J-Lay [9]

2.1.3 Reeling Method

The concept of reeling pipes on barges, and then unwinding them along the way was initially developed as part of the PLUTO (Pipeline Under the Ocean) project at the end of world war 2. It was initiated to send gas over the English troops located in France. The technology had a lot of problems and was not used for another 30 years, until the technology was “rediscovered” and further developed in the '60s [1]. The benefit of reeling is that the pipe can be constructed onshore, wound up on a reel, transported to the location, and then unreeled a few hours later. Figure 2-3 shows a typical reel-lay vessel.

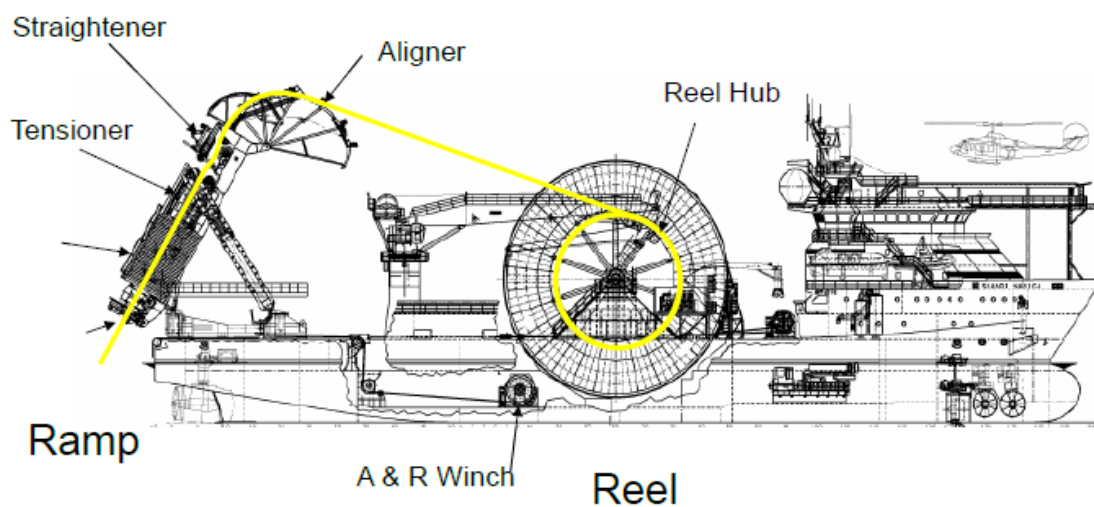


Figure 2-3 Illustration of Reeling [10]

High production rates and the relocation of work onshore makes reeling a beneficial laying method. Reeling removes high support costs involved in offshore operations and makes the process less sensitive to weather conditions. However, as the technique requires large bending strains makes concrete coating not applicable. Thus, wall thickness has to be increased or apply another type of coating such as FBE or solid polypropylene, to withstand the induced bending moment and stabilize the pipe against environmental loads. As the pipeline is bent plastically in the horizontal plane it needs to be straightened before it is laid. Nowadays, the outer diameter constraint for pipelines using the reeling method is 18” and is governed by the reeling criteria [10].

2.1.4 Selected Installation Method

Based on the discussed advantages and disadvantages in Section 2.1.1 to 2.1.3, J-Lay and S-Lay are generally favourable for deepwater pipelaying operations primarily because of:

- The allowable pipeline diameter. Reel-Lay is limited to pipeline diameters up to 18”, whilst J-Lay and S-Lay have significantly larger diameter capacities.
- The allowable wall thickness is higher compared to Reel-Lay
- Well established pipelaying methods

Herdianti (2013) investigated how bending, tension, and external hydrostatic pressure affect the lay-ability of a pipe [11]. The purpose of the study was to investigate the feasibility of pipelaying operations up to 4000 meters of water depth. The study concluded that J-Lay requires substantially lower top tension than S-Lay, and in general, can reach deeper waters than S-Lay. The selected pipelaying method is J-Lay due to the significantly lower top tension requirement [1].

2.2 Guideline on Laying Operation

Specific requirements for installations vessels, monitoring systems, and other essential parameters for pipeline installation procedures are defined in DNV-OS-F101 [12]. The tensioning system is required to operate in a fail-safe mode where the holding force, pulling force, squeeze pressure, and braking capacity is to be adequate under controlled tension. The tension equipment is to be constructed in a manner that does not cause damage to the pipeline or coating. The pipeline is to be sufficiently supported by the rollers to ensure axial movement without damage to the coat, joints and other in-line assemblies.

Pipelaying operations require sufficient measuring tools to monitor relevant parameters and to ensure that the operation is held within operational limits. DNV-OS-F101 defines the minimum required monitoring systems as:

- Tension system
 - Actual tension
 - Squeeze pressure
- Stinger

- Roller reaction loads
- Stinger and ramp configuration
- Pipeline position relative to the last roller
- Touch down point
 - Monitoring of touch down point
- Buckle detection
- Vessel
 - Vessel position
 - Vessel response
 - Vessel draft
 - Water depth
 - Direct/Indirect implication of sagbend strain and curvature

The original and most frequently used method in the world is S-laying. However, when moving towards ultra-deep waters, J-lay has qualities that make it a favourable laying method, as discussed in Section 2.1.4.

Simplified laying criteria

In the early design stages, DNV-OS-F101 specifies preliminary criteria for both overbend and sagbend.

- Overbend static strains shall be calculated according to “criterion 1” specified in Table 2-1. This includes strains induced by axial force, bending loads, local roller loads. Varying stiffness effects can be neglected. “Criterion 2”, shown in Table 2-1 is for combined static and dynamic loading, which includes all effects (including varying stiffness). See Section 3.2.2 for further information concerning material grades.

Table 2-1 Simplified laying criteria, overbend

<i>Criterion</i>	<i>X70</i>	<i>X65</i>	<i>X60</i>	<i>X52</i>
1	0.270%	0.250%	0.230%	0.205%
2	0.325%	0.305%	0.290%	0.260%

- For combined static and dynamic loads, the equivalent stress at the stinger end and sagbend region shall not exceed:

$$\sigma_{eq} < 0.87 \cdot f_y \quad (2.1)$$

Where:

f_y = yield stress

σ_{eq} = equivalent stress

The present study performs static analysis, meaning all effects due to stiffness variation and residual strain are neglected. Large water depths induce high hydrostatic pressures, resulting in critical limitations due to pipeline collapse. Therefore, it is vital to meet the buckling and collapse criteria, further discussed in Section 3.3. The design in the sagbend region should follow the requirements for the load-controlled condition addressed in Section 3.3.

2.3 Pipeline Systems

A subsea pipeline system can be complicated and consists of several components. The main task of a subsea pipeline system is to transport a medium from one point to another. In a conventional offshore system, hydrocarbons are transported from the wellhead to a processing facility. Subsea, Umbilicals, Risers, and Flowlines (SURF) is a common denotation for subsea pipeline systems. SURF can be split into two main groups:

- Umbilicals are used for data transmission and control of components.
- Flowlines and risers are used as transportation system for the produced fluid. Flowlines are responsible for transporting the fluid at the seabed, while risers are responsible for transporting the fluid from seabed to surface.
- Pipelines used in the present study are either flowlines or export pipelines. Flowlines are pipelines used for transportation of untreated fluids, whilst export pipelines transport the processed fluid.

2.4 Flow Assurance

To ensure steady- production and operation of offshore fields, maintenance and flow assurance of the subsea pipelines are essential. For pipelines in ultra-deep waters, any external operation

concerning repairs or maintenance will be complex and expensive. It is vital to design sustainable pipelines without the need for excessive intervention.

Flow assurance in deepwater environments is complicated due to the significant temperature difference between pipeline and environment, in combination with the high hydrostatic pressure. Furthermore, the formation of wax, hydrates, asphaltenes, and scale deposits are more frequent used in deepwater environments compared to shallower waters and can result in undesired fluid properties or even blocking of the wellstream. Therefore, it is essential to investigate the flow assurance for all subsea pipelines, especially in ultra-deep waters.

2.4.1 Coating

Several measures can be implemented to reduce the impact of ultra-deepwater environment conditions. The pipeline needs a specified minimum wall thickness to withstand the high hydrostatic pressure, further investigated in Section 3.3. Due to the long span in ultra-deep pipelaying operations, the weight of the pipeline is significantly increased compared to operations at intermediate waters. It requires large top tension capacities from the lay-vessel to avoid buckling in either the sagbend or overbend region. At the same time, the weight of the pipeline is directly affected by the wall thickness and coating. Wall thickness is essential to resist the hydrostatic pressure and other imposed loads. It also supplies necessary axial- and bending stiffness for the pipeline. Complications related to trawling and dropped objects are negligible in ultra-deep waters. Meaning, the primary drivers of the coating design are corrosion resistance and thermal insulation.

2.4.2 Piggyback

There are several other methods typically applied to ensure a steady flow in subsea pipelines. One approach is called piggyback, which is the mounting of an additional smaller pipeline to the main line. A typical piggyback cable/pipeline can be one of the following:

- Chemical injection pipeline: Chemicals like MEG (Mono-Ethylene Glycol) or Methanol are injected from a separate pipeline into the main line to prevent the formation of wax and hydrates.
- DEH (Direct Electrical Heating) cable: A DEH cable is strapped to a pipeline from a power source, like a platform, connecting to the pipeline end opposite from the power source. Alternating current is sent from the power source through the DEH cable and returned

through the pipeline. The electrical resistance within the pipeline will generate heat which can prevent the formation of wax and hydrates, further discussed in Section 2.4.3.

2.4.3 Hydrate Control

Hydrates are formed as a result of a crystallization process between liquid, gas, and solid phases [13]. Four conditions must be met for hydrates to form:

- Accessibility of small molecules like C₁, C₂, C₃, CO₂, H₂S and N₂
- Accessibility to free water. Even condensed water can be enough.
- High pressures. Hydrates are formed and are stable when the pressure is larger than 10-15 bar.
- Low temperatures.

All methods mentioned for flow assurance correlates with Figure 2-4. Chemical injection changes the fluid composition and shifts the hydrate formation curve to the left by increasing the hydrate free region. DEH increases the fluid temperature and maintains the fluid temperature within the hydrate free region.

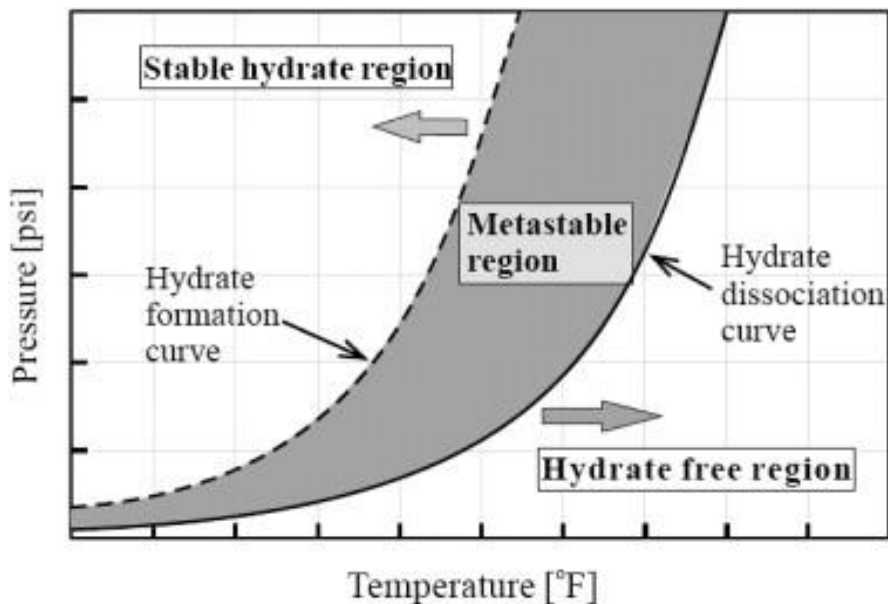


Figure 2-4. Hydrate region [13]

3 Design Criteria

The present section provides applied design criteria used to verify the design of the pipelaying process fulfils operational criteria. Different loads are identified, with the effects and uncertainties categorized. Furthermore, pipeline material selection and wall thickness design are examined.

3.1 Classifications

DNV-OS-F101 has been utilized throughout the design process to ensure the viability of the present report. The standard gives criteria and recommendations on aspects such as submarine pipeline- design and construction. In this section, the applied classifications are discussed and categorized.

3.1.1 Loads

Loads are categorized in different load categories to better relate to associated loads of a pipelaying operation to its respective uncertainties.

Functional Loads

Loads induced by the physical presence of the pipe are defined as functional loads. Relevant functional loads are [12]:

- Weight
- Response reaction from installation vessel (stinger, tensioner)
- Hydrostatic pressure (external)
- The reaction force from the soil in the sagbend
- Pre-induced stress
- Installation induced static hydrodynamic forces

Weight includes parameters such as the weight of pipe, coating, buoyancy, and all attachments to the pipe.

Environmental Loads

The loads acting on the pipeline caused by the surrounding environment are defined as environmental loads. Environmental loads include all loads which are not classified as accidental or functional loads [12]. Accidental loads are loads with an occurrence of less than 10^{-2} each year, such as extreme weather conditions, dropped objects and vessel impact. In the present study, the effects of hydrodynamic current loads on pipelaying operations are investigated and can be listed as:

- Lift and drag forces in phase with the relative sea particle velocity
- Inertia forces in phase with the relative sea particle acceleration
- Cyclic loads caused by vortex shredding or other unstable phenomena

Construction Loads

Loads that occur during the installation of pipelines are classified as functional or environmental loads. Pipe loads that arise during construction are defined as construction loads and can be listed as:

- Bundling of pipes
- Transportation loads
- Pipe handling, such as lifting or joining.
- Dynamic and static installation loads.
- Commissioning loads, such as pressure difference due to vacuum drying.

In addition, fatigue loads should to be checked and verified to be within limits. However, this is not investigated in the present study.

The different characteristic loads are shown in Table 3-1 with their corresponding return periods in Table 3-2 [12].

Table 3-1 Characteristic loads

<i>Extreme Load</i>	<i>Load effect factor combination¹⁾</i>	<i>Functional load</i>	<i>Environmental load</i>	<i>Interference load</i>	<i>Accidental load</i>
Functional load effect	a, b	100-year ²⁾	1-year	Associated	NA
Environmental load effect	a, b	Associated ³⁾	100-year ⁴⁾	Associated	NA
Interference load effect	b	Associated ³⁾	Associated	UB	NA
Fatigue load effect	c	Associated	Associated	Associated	NA
Accidental load effect	d	Associated	Associated	Associated	BE

Characteristic load definition:

n-year: Most probable maximum in n years, BE: Best estimate, UB: Upper Bound

- 1) Load effect factor combinations can be seen in Table 3-16
- 2) 100-year functional load effect are usually equivalent to an internal pressure. The internal pressure will be a combination of local incidental pressure and expected values of other associated functional loads
- 3) Will usually be equivalent to a temperature and internal pressure larger than or equal to the operating temperature profiles and operating pressures.

Table 3-2 Return period for characteristic environmental loads [12]

<i>Wind</i>	<i>Wave</i>	<i>Current</i>	<i>Ice</i>	<i>Earthquake</i>
Permanent condition				
100-year	100-year	10-year		
10-year	10-year	100-year		
10-year	10-year	10-year	100-year	
10-year	10-year	10-year		100-year
Temporary condition				
10-year	10-year	1-year		
1-year	1-year	10-year		
1-year	1-year	1-year	10-year	
1-year	1-year	1-year		10-year

The table is in compliance with ISO 16708, but if the design life is less than 33 years in conflict with ISO13623

3.1.2 Limit States

Different scenarios require different limit states which shall be considered for the relevant scenarios. The limit state design is to ensure that possible failure modes are accounted for and actions have been implemented to avoid them. DNV-OS-F101 guideline defines the typical links between scenarios and limit states as shown in Table 3-3 [12].

Table 3-3 Normal links between limit states and scenarios [12]

Scenario	<i>Ultimate Limit State</i>						<i>Serviceability Limit State</i>			
	Bursting	Fatigue	Fracture	Collapse	Propagating buckling	Combined loading	Dent	Ovalisation	Ratcheting	Displacement
Wall thickness design	X			X	X					
Installation		X	X	X	X	X		X		X
Riser	X	X	X	X	X	X		X		X
Free-Span	(X)	X	X			X				
Trawling/3 rd Party	(X)	X				X	X			
On-Bottom Stability	(X)	(X)	(X)			(X)	(X)	(X)		X ¹⁾
Pipeline Walking		X				X				
Global Buckling	(X)	X	X			X			X	

1)This is normally simplified to avoid the necessity for checking every relevant limit state.

- Ultimate Limit State (ULS) is defined as an elastic condition, which is around 15% below the limit for elasticity. By exceeding the ULS, the integrity of the pipe system is threatened.
 - Accidental Limit State and Fatigue Limit State are sub-categories of ULS as it accounts for accidental- and cyclic loads.
- Serviceability Limit State (SLS) is to ensure that the design is applicable and comfortable during normal operation.

3.1.3 Risk classifications

In this section, the location classes, fluid classes and safety classes are investigated. The design format is based on characterizing the consequence of failure, called the Load and Resistance Factor Design (LRFD) format.

Location Classes

Location classes are defined in DNV-OS-F101 by Table 3-4, where the definition of location classes defines what equations can be used. Location class 1 is applied for the calculations and simulations.

Table 3-4 Location class

<i>Location</i>	<i>Definition</i>
1	Human activity is non-frequent, and no activity is planned or anticipated along the subsea pipeline.
2	In risk of frequent human activity. Subsea pipeline or riser can be near a manned platform. A risk analysis should be performed to identify to which extent location class 2 should be applied. A minimum horizontal distance of 500 meters if no such analysis is performed.

Fluid Classes

Fluids that are being transported by pipelines shall be categorized after their hazard potential shown in Table 3-5.

Table 3-5 Fluid classifications

<i>Category</i>	<i>Description</i>
A	Normal non-flammable water-based fluids
B	Toxic and/or flammable fluids which are in liquid phase at atmospheric pressure and ambient temperatures. This can be oil and other petroleum products.
C	Non-flammable fluids which at atmospheric pressure and ambient temperatures are non-toxic gasses. This can be nitrogen, argon, air and carbon dioxide.
D	Single-phase natural gas, non-toxic
E	Toxic and/or flammable fluids which are in gaseous phase at atmospheric pressure and ambient temperatures. It which are conveyed as liquids and/or gases. This can be hydrogen, ethane, ammonia, chlorine or other natural gasses not covered by category D.

Safety Classes

DNV-OS-F101 defines the standard classification of safety classes in Table 3-6. The safety class for a given operation is defined by utilizing the combination of location class and fluid category.

Table 3-6 Safety class classification

Phase	Fluid Category A and C		Fluid Category B, D and E	
	Location Class		Location Class	
	1	2	1	2
Temporary	Low	Low	-	-
Operational	Low	Medium	Medium	High

It is expected that the pipeline operation is performed in Location Class 1 with Fluid Category B. However, DNV-OS-F101 states that pipelaying operations can apply Safety Class Low for calculations.

3.2 Pipeline Material

Material type and properties are determined by factors such as external pressure, internal pressure, fluid properties, mechanical requirements, weight requirements and cost. DNV-OS-F101 defines the following material characteristics to be considered for submarine pipelines:

- Weldability
- Mechanical properties
- Corrosion resistance
- Fatigue resistance
- Hardness
- Fracture toughness

The present section will investigate key parameters concerning material- selection and features.

3.2.1 Material Selection

Material selection is essential to obtain sustainable subsea pipelines both during installation, and operation. It defines the pipeline corrosion resistance, strength, weight, and weldability. The main limitation for pipeline installations in ultra-deep waters is identified to be the vessel top tension

capacity [1]. It needs to be large enough to avoid plastic deformation in the sagbend area for J-Laying operations. The environment of ultra-deep waters will be considerably harsher than for pipelines installed in shallow and midwaters due to high hydrostatic pressure and significant temperature differences. It is essential to select a proper material with suitable pipeline thickness to withstand the sagbend moment and environmental loads with sufficient on-bottom stability.

3.2.2 Material Grades

API requirements and standards define material grades, from X42 to X80. Full definitions and further details are given in API-5L “Specification for Line Pipe” [14]. The API grades are given in ksi and MPa by Table 3-7, where the material grades define required- Specific Minimum Yield Strength (SMYS) and Specified Minimum Tensile Strength (SMTS).

Table 3-7 Material grades [12]

<i>API Grade</i>	<i>SMYS</i>		<i>SMTS</i>	
	ksi	MPa	ksi	Mpa
X42	42	289	60	413
X46	46	317	63	434
X52	52	358	66	455
X56	56	386	71	489
X60	60	413	75	517
X65	65	448	77	530
X70	70	482	82	565
X80	80	551	90	620

Note: 1MPa = 0.145 ksi, 1 ksi = 1000 psi

The most common material grade for subsea pipelines is X65 and is applied in all calculations and simulations presented in the present study. API-5L-X65 is a manganese stainless steel alloy with the material properties listed in Table 3-8 [15].

Table 3-8 Material properties – X65 [15]

<i>Characteristics</i>	<i>Unit</i>	<i>Values</i>
Density	Kg/m ³	8000
Poisson’s number	-	0.3
Elastic Modulus	GPa	206

Thermal Expansion Co.	-	1.17×10^{-5}
Thermal Conductivity	W/m.K	50
Heat Capacity	J/kg.K	800
Shear Modulus	GPa	80

3.2.3 Characteristic Wall Thickness

Pipeline wall thickness must have a minimum wall thickness to avoid the following three failures:

- Collapse due to external pressure only (local buckling)
- Propagation buckling for external pressure only
- Bursting (containment of internal pressure)

The pipeline wall thickness is primarily influenced by the high hydrostatic pressure experienced in ultra-deep waters. Hydrostatic pressure increases linearly with depth, using a rule of thumb; at 3000 meters of water depth, the hydrostatic pressure will be around 300 bars. A corrosion allowance is to be added for the calculated wall thickness, as shown in Table 3-9. The installation loading, external impact loads, and bending loads can also influence the wall thickness. External impact loads are deemed unlikely in ultra-deep waters and therefore not accounted for in the present study.

Pipeline wall thickness in ultra-deep waters will be defined by the combination of external hydrostatic pressure and bending moment induced by the pipelaying operation. The allowable wall thickness must resist system collapse due to the combination of external hydrostatic pressure and installation bending moment. This combined loading will experience the largest stress magnitude in the sagbend region.

Two characteristics of wall thicknesses are defined in DNV-OS-F101 for different design scenarios.

- t_1 : defined by situations where failure is likely to occur due to low capacity, this is the minimum wall thickness.
- t_2 : thickness is defined by scenarios where failure is likely to occur due to an extreme load at a location with the defined average thickness.

These characteristic wall thicknesses are defined in Table 3-9.

Table 3-9 Characteristic wall thickness

	<i>Before operation</i> ¹⁾	<i>Operation</i> ²⁾
t ₁	t – t _{fab}	t – t _{fab} – t _{corr}
t ₂	t	t – t _{corr}
1) Intended where the corrosion is deemed negligible (pressure test, construction). 2) Intended where corrosion is present.		

Where:

t_{fab} = Fabrication thickness tolerance.

t_{corr} = Corrosion allowance

- A fabrication thickness allowance of 1.0mm is given by DNV-OS-F101 to be used for pipelaying operations.
- Failure statistics indicate that corrosion and impact loads are the most common failures for pipeline and are therefore decisive for the thickness design. For ultra-deep oceans, only corrosion allowance is accounted for. The following recommendations for corrosion allowance are given:
 - An internal corrosion allowance of 3 mm is recommended to be applied for steel pipelines with safety class medium or high transporting hydrocarbon fluids likely to contain water. This is utilized in the calculations.
 - External corrosion allowance of 3 mm is recommended to be applied for steel risers with safety class medium and high. This is not relevant for calculations.
- Wall thickness tolerances are defined by DNV-OS-F101 to be in accordance with Table 3-10 for the different pipeline types.

Table 3-10. Wall thickness tolerance

<i>Type of pipe</i>	<i>Wall thickness (mm)</i>	<i>Frequency of inspection</i>	<i>Tolerances</i>
SMLS	t < 4.0	100 %	+ 0.6 mm – 0.5 mm
	4.0 ≤ t < 10.0		+ 0.15 t – 0.125 t
	10.0 ≤ t < 25.0		± 0.125 t
	t ≥ 25.0		+ 0.10 t or + 3.7 mm, whichever is greater MR – 0.10 t or – 3.0 mm, whichever is greater MR

HFW, EBW, LBW and MWP	$t \leq 6.0$	100 %	± 0.4 mm
	$6.0 < t \leq 15.0$		± 0.7 mm
	$t > 15.0$		± 1.0 mm
SAW	$t \leq 6.0$		± 0.5 mm
	$6.0 < t \leq 10.0$		± 0.7 mm
	$10.0 < t \leq 20.0$		± 1.0 mm
	$t > 20.0$		+ 1.5 mm – 1.0 mm

Where:

t = Nominal wall thickness.

SMLS = Seamless Pipe

HFW = High Frequency Welding

EBW = Electronic Beam Welded

LBW = Laser Beam Welded

MWP = Multiple Welding Process

SAW = Submerged Arc-Welding

3.3 Pipeline Wall Thickness Design

The present section investigates significant criteria that have to be met to ensure a reliable pipelaying operation. Pipeline wall thickness design criteria are based on DNV-OS-F101. Situations with high potential for failure can be such as collapse due to external pressure, propagation buckling, and on-bottom stability. To ensure a sustainable pipeline wall thickness, all parameters discussed in this section are verified before a wall thickness is selected.

3.3.1 Collapse due to External Pressure, Local Buckling

The external pressure at any point along the pipeline must satisfy the criterion:

$$P_e - P_{min} \leq \frac{P_c(t_1)}{\gamma_m * \gamma_{SC}} \quad (3.1)$$

Where:

P_e = External pressure

P_{min} = Internal pressure

$P_c(t_1)$ = Minimum collapse pressure

γ_m = Material resistance factor

γ_{sc} = Safety class resistance factor

The minimum internal pressure is ordinarily equal to zero for as-laid pipelines. The external pressure, P_e , is the hydrostatic pressure due to seawater weight and is given by Equation 3.2.

$$P_e = \rho_{sea} \cdot g \cdot h \quad (3.2)$$

Where:

ρ_{sea} = Sea density

g = Gravity

h = Water depth

Material Resistance Factor

Following the Load and Resistance Factor Design method, a material resistance factor (γ_m) is accounted for to ensure the reliability of the design. DNV-OS-F101 states the requirements for different limit states, shown in Table 3-11.

Table 3-11. Material resistance factor

<i>Limit state category</i>	<i>SLS/ULS/ALS</i>	<i>FLS</i>
γ_m	1.15	1.00
Note: The different limit states are defined in Section 3.1.2.		

Safety Class Resistance Factor

All pipelines are classified by a safety class to avoid potential failures and identify the consequences. The safety level of the safety class is reflected by the safety class resistance factor (γ_{sc}) shown in Table 3-12. Different phases or locations may require different safety classes.

Table 3-12 Safety class resistance factor, γ_{SC}

<i>Safety class</i>	γ_{SC}		
	<i>Low</i>	<i>Medium</i>	<i>High</i>
Pressure containment	1.046	1.138	1.308
Other	1.040	1.140	1.260

To decide what safety class to apply, one must identify several parameters. DNV-OS-F101 states that the installation of pipelines is classified as Safety Class Low, resulting in a safety class resistance factor, γ_{SC} equal to 1.046.

Collapse Pressure

$P_c(t_1)$ is the characteristic resistance for external pressure, calculated using Equation 3.3. A system collapse will happen at the weakest point along the pipeline, represented by f_y and the minimum wall thickness t_1 . Several parameters are solved separately before being applied in Equation 3.3, identifications of these parameters are presented below.

$$P_c(t) - P_{el}(t) \cdot (P_c(t)^2 - P_p(t)^2) = P_c(t) \cdot P_{el}(t) \cdot P_p(t) \cdot f_0 \cdot \frac{D}{t} \quad (3.3)$$

Where:

$P_{el}(t)$ = Elastic collapse pressure eq. (3.4)

$P_p(t)$ = Plastic collapse pressure eq. (3.5)

f_0 = Initial ovality of the pipeline eq. (3.6)

$$P_{el}(t) = \frac{2 \cdot E \cdot \left(\frac{t}{D}\right)^3}{1 - \nu^2} \quad (3.4)$$

$$P_p(t) = f_y \cdot \alpha_{fab} \cdot \frac{2 \cdot t}{D} \quad (3.5)$$

The ovalisation caused by the construction phase is included in the total ovality. Ovalisation caused by external hydrostatic pressure or bending moment is not included, and the ovalisation cannot exceed 3% [12].

$$f_0 = \frac{D_{max} - D_{min}}{D} \leq 0.03 \quad (3.6)$$

In the formulas above, the characteristic wall thickness t , shall be replaced by t_1 or t_2 given specific design criteria. Further explanation of parameters used in the calculation of the characteristic resistance to external pressure, $P_c(t)$, is listed below.

- f_y is the characteristic material strength of the pipeline. Limit state criteria define this value as:

$$f_y = (SMYS - f_{y,temp}) \cdot \alpha_U \quad (3.7)$$

- $f_{y,temp}$ is the de-rating value due to the temperature of yield strength. For the installation procedure, no high temperatures are expected. Thus, the de-rating value is neglected.
 - α_u is a material strength factor given in Table 3-13 . A material strength factor of 0.96 is used in the calculations.
- f_u is like f_y a characteristic material strength of the pipeline defined by the specified minimum tensile strength with negligible de-rating values, shown in Equation 3.8.

$$f_u = (SMTS - f_{u,temp}) \cdot \alpha_U \quad (3.8)$$

- A material strength factor, α_u , is accounted for when calculating the material strength of the pipeline. Applicable values are shown in Table 3-13.

Table 3-13 Material Strength factor, α_U

<i>Factor</i>	<i>Normally</i>	<i>Supplementary requirement, U</i>
α_u	0.96	1.00

- During the laying operation, segments of pipes will be welded together and form the pipeline. This operation will introduce cold deformations resulting in varying strength in tension and compression. The fabrication factor, α_{fab} is determined to account for this. Table 3-14 supplies the maximum fabrication factor for different fabrication processes. A maximum fabrication factor of 0.85 is used in the calculations.

Table 3-14 Maximum fabrication factor, α_{fab}

<i>Pipe</i>	<i>Seamless</i>	<i>UO & TRB & ERW</i>	<i>UOE</i>
α_{fab}	1.00	0.93	0.85

Where:

UO = Pipe fabrication process for welded pipes

TRB = Three Rolled Bending

ERW = Electrical Resistance Welding

UOE = Pipe fabrication process for welded pipes, expanded

3.3.2 Simplified Laying Criteria

DNV-OS-F101 defines a simplified laying criterion which can be used as a preliminary criterion to check the pipeline for buckling during the early design phases. In addition to the simplified stress criteria given in Equation 3.9, limit states for fatigue, concrete crushing and rotation must be satisfied, and are found in DNV-OS-F101 under Sec.5 D800, K200, and H200 respectively [12]. The equivalent stress for combined static and dynamic loads in the sagbend region and stinger tip must be less than 87 % of the yield stress.

$$\sigma_{eq} < 0.87f_y \quad (3.9)$$

3.3.3 Combined Loading Criteria

There are two main differentiations in combined loading criteria

- Load Controlled Condition (LC-condition)
- Displacement Controlled Condition (DC-condition)

The two different differentiations require different limit states. For LC-condition, the structural response is governed by the imposed loads. For DC-condition, the structural response is governed by the geometric displacements. Pipelines utilizing the displacement-controlled criteria will usually have tensile strains over 0.4%. If the tensile strains exceed 0.4%, a fracture assessment is required.

Load Controlled Condition (LCC)

All pipe segments subjected to effective axial force, bending moment, and external overpressure is to be designed at all cross sections by the criterion given in Equation 3.10.

$$\gamma_m \cdot \gamma_{SC} \cdot \frac{|M_{sd}|}{\alpha_c \cdot M_p(t_2)} + \left\{ \left(\frac{\gamma_m \cdot \gamma_{SC} \cdot S_{sd}}{\alpha_c \cdot S_p(t_2)} \right)^2 \right\} + \left(\gamma_m \cdot \gamma_{SC} \cdot \frac{P_e - P_{min}}{P_c(t_2)} \right)^2 \leq 1 \quad (3.10)$$

Equation 3.10 is valid when the following criteria are met:

$$15 \leq \frac{D}{t_2} \leq 45, \quad P_i < P_e, \quad \frac{|S_{sd}|}{S_p} < 0.4$$

Where:

- M_{sd} = Design moment
- S_{sd} = Design effective axial force
- P_{min} = Minimum sustainable internal pressure (= 0)
- P_e = External pressure
- S_p = Plastic capacity eq. (3.11)
- M_p = Plastic capacity eq. (3.12)
- α_c = Stress flow parameter eq. (3.13)
- α_p = Details the effect of D/t₂ ratio eq. (3.14)
- β = Details the effect of D/t₂ ratio eq. (3.15)
- P_b = Burst pressure eq. (3.16)

$$S_p(t) = f_y \cdot \pi \cdot (D - t) \cdot t \quad (3.11)$$

$$M_p(t) = f_y \cdot \pi \cdot (D - t)^2 \cdot t \quad (3.12)$$

$$\alpha_c = (1 - \beta) + \beta \cdot \frac{f_u}{f_y} \quad (3.13)$$

$$\alpha_p = \begin{cases} 1 - \beta & \frac{P_i - P_e}{P_b} < \frac{2}{3} \\ 1 - 3\beta \left(1 - \frac{P_i - P_e}{P_b} \right) & \frac{P_i - P_e}{P_b} \geq \frac{2}{3} \end{cases} \quad (3.14)$$

$$\beta = \frac{60 - \frac{D}{t_2}}{90} \quad (3.15)$$

$$P_b(t) = \frac{2 \cdot t}{D - t} f_{cb} \frac{2}{\sqrt{3}} \quad (3.16)$$

$$f_{cb} = \text{MIN} \left[f_y; \frac{f_u}{1.15} \right] \quad (3.17)$$

Displacement Controlled Condition (DCC)

Displacement Controlled Condition is a situation in which the established geometric displacement governs the structural response. For a pipeline exposed to compressive longitudinal strain (axial force and bending moment) and external pressure, the criterion given in Equation 3.18 must be satisfied:

$$\left(\frac{\frac{\varepsilon_{sd}}{\varepsilon_c(t_2)}}{\gamma_\varepsilon} \right)^{0.8} + \frac{P_e - P_{min}}{\gamma_m \cdot \gamma_{SC}} \leq 1 \quad (3.18)$$

Equation 3.18 is valid when the following criteria are met:

$$\frac{D}{t_2} < 45, \quad P_{min} < P_e$$

Where:

- ε_{sd} = Design compressive strain
- ε_c = Characteristic bending strain resistance
- γ_ε = Resistance strain factor, defined for different safety classes

Design Load Effect

Different limit states apply for the two conditions given above. DNV-OS-F101 states that the LCC can always be used instead of the DCC for all applications. Therefore, the Load Controlled Condition is used in the wall thickness calculations, seen in Appendix A. The design load effect can be calculated from the following three equations:

$$M_{Sd} = M_F \cdot \gamma_F \cdot \gamma_C + M_E \cdot \gamma_E + M_I \cdot \gamma_F \cdot \gamma_C + M_A \cdot \gamma_A \cdot \gamma_C \quad (3.19)$$

$$\varepsilon_{Sd} = \varepsilon_F \cdot \gamma_F \cdot \gamma_C + \varepsilon_E \cdot \gamma_E + \varepsilon_I \cdot \gamma_F \cdot \gamma_C + \varepsilon_A \cdot \gamma_A \cdot \gamma_C \quad (3.20)$$

$$S_{Sd} = S_F \cdot \gamma_F \cdot \gamma_C + S_E \cdot \gamma_E + S_I \cdot \gamma_F \cdot \gamma_C + S_A \cdot \gamma_A \cdot \gamma_C \quad (3.21)$$

Where:

- M_{sd} = Design Moment
- M_F = Moment due to functional loads
- M_E = Moment due to environmental loads
- M_I = Moment due to interference loads
- M_A = Moment due to accidental loads
- ε_{sd} = Design compressive strain
- ε_F = Strain due to functional loads
- ε_E = Strain due to environmental loads
- ε_I = Strain due to interference loads
- ε_A = Strain due to accidental loads
- S_{sd} = Design axial force
- S_F = Axial force due to functional loads
- S_E = Axial force due to environmental loads
- S_I = Axial force due to interference loads
- S_A = Axial force due to accidental loads

Condition load effect factor (γ_c) equal to 1.07 is given to account for uncertainties connected to load effects for pipelines resting on an uneven seabed, given in Table 3-15 [12]. Meaning, γ_c is not applicable for pipelaying operation analysis where the sagbend region of the pipeline is evaluated, even if the operation is conducted on an uneven seabed.

Table 3-15 Condition load effect factors, γ_c

<i>Condition</i>	γ_c
Pipe resting on uneven seabed	1.07
Reeling on and J-tube pull-in	0.82
System pressure test	0.93
Otherwise	1.00

The calculation of design load effects for characteristic loads is to be done in accordance with DNV standards. This includes the load effect combination following the different limit states. Different conditions for the pipelaying operation results in different condition load effect factors, shown in Table 3-16.

Table 3-16 Load effect factor combinations

<i>Limit state</i>	<i>Combinations</i>		<i>Functional loads¹⁾</i>	<i>Environmental loads</i>	<i>Interference loads</i>	<i>Accidental loads</i>
			γ_F	γ_E	γ_I	γ_A
ULS	a	System check ²⁾	1.2	0.7		
	b	Local check	1.1	1.3	1.1	
FLS	c		1.0	1.0	1.0	
ALS	d		1.0	1.0	1.0	1.0
1) The functional load effect γ_F can be taken as 1/1.1 if it reduces the combined load effects 2) The necessity to check the load effect factor combination is only necessary if system effects are present. This is relevant for pipelaying operations as most of the pipeline is exposed to the same functional load.						

3.3.4 Collapse Pressure

As discussed in Section 3.3.1, the collapse pressure is a function of the elastic capacity, plastic capacity, and the ovality. The collapse pressure is defined by Equation 3.3, where the elastic and plastic capacities are defined by Equation 3.4 and Equation 3.5, respectively. DNV-OS-F101 defines a third-degree polynomial solution to apply when solving for the collapse pressure, shown in Equation 3.22 to Equation 3.29.

$$P_c = y - \frac{1}{3}b \quad (3.22)$$

Where:

$$b = -P_{el}(t) \quad (3.23)$$

$$c = -\left(P_p(t)^2 + P_p(t) \cdot P_{el}(t) \cdot f_0 \cdot \frac{D}{t}\right) \quad (3.24)$$

$$d = P_{el}(t) \cdot P_p(t)^2 \quad (3.25)$$

$$u = \frac{1}{3} \left(-\frac{1}{3} b^2 + c \right) \quad (3.26)$$

$$v = \frac{1}{2} \left(\frac{2}{27} \cdot b^3 - \frac{1}{3} \cdot b \cdot c + d \right) \quad (3.27)$$

$$\Phi = \cos^{-1} \left(\frac{-v}{\sqrt{-u^3}} \right) \quad (3.28)$$

$$y = -2 \cdot \sqrt{-u} \cdot \cos \left(\frac{\Phi}{3} + \frac{60 \cdot \pi}{180} \right) \quad (3.29)$$

Calculations, in which the equations are applied for a 20" pipeline with piggyback, can be found in Appendix A.

3.3.5 Propagation Buckling due to External Pressure

Propagation buckling occurs as a result of local buckling. Equation 3.30 defines the maximum allowable external pressure before buckle arrestors must be installed on the pipeline. The spacing of the buckle arrestors is based on cost and spare pipe philosophy.

$$P_e - P_{min} \leq \frac{P_{pr}}{\gamma_m \cdot \gamma_{sc}} \quad (3.30)$$

Where the propagation pressure is defined by Equation 3.31.

$$P_{pr} = 35 \cdot f_y \cdot \alpha_{fab} \left(\frac{t_2}{D} \right)^{2.5} \quad (3.31)$$

Given the criterion:

$$15 \leq \frac{D}{t_2} \leq 45$$

The propagation pressure, P_{pr} , is the required pressure to continue an initiated propagation buckle. If the pressure is lower than the propagation pressure, the buckle will stop. The initiation pressure, P_{init} , is defined as the required pressure to start propagation buckle from an initial buckle. A relationship between the pressures is given in Equation 3.32.

$$P_c > P_{init} > P_{pr} \quad (3.32)$$

A buckle arrestor can be installed on pipeline to increase the bending stiffness and its capacity depends on several parameters such as:

- Length of buckle arrestor
- The resistance of propagating buckle of adjacent pipe
- The resistance of propagating buckle of an infinite buckle arrestor.

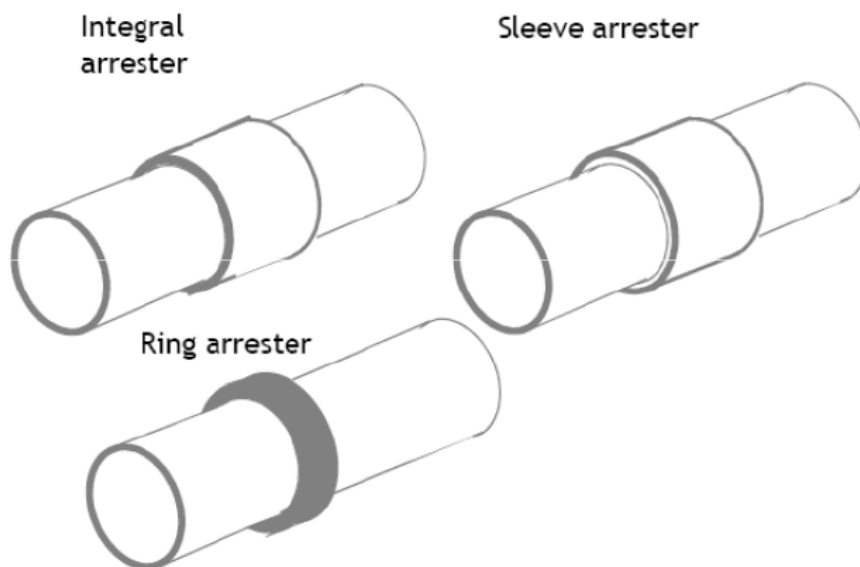


Figure 3-1. Three types of buckle arrestors, [10]

To design a buckle arrestor, the relationship given by Equation 3.33 can be applied:

$$P_e \leq \frac{P_x}{1.1 \cdot \gamma_m \cdot \gamma_{SC}} \quad (3.33)$$

$$P_x = P_{pr} + (P_{pr,BA} - P_{pr}) \left[1 - \text{EXP} \left(-20 \frac{t_2 \cdot L_{BA}}{D^2} \right) \right] \quad (3.34)$$

Where:

P_x = Crossover pressure eq. (3.34)

$P_{pr,BA}$ = Propagation buckle capacity for an infinite buckle arrestor eq. (3.31)

L_{BA} = Buckle arrestor length

3.3.6 On-Bottom Stability

On-bottom stability is applied to any subsea pipeline with a simple criterion: the pipeline is not to move from its installed position/location. Thermal expansion, permissible vertical or lateral movements and limited settlement movement is not included. On-bottom stability applies for the entire designed lifetime of the pipeline, metal loss due to corrosion and erosion is also to be accounted for. When calculating the weight of the pipeline, the nominal thickness shall not include the corrosion allowance to ensure on-bottom stability independent of corrosion allowance.

To avoid flotation, the specific gravity of the subsea pipeline must comply with the following criterion:

$$\gamma_w \cdot \frac{b}{W_{sub} + b} \leq 1.00 \quad (3.35)$$

Where:

γ_w = Weight safety factor = 1.1

b = Buoyancy

W_{sub} = Submerged weight

3.3.7 Summary of Wall Thickness Design.

Figure 3-2 summarizes the process of selecting a suitable pipeline thickness. It identifies the complexity of pipeline wall thickness calculations.

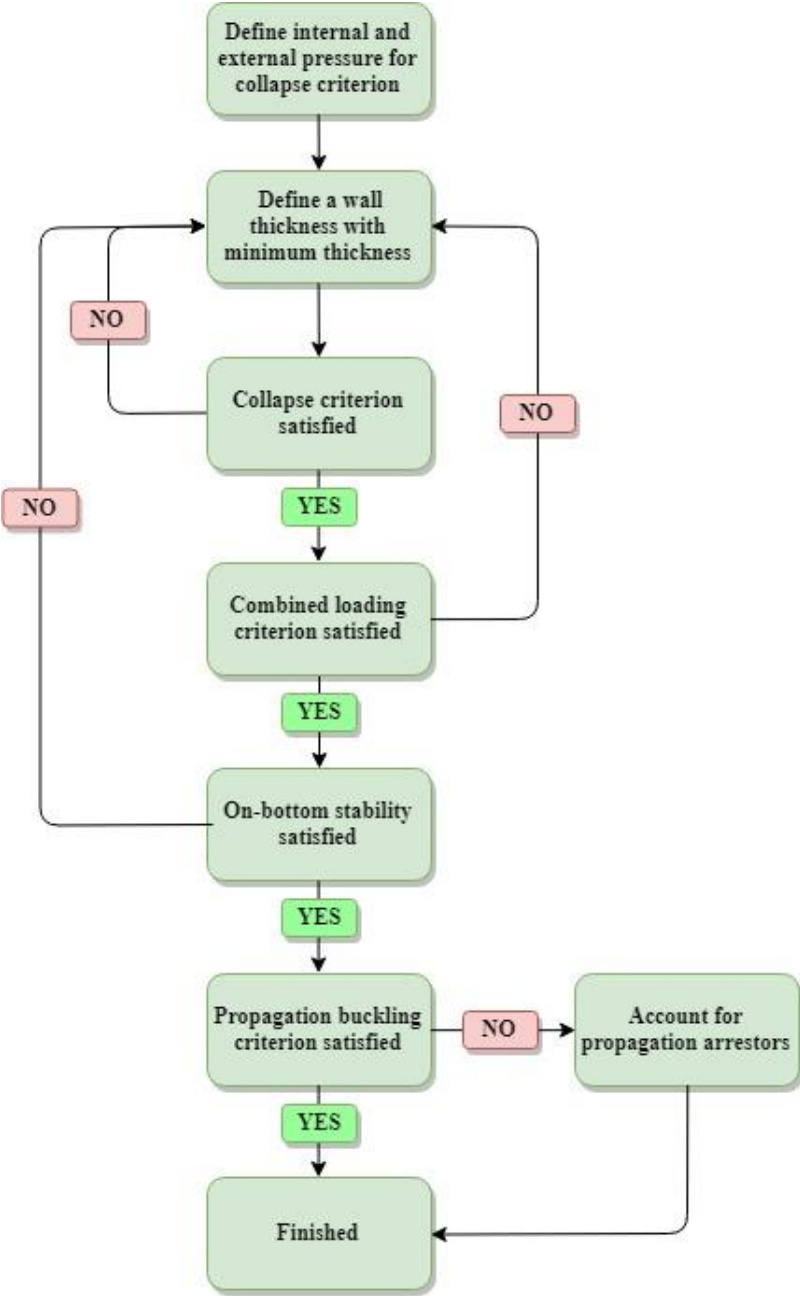


Figure 3-2 Wall thickness design flowchart

Constant values used in wall thickness calculations for the different pipeline geometries in the present study are summarized in Table 3-17. Other parameters based on pipeline/cable geometry varies for the different scenarios, see Appendix A.

Table 3-17 Summary of applied constants in wall thickness design.

<i>Characteristics</i>	<i>Unit</i>	Value
t_{fab}	mm	1.0
t_{corr}	mm	3.0
γ_m	-	1.150
γ_{SC}	-	1.046
f_0	-	0.015
SMYS	MPa	482
SMTS	MPa	530
α_u	-	0.96
α_{fab}	-	0.85
γ_c	-	1.07
γ_F	-	1.2
γ_E	-	0.7
γ_W	-	1.1
ρ_{sea}	kg/m ³	1026

3.4 Coating

The significant limitation for ultra-deep pipelaying operations is vessel top tension capacity; it is favourable to minimize the weight increase due to coating. The traditional coating solutions such as cement is discarded. For deepwater laying operations, coating compositions consisted of polymer materials are typically used. The following three compositions were suggested by the pipelaying company, Subsea7, to be feasible coating solutions for a pipeline at 3000 meters of water depth [18].

If the coating is designed for corrosion protection, it will usually be three-layer polypropylene (3LPP), shown in Table 3-18.

Table 3-18. Corrosion resistant coat (3LPP)

<i>Layer</i>	<i>Thickness</i>	<i>Density</i>
FBE (Fusion-bonded epoxy)	300 microns	1300kg/m ³
Copolymer adhesive	300 microns	900kg/m ³
Solid Polypropylene	2.6mm minimum, typical 5mm max.	900kg/m ³

Solid polypropylene with glass syntactic PP (GSPP) or solid Ultra (Ultra is a brand name from ShawCor for insulation based on polystyrene) is typically used if insulation is required, The choice of coating is primarily based on application cost, but coating thickness and specific gravity requirements also affect the composition. Table 3-19 and Table 3-20 are typical coating compositions for thermal insulation and corrosion resistance.

Table 3-19. Insulation and corrosion resistant coat (Alternative 1)

<i>Layer</i>	<i>Thickness</i>	<i>Density</i>
FBE (Fusion-bonded epoxy)	300 microns	1300kg/m ³
Copolymer adhesive	300 microns	900kg/m ³
Solid Polypropylene	5.4mm	900kg/m ³
Syntactic PP	To suit insulation design, 20- 70mm typical	650 - 780kg/m ³
Solid Polypropylene	4mm	900kg/m ³

Table 3-20. Insulation and corrosion resistant coat (Alternative 2)

<i>Layer</i>	<i>Thickness</i>	<i>Density</i>
FBE (Fusion-bonded epoxy)	300 microns	1300kg/m ³
Adhesive	300 microns	1030kg/m ³
Solid Ultra (polystyrene)	To suit insulation design, 20- 70mm typical	1030kg/m ³
Ultra-top layer	4mm	1050

The coating composition shown in Table 3-19 is used in current simulations due to the lower coating density as it does not affect the top tension. All pipeline-configurations have the same coating thickness applied to them.

For pipelines in ultra-deep waters, the change in coating thickness relative to the pipeline dimension is small. Langhelle (2011) studied the effect of pipeline dimension and sea depth on coating thickness [16]. It discovered that an insulation-coating for a 20” pipeline relative to a 28” pipeline at 3500 meters depth requires an increase of 2mm in coating thickness. The coating thickness is reduced from 41 mm for 20”-configuration to 39 mm for the 28”-configuration. As a simplification, the pipeline-configurations used in the simulations are applied the same coating thickness.

3.5 DEH Cable

For the pipeline with piggyback solution, it is assumed that the piggyback cable is a DEH cable in the present study. The typical DEH cable consists of an outer HDPE (High-Density Polyethylene) layer, with copper wires as a core, and the material properties of HDPE and copper are shown in Table 3-21 and Table 3-22. Figure 3-3 shows a simple cross-sectional model of the DEH cable made in Inventor, a 3D CAD software.

Table 3-21. HDPE Properties

<i>Steel Pipe Diameter (inches)</i>	<i>Young’s Modulus (GPa)</i>	<i>Outer Diameter (mm)</i>	<i>Inner Diameter (mm)</i>	<i>Density (kg/m³)</i>
20	1.5	150	50	950
28		210	70	
30		225	75	

Table 3-22. Copper C11000 Properties

<i>Steel Pipe Diameter (inches)</i>	<i>Young’s Modulus (GPa)</i>	<i>Outer Diameter (mm)</i>	<i>Wire Diameter (mm)</i>	<i>Density (kg/m³)</i>
20	115	50	5	8890
28		70	5	8890
30		75	5	8890

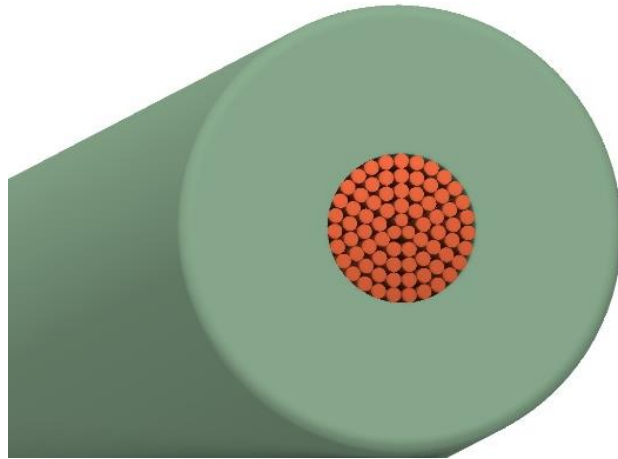


Figure 3-3. DEH cable model

SIMLA does not process multiple material properties for a single pipeline/cable. A uniform material had to be composed of the material properties of the DEH cable components. A uniform weight is established by adding the cross-sectional weight per unit length. The axial and bending stiffness are calculated for each material using Equation 3.36 to Equation 3.39.

$$F_{a,HDPE} = E_{HDPE}A_{HDPE} = E_{HDPE} \frac{\pi}{4} (OD_{HDPE}^2 - OD_{cu}^2) \quad (3.36)$$

$$F_{a,cu} = E_{cu} \cdot n_w \cdot \frac{\pi}{4} \cdot (D_w)^2 \quad (3.37)$$

$$\delta_{HDPE} = E_{HDPE} \cdot I_{HDPE} = E_{HDPE} \cdot \frac{\pi}{64} (OD_{HDPE}^4 - OD_{cu}^4) \quad (3.38)$$

$$\delta_{cu} = E_{cu} \cdot I_{cu} = E_{cu} \cdot n_w \cdot \frac{\pi}{64} (D_w)^4 \quad (3.39)$$

Where:

F_a = Axial stiffness

δ = Bending stiffness

OD_{HDPE} = Outer diameter, HDPE

OD_{cu} = Outer diameter, copper

D_w = Wire diameter

n_w = Number of wires eq. (3.40)

$$n_w = \frac{OD_{cu}^2}{D_w^2} \quad (3.40)$$

The axial and bending stiffness for each material is added together. Young's modulus is then calculated from the axial stiffness equation, see Equation 3-41.

$$F_{a,cable} = E_{cable}A_{cable} = F_{a,HDPE} + F_{a,cu} \rightarrow E_{cable} = \frac{F_{a,cable}}{A_{cable}} \quad (3.41)$$

The applied DEH cable material properties are shown in Table 3-23.

Table 3-23. DEH material properties

Pipe diameter (inch)	DEH diameter (mm)	F_a (kN)	δ (kNm ²)	E (GPa)	W_{dry} (kg/m)	W_{sub} (kg/m)
20	150	2.49E+05	37.17	14.11	32.38	14.25
28	210	4.89E+05	142.12		63.46	27.92
30	225	5.61E+05	187.17		72.85	32.06

The ratio between the outer diameter of the DEH cable and the pipeline is maintained for all pipeline configurations. This reduces the required CFD simulations for drag- and lift coefficients. The CFD results from 20" pipeline with DEH cable are used for all three diameters of the pipeline with DEH cable as the pipeline-DEH-ratio is equivalent.

3.6 Strap Material

To ensure that the DEH cable is fastened to the pipeline according to functionality, High Tensile Carbon Steels are used as strapping materials. In the calculations, it is assumed that the material AISI 4140 is a representative strap material. AISI 4140 is a chromium, manganese, molybdenum low alloy steel with high fatigue strength, impact resistance, torsional strength, toughness, and abrasion [17]. It is ensuring that the strap maintains the cable position relative to the pipeline. Table 3-24 summarizes the applied strap material properties.

Table 3-24. High tensile carbon steel material properties

<i>Property</i>	<i>Unit</i>	<i>Value</i>
Density	Kg/m ³	7850
Tensile Strength	MPa	655
Yield Strength	MPa	415
Shear Modulus	GPa	80
Elastic Modulus	GPa	210
Poisson's ratio	-	0.3
Thermal expansion coefficient	1/K	1.22e-5
Thermal conductivity	W/m·K	42.6

During pipelaying operation, several issues can occur to the strapped geometry. Pipelines are installed with coating as part of the flow assurance scheme, discussed in Section 2.4. External hydrostatic pressure induces compression to the coating material and can significantly affect the design of clamps and straps. The pipelaying company, Subsea7 recently experienced two scenarios where pipeline coating compression/reduction affected the piggyback strap design [18].

- Insulation design for a 350 m water depth pipeline was predicted to have a 3 mm reduction in coating thickness. The coating was comprised of Polypropylene (PP) foam with an initial thickness of 78 mm. The coating thickness would be reduced with 3.85 % due to a combination of high pipeline temperature and external hydrostatic pressure.
- A coating designed for 1500 m water depth was predicted to experience a 3mm reduction relative to an original coating thickness of 52 mm. Resulting in a 5.77% reduction in coating thickness. For this project, the anode had to be directly attached to the pipeline, as the bracelet anode clamps will become too loose.

In the present study, the relationship between coating compression and strap-functionality is not investigated. However, the industry is faced with complications due to this relationship, and it should be accounted for in future applications.

3.7 Current Velocity Profile

Environmental loads induced by currents should be considered for both the operation and installation of offshore structures. Currents can cause a lot of challenges for the installation of pipelines, especially in deep and ultra-deep waters. Several aspects must be considered such as:

- Currents can cause steady, but large drift motions to laying barge.
- Currents can induce lift and drag forces to submerged pipe sections. These will increase with the depth as the exposed surface area subjected to currents will increase.
- Currents can change the seabed topography.
- Seabed scour induced by the current loads can undermine structural stability.
- Currents acting on slender structures can cause vortex-induced vibrations (VIV's) and vortex induced motions (VIM's) for large structures.

However, appropriate currents are not easy to include in the simulation as data for current distribution and velocity profiles are scarce. General information for regional currents can be found in ISO 19901-1:2015 “Metoccean design and operating considerations” [19]. If site-measurements are not available, the conservative solution would be to apply joint wave-current standards as specified in NORSOK N-003 or DNV-RP-C205 for the simulation [20][21].

Ocean currents can be divided into several sub-categories as follows:

- Eddy and loop currents
- Currents generated by wind
- Currents generated by tides
- Longshore currents
- Soliton currents
- Circulation currents

For deepwater and ultra-deepwater applications, tidal and circulation currents are most relevant. Wind currents are also usually included in numerical models but will diminish at 50 meters of water depths [20].

- Tidal currents are induced by planetary motions and will have its maxima according to astronomical high tides and low tides. Strong tidal currents are typically located at straights and inlets in coastal regions.

- Circulation currents are large-scale steady currents induced by the circulation of the ocean, such as the Gulf Stream. Sections of these currents can break free and form large-scale eddies with velocities exceeding that of the main current.
- Wind currents are caused by changes in atmospheric pressure and wind stress.

Current velocity is a function of the water depth and can vary substantially. The current velocity can either be compressed or stretched at the sea surface dependent on the waves. Due to changes in the flow caused by turbulence the current will be time-dependent, resulting in a velocity vector that will be a function of both space and time.

$$\mathbf{v}_c = \mathbf{v}_c(x, y, z, t) \quad (3.42)$$

For most applications, currents can be considered as steady flow fields and a function of the depth [10]. The velocity vector for the current at the location (x,y) is given by the sum of all current vectors such as wind, circulation, and tide.

$$\mathbf{v}_c(z) = \mathbf{v}_{c,wind}(z) + \mathbf{v}_{c,circ}(z) + \mathbf{v}_{c,tide}(z) + \dots \quad (3.43)$$

Current velocity profiles are complicated as they depend on the vertical density distribution of water, the flow of water coming into the control volume and the local climate. Seabed friction decreases the current velocity progressively as it reaches the seabed, resulting in $\mathbf{v}_c(\text{seabed}) = 0$. Magnitude and direction of currents vary with seasons and at some locations, the current direction can change 180° over short spans. This makes current profiles for deep and ultra-deep waters complicated and unpredictable. The most viable solution is to perform on-site measurements.

Tidal Current Profile

The depth varying tidal current velocity profile is defined in DNV-RP-C205 as [20]:

$$v_{c,tide}(z) = v_{c,tide}(0) \left(\frac{d+z}{d} \right)^\alpha \quad \text{for } z \leq 0 \quad (3.44)$$

Where

$v_{c,tide}(0)$ = tidal surface current (at $z = 0$)

$\alpha = \text{constant} = 1/7$

$d = \text{water depth}$

$z = \text{distance from water surface (positive upwards)}$

Wind Current Velocity Profile

The depth varying wind current velocity profile is defined by the following equation in DNV-RP-C205[20]:

$$v_{c,wind}(z) = v_{c,wind}(0) \left(\frac{d_0 + z}{d_0} \right) \text{ for } -d_0 \leq z \leq 0 \quad (3.45)$$

$v_{c,wind}(0)$ for deep waters in open environments can be calculated with the following equation:

$$v_{c,wind}(0) = kU_{1 \text{ hour}, 10 \text{ m}} \text{ where } 0.015 \leq k \leq 0.03 \quad (3.46)$$

Where:

$v_{c,wind}(0)$ = wind-generated current velocity at sea surface

d_0 = constant reference water depth = 50 m

Circulation Currents

The mean circulation current needs to be measured at a specific location. As a rule of thumb, it is sufficient to use the average of a recording of a 10 minute period or larger. There are no formulas defined to express a theoretical velocity profile for circulation currents.

Deep Water Currents

Data concerning deepwater currents are scarce. Some studies have been carried out investigating this phenomenon, such as YoMaHa'07 [22]. YoMaHa'07 is a dataset containing velocity estimates for surface and deep currents. The data is sampled through trajectories of floaters called Argo. The data is collected over a 10-year period and has around 297'000 velocity readings. The readings are worldwide and shown in Figure 3-4.

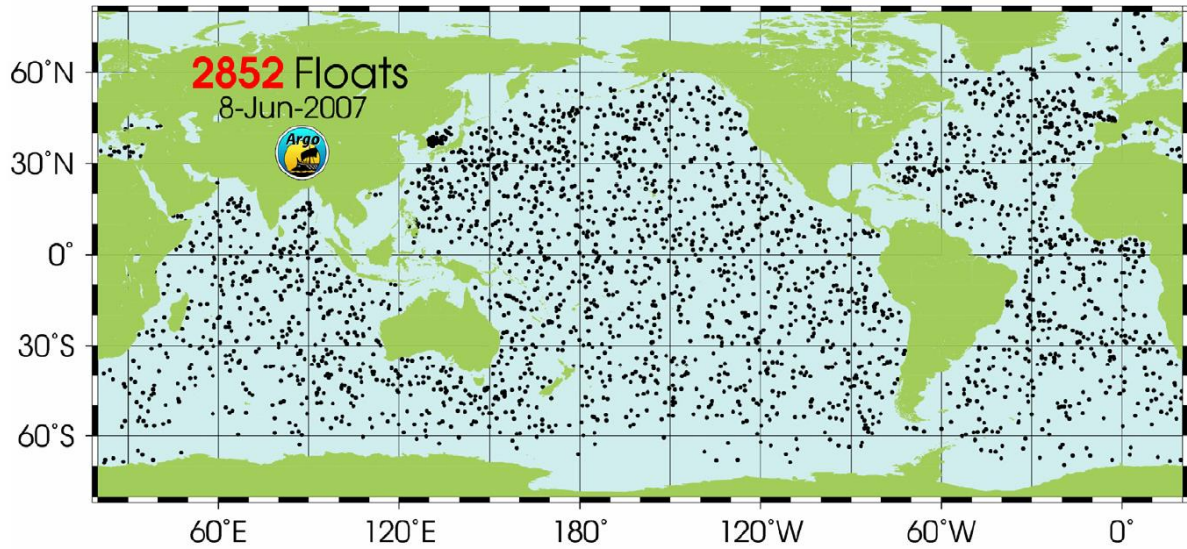


Figure 3-4 YoMaHa'07 readings [8]

The measurements are obtained by sinking a floater 2km below sea surface followed by a slow and controlled rise to the surface. The rise takes about ten days, and during this period, temperature and salinity data are collected. With the data from the float displacement, researchers are able to calculate the horizontal velocities comprising deep water currents. When surfaced, the floater provides data through satellite communication during a 24h period and the cycle is repeated. Error estimates are included to account for deviations caused by surface and intermediate currents. Deepwater velocities are taken at a minimum of 750 m depths with a less than 2 cm/s error. By averaging the data in $3^\circ \times 3^\circ$ sections, the researchers were able to make a deep water current velocity distribution, shown in Figure 3-5. It is interesting to note that deepwater currents often reach velocities over 10 cm/s.

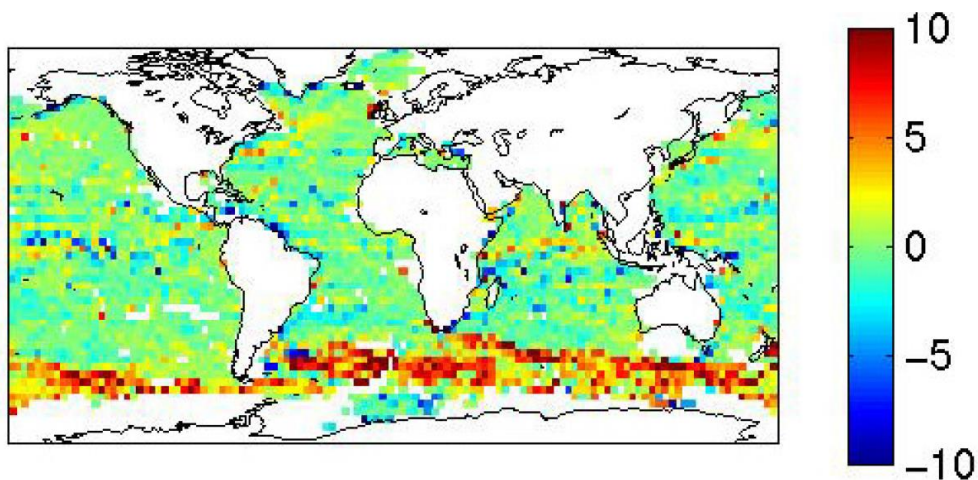


Figure 3-5 Deep water currents, given in cm/s [22]

Formations in the seabed such as gullies or trenches can further increase the deepwater currents. Gullies can become quite large and will affect the current velocity profiles greatly. Sherwin (2009) investigated a gully with a corresponding geometry shown in Figure 3-6 [23]. Velocities are given in cm/s, with downstream positive. Interesting aspects can be seen both with the high magnitude of current velocity close to the seabed, but also the positive upstream over the overflow centre.

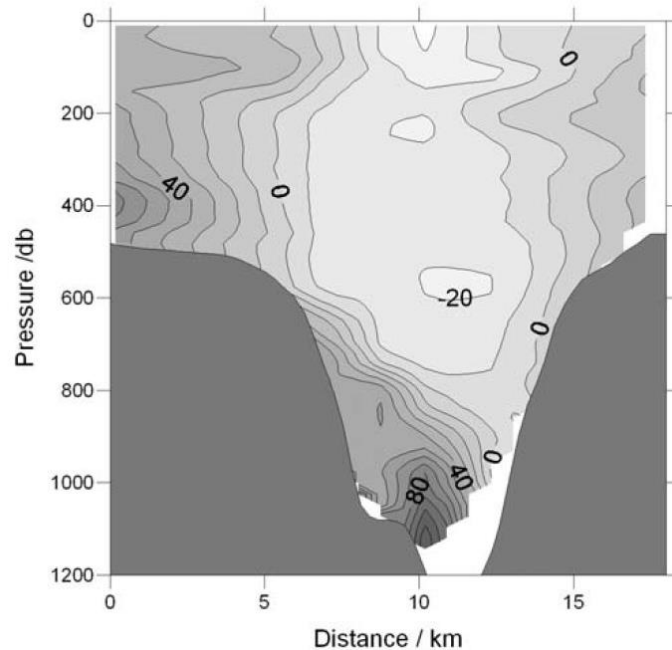


Figure 3-6 Mean current velocity in gully, given in cm/s [23]

Johnson (1998) conducted a study over the Kermadec Trench to investigate the vertical velocity profiles [24]. Recordings were done using a current meter array, deploying 20 moorings in a 22-month period. The current direction is denoted as °T, which is degrees clockwise from north (I.E. 90°T is east). Measurements were taken at 2500, 4000 and 6000 meters of water depth (or close to the bottom if shallower than 6000 m) and is further discussed by Johnson (1998). The mean current velocities for 27°T are shown in Figure 3-7.

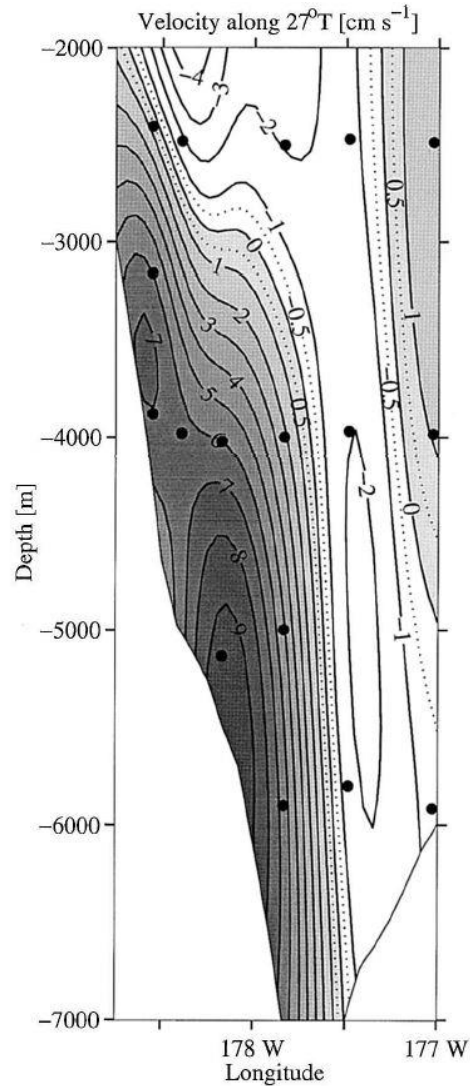


Figure 3-7 Velocity along deep water ocean trench [24]

Based on the discussed studies and DNV standards, it is evident that deep water currents are complicated. The current profile applied in the present study is based on wind currents (down to 50m), tidal currents and circulation currents (down to the seabed, 3000m). The detailed information can be found in Table 3-25 where the selected current velocity profile is described, and the current velocity profile implemented in SIMLA is shown in Appendix B.

Selected Current Velocity Profile

Based on the discussion above, a current velocity profile consistent of wind, tidal and circulation currents is selected in accordance with DNV-RP-C205 [20]. The total current velocity profile used in the simulations is shown in Table 3-25 and Figure 3-8.

Table 3-25. Selected current velocity profile

<i>Depth</i> (m)	<i>Wind currents</i> (m/s)	<i>Tidal currents</i> (m/s)	<i>Circulation</i> (m/s)	<i>Total</i> (m/s)
0	0.3	0.20	1.50	2.00
-25	0.15	0.20	1.45	1.80
-50	0	0.20	1.40	1.60
-100	0	0.20	1.30	1.50
-250	0	0.20	1.00	1.20
-348	0	0.20	0.80	1.00
-500	0	0.19	0.50	0.69
-740	0	0.19	0.31	0.50
-1000	0	0.19	0.10	0.29
-1500	0	0.18	0.10	0.28
-2000	0	0.17	0.10	0.27
-2500	0	0.15	0.10	0.25
-3000	0	0.00	0.10	0.10

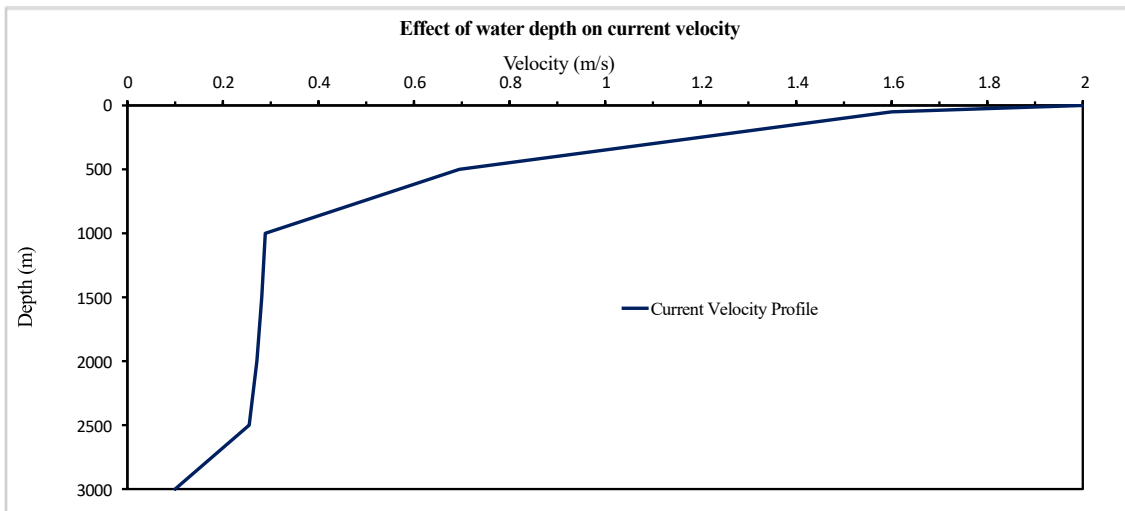


Figure 3-8. Current velocity profile

4 Pipelaying Operation Modelling

Pipelaying operations are performed with the primary purpose to install a pipeline on the seabed without exceeding the pipeline integrity. The pipeline must be installed with a top tension and curvature to avoid excessive bending moments in the sagbend region, within criteria given by DNV-OS-F101. A numerical study is performed as a static pipelaying operation, for pipelines with and without piggyback, using the finite element method (FEM) software SIMLA. The model build-up and input parameters will be discussed. In order to fully understand the pipeline-flow interaction, a series of two-dimensional numerical simulations are performed for singular pipelines and piggyback-solutions, using the open source CFD code OpenFOAM. CFD is a useful analytical tool to gain insight into the pipe, cable, and flow interactions. The governing equations and applied simulation methods will be further discussed in this section. Furthermore, key simulation assumptions will be discussed, and an analysis matrix of all performed simulations will be detailed at the end of the section.

4.1 SIMLA - Software

The numerical analysis is carried out using SIMLA which is developed by SINTEF Ocean [25]. SIMLA is an engineering analysis software using the finite element method (FEM) to simulate offshore pipeline installation, design and operations. In mechanical simulations, nonlinearities are common, usually caused by nonlinear- geometry, material, and boundary conditions. These nonlinearities are accounted for in the software

The principle for SIMLA is to analyse the pipe from the vessel to the touchdown point, including affected parts of the pipeline resting on the seabed. Important output parameters are calculated, such as curvatures in the sagbend and overbend region, moments, and axial tension. The global coordinate system is shown in Figure 4-1. It is righthanded Cartesian with the sea surface located at $z = 0$. Each model consists of elements and nodes, where the nodes are governed by the node coordinate system, as shown in Figure 4-2 [26].

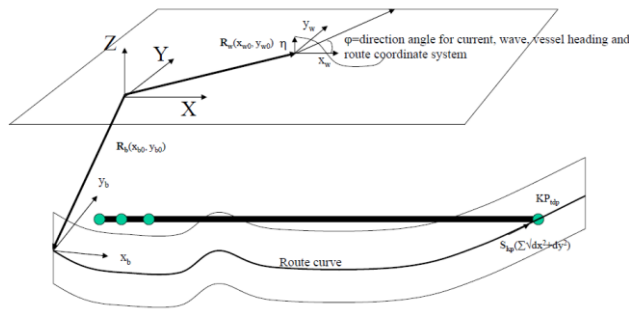


Figure 4-1 Global coordinate system [26]

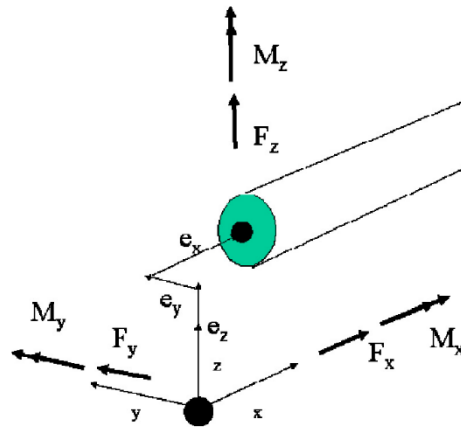


Figure 4-2 Nodal coordinate system [26]

SIMLA is part of a larger module tree, where other modules are responsible for tasks such as visualisation, result processing, and plotting, as seen in Figure 4-3 [27].

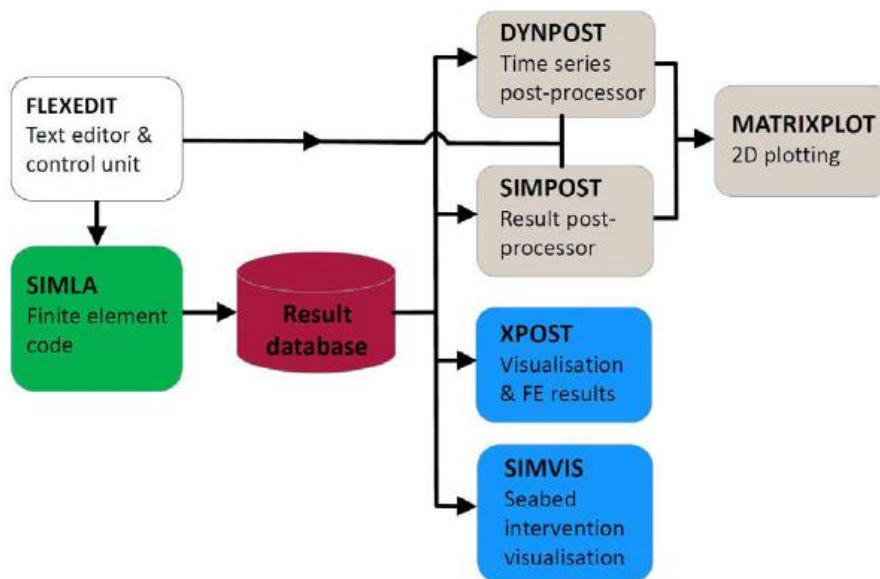
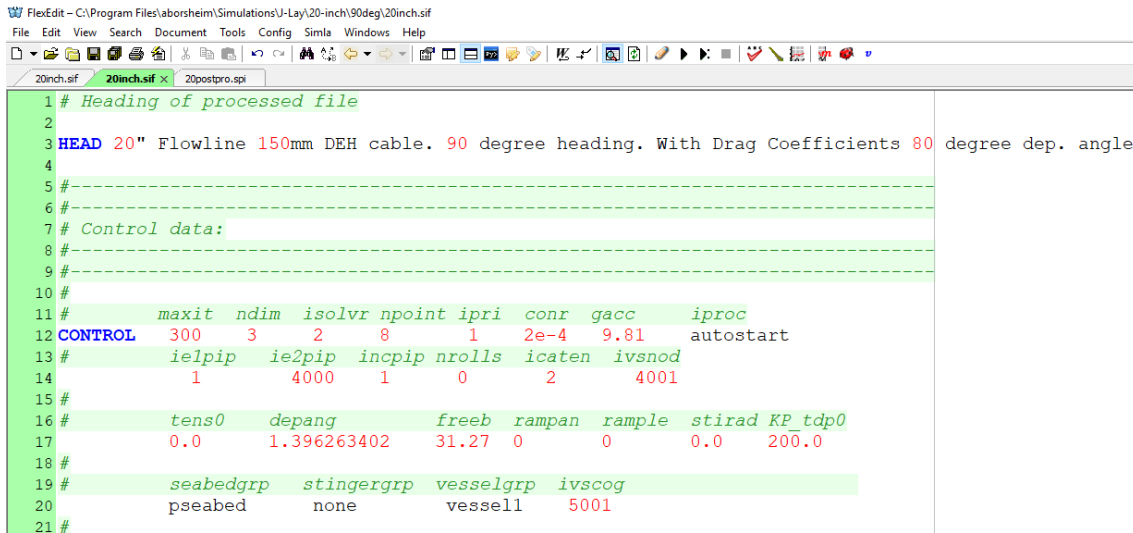


Figure 4-3 SIMLA module tree [27]

FlexEdit

FlexEdit is a text editor program used for editing input data used in the SIMLA analysis. A typical software view is shown in Figure 4-4, and a reference code is found in Appendix B. Figure 4-3 details how FlexEdit is used to communicate with all the respective programmes in the SIMLA-package.



```
FlexEdit - C:\Program Files\laborsheim\Simulations\J-Lay\20-inch\90deg\20inch.sif
File Edit View Search Document Tools Config Simla Windows Help
20inch.sif 20inch.sif x 20postpro.spl
1 # Heading of processed file
2
3 HEAD 20" Flowline 150mm DEH cable. 90 degree heading. With Drag Coefficients 80 degree dep. angle
4
5 #-----
6 #-----
7 # Control data:
8 #-----
9 #-----
10 #
11 #          maxit  ndim  isolvr  npoint  ipri  conr  gacc  iproc
12 CONTROL  300    3    2    8    1  2e-4  9.81  autostart
13 #          ielpip  ie2pip  incpip  nrolls  icaten  ivsnod
14          1          4000  1    0    2    4001
15 #
16 #          tens0  depang  freeb  rampan  rample  stirad  KP  tdp0
17          0.0    1.396263402  31.27  0    0    0.0  200.0
18 #
19 #          seabedgrp  stingergrp  vesselgrp  ivscog
20          pseabed    none        vessel1    5001
21 #
```

Figure 4-4. FlexEdit layout

SIMPOST

SIMPOST is a post-processing program used to obtain SIMLA results. SIMPOST will arrange the data, so it is applicable for plotting. The input file of SIMPOST has the suffix spl., a typical post-processing file used in the present study is shown in Figure 4-5.

20postpro.spl x											
1	GNPLOT	"20inch"	"xy-config"	"X"	X-COR	"Y"	Y-cor	1	4001	1	1
2	GNPLOT	"20inch"	"xz-config"	"X"	X-COR	"Z"	Z-cor	1	4001	1	1
3											
4	GLPLOT	"20INCH"	"Axforce-alongpipe"	"X-COR"	X-COR	"Axial force"	ELFORCE-X	1	4000	1.0	1.0 2
5	GLPLOT	"20INCH"	"YBendMom-alongpipe"	"X-COR"	X-COR	"Y-moment"	ELMOM-Y	1	4000	1.0	1.0 2
6	GLPLOT	"20INCH"	"Stress_xx-alongpipe"	"X-COR"	X-COR	"Stress-XX"	Sigma-xx	1	4000	1.0	1.0 2
7											
8	GLPLOT	"20INCH"	"CONFORZ-seabed"	"X-COR"	X-COR	"CONTACTFORCE-Y"	CONFOR-Y	25001	26000	1.0	
9	GLPLOT	"20INCH"	"CONFORZ-seabed"	"X-COR"	X-COR	"CONTACTFORCE-Z"	CONFOR-Z	25001	26000	1.0	
10											
11	ELPLOT	"20inch"	"Axforc-sagbend-time"	"TIME"	TIME	"Axial Force"	ELFORCE-X	490	500	1.0	1.0 2
12	ELPLOT	"20inch"	"YBendMom-sagbend-time"	"TIME"	TIME	"Y-moment"	ELMOM-Y	440	460	1.0	1.0 2
13	ELPLOT	"20inch"	"top-tension"	"TIME"	TIME	"Axial Force"	ELFORCE-X	4000	4000	1.0	1.0 2
14											
15	GLPLOT	"20inch"	"CurvatureZ-alongpipe"	"X-COR"	X-COR	"Z Curvature"	ELCUR-Z	1	4000	1.0	1.0 2
16	GLPLOT	"20inch"	"CurvatureY-alongpipe"	"X-COR"	X-COR	"Y Curvature"	ELCUR-Y	1	4000	1.0	1.0 2
17	GLPLOT	"20inch"	"TorsionX-alongpipe"	"X-COR"	X-COR	"X torsion"	ELTOR-X	1	4000	1.0	1.0 2

Figure 4-5 SIMPOST layout

MatrixPlot

MatrixPlot is a post-processing program used to plot the extracted simulation results from SIMPOST. The values can either be viewed graphically, as shown in Figure 4-6 or as a table. Figure 4-6 shows a graphical plot of elastic y-moment in the sagbend region in the element interval [440, 460] over time.

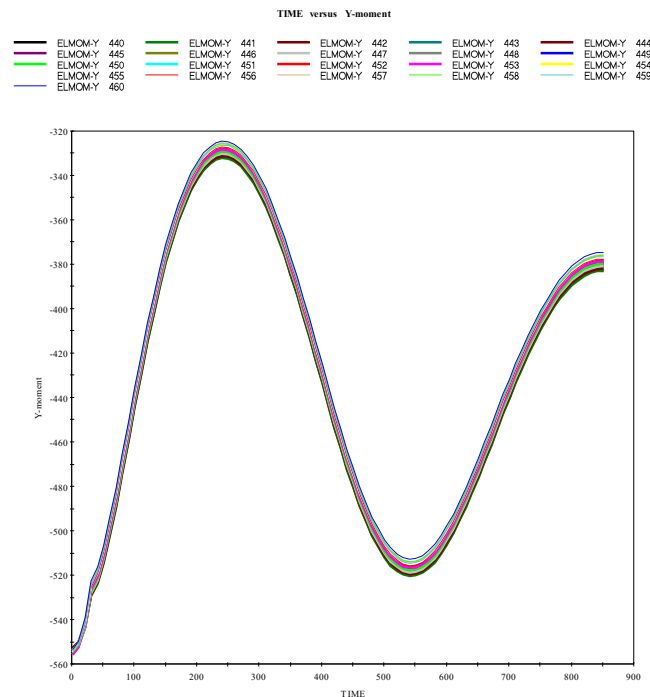


Figure 4-6 MATRIXPLOT layout

XPOST

XPOST is used for post processing giving a 3D visualization of the numerical model and results. Figure 17 shows an example of the numerical model. Only results stored in a .raf file at specified time steps are shown in XPOST.

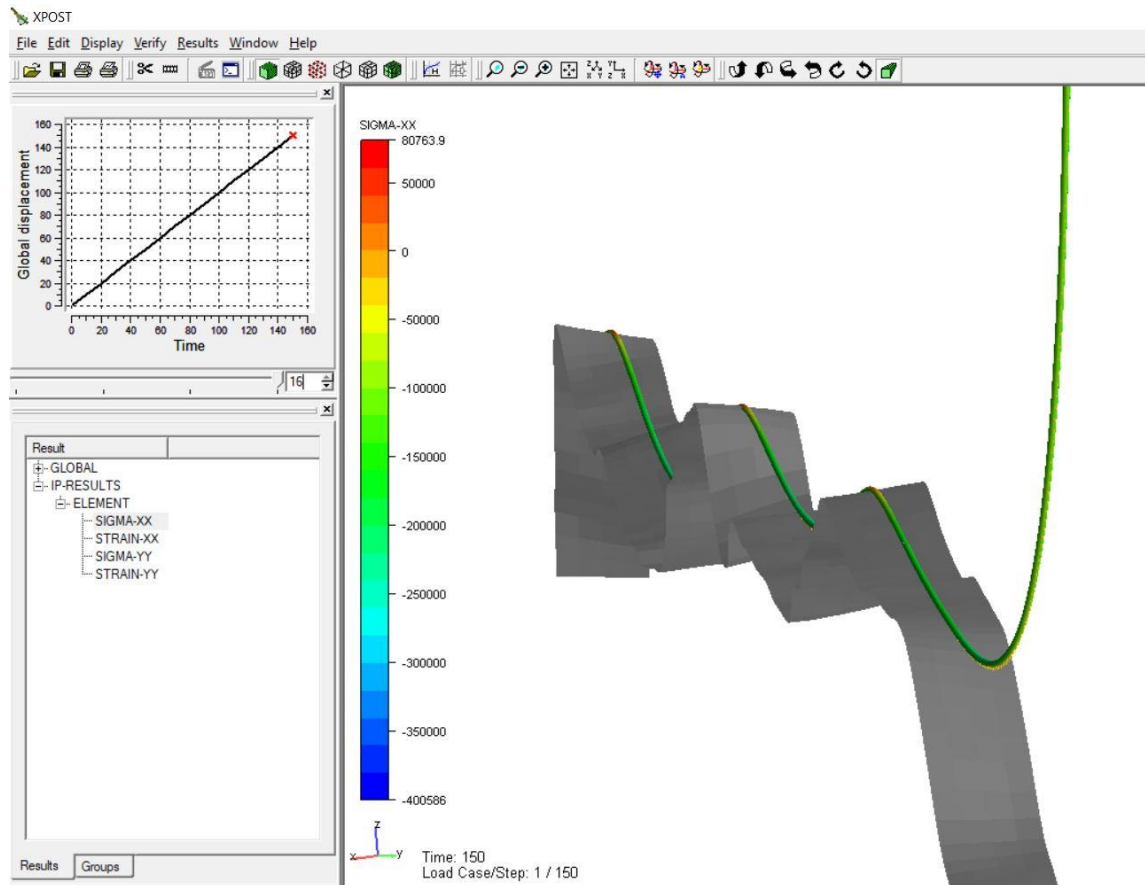


Figure 4-7 Pipeline interaction with seabed – XPOST

4.2 Pipelaying Parameters

There are several features included in SIMLA, such as:

- Nonlinear dynamic and static FEM analyses
- Lateral buckling analysis
- Pipeline stability
 - Screening analysis to find locations that might be critical concerning the stability.
 - FEED analysis to study of sliding numerically.

In the present study, static analysis is performed in SIMLA. The input files for SIMLA are generated in FlexEdit, results are processed by SIMPOST, and visualized in XPOST.

The main parameters have been considered in the current simulation as follows.

- Water depth

- Departure Angle
- Vessel freeboard
- Pipeline- and cable length
- Number of straps
- Pipeline, cable and strap material properties
- Soil material properties
- Drag coefficients for both pipeline and cable relative to current heading and geometry inclination.
- Current velocity profile
- Contact interfaces

The parameters listed above will affect significant aspects of pipelaying operations, such as.

- Sagbend moments and strains
- Required top tension
- Interaction forces between pipe and seabed
- Pipeline span from vessel to seabed
- Drag forces
- Pipeline displacement

The impact of current loads on pipelines in ultradeep waters was investigated through three main parameters.

- Current heading relative to pipeline/pipeline-cable geometry.
- Effects of piggyback.
- Effects of change in pipeline- and cable diameter.

Other parameters could have been investigated, such as steel grades, water depth, and change in the current velocity profile. However, this would expand the scope considerably and should be investigated in future works.

The set-up of the SIMLA model for the two base cases are described in Section 4.3. The first is a J-Lay model with 80 degrees departure angle, without piggyback cable. The second base case is almost identical to the first, except that a piggyback cable is mounted to the pipeline.

4.3 J-Lay Model

J-Lay was selected as the suitable pipelaying method. This section presents parameters used in the SIMLA model for a pipeline with and without piggyback.

Without Piggyback

The SIMLA code is defined by different cards, a “card” is a specific function in SIMLA which has designated parameters. An example is the UNIT-card, this card has the pre-defined parameters of mass, length and time. By defining the mass as 10^{-3} , all mass inputs are given in tonnes, and not kilogrammes.

The first card in most SIMLA codes is the CONTROL-card; for the present study, the model is defined as 3-dimensional with a convergence limit of 10^{-5} . SIMLA determines the initial pipeline configuration through the "Autostart"-procedure, where a catenary configuration is established based on lay vessel parameters [25].

The model length of the pipeline is 4000 meters, it consists of 4001 nodes and 4000 pipe elements with the element length of 1 meter. The pipe element has eight integration points around the cross section; Seabed, sea, and vessel are also modelled in the SIMLA. The nodes are defined in the NOCOOR card, and elements generated between nodal points by the ELCON (Element Connectivity) card. Element types such as pipe, body, contact, or sea elements are defined in the ELCON-card.

The initial element orientation is defined in the ELORIENT-card, and for pipe elements, a position vector **R** is set, specifying the local element position relative to the global coordinate system. Three Tait-Bryan angles define the body and contact elements. The Tait-Bryan angles rotate the elements corresponding to the coordinate system specified in the NOORIENT-card. The NOORIENT-card, in turn, rotates nodal points relative to the global coordinate system, as seen in Figure 4-8.

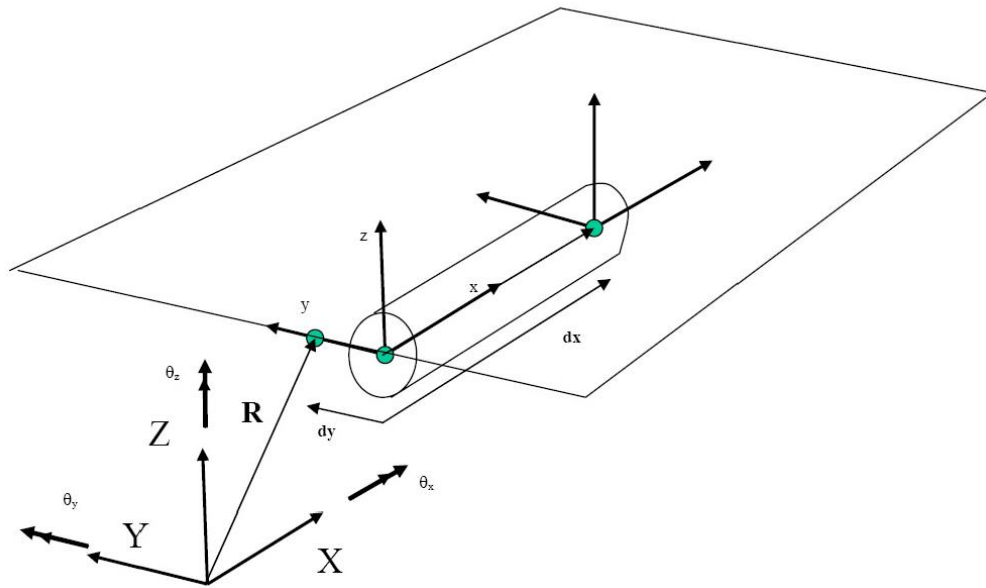


Figure 4-8. Relative position and rotation of elements to the global coordinate system [25]

Element properties are defined in the ELPROP-card with specifications related to the element types. Current velocity profiles are defined through the CURLOAD-card, where current- headings and velocities are shown in Table 3-25, and further discussed in Section 3.7.

The SIMLA-card defines the lay simulation scenario with information concerning steering type, pipeline yield strength, and connects the vessel with pipeline and seabed groups. Steering type is defined as “J Lay,” with a constant pipeline departure angle of 80 degrees.

The first node is located at the bottom end of the pipeline and is constrained to displacement in x, y, and z-direction. At top end pipeline is connected with the vessel through a specific linear constraint between master and slave nodes. The pipelaying vessel has the role of “master” where the vessel response controls all six degrees of freedom; the pipe node at that location will respond correspondingly. The slave nodes from the pipeline will always follow the displacements of the master nodes of the vessel. Figure 4-9 shows the pipeline-vessel interaction.

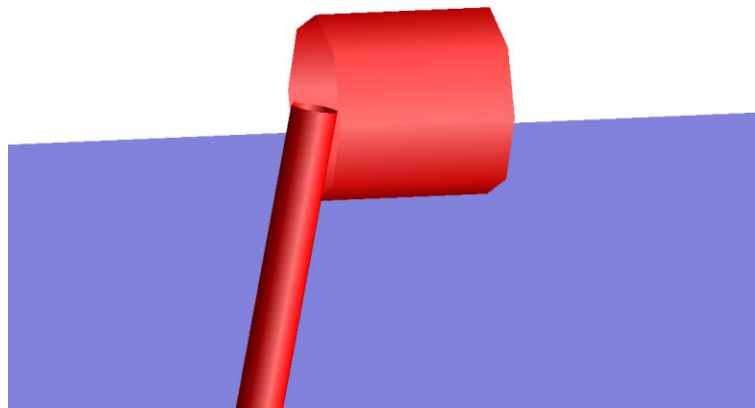


Figure 4-9. Pipe-vessel interaction

Beam elements with linear material properties represent the pipeline model. The pipeline material properties used in the present study are shown in Table 3 8. Soil properties of the seabed are modelled as an elastoplastic material with isotropic/kinematic hardening in x and y-direction, and hyperelastic (non-linear) in the z-direction. The pipelaying vessel is modelled as a linear elastic beam and can be regarded as a rigid beam, as it has considerably larger axial- and bending stiffness compared to the pipeline. Figure 4-10 shows the model of a 20-inch pipeline at 3000 meters of water depth utilizing the J-Lay method.

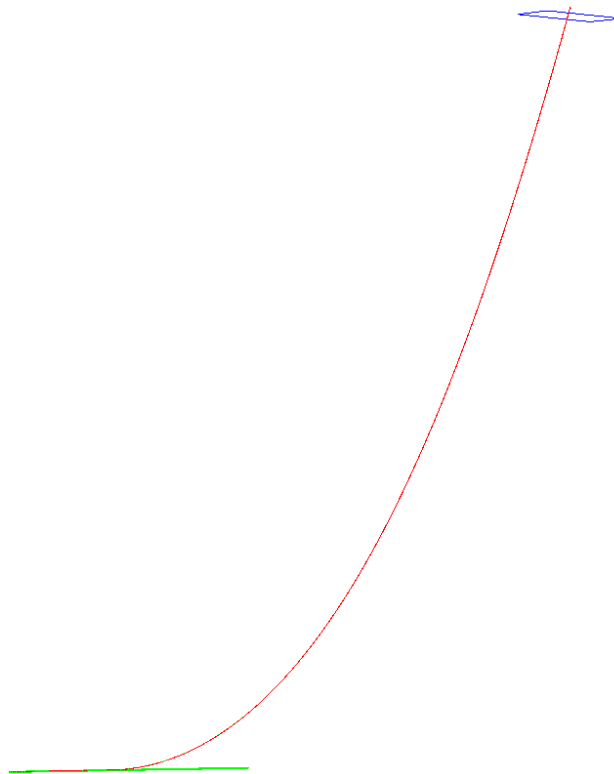


Figure 4-10 J-Lay model

With Piggyback

The simulation model for the pipeline with piggyback is based on the same input parameters for the pipeline without piggyback. It extends the model by adding parameters such as DEH- and strap elements. The piggyback is modelled to be a composite cable consists of a copper core with HDPE coating, further discussed in Section 3.5. The model length of the DEH cable is 3997 meters and is comprised of 3998 nodes with 3997 beam elements. The beam element has 8 integration points around the cross-section. The cable is reduced in length relative to the pipeline due to the pipeline-vessel constraints at the top. This does not affect the results, as the cable is mounted right after the pipeline-vessel top constraint, shown in Figure 4-11.

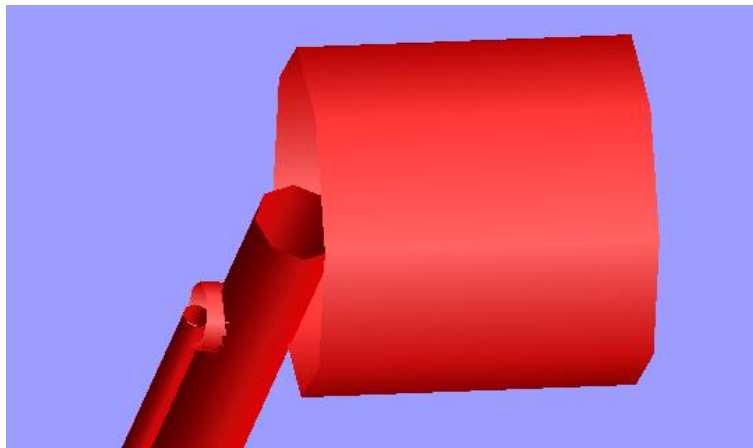


Figure 4-11. Pipeline-DEH interaction with vessel

The strap nodes are defined in intervals of 3 meters, constrained to every third pipeline and cable node. It is this constraint that maintains the pipeline-DEH relative position during the laying operation.

To model the hydrodynamic loads for pipeline and cable a dummy body element without mass is attached to the pipeline and cable. The nodes of the cable are initially constrained in translation in the local z-direction.

The cable and straps are modelled as beam elements with linear material properties. The element properties of the cable and straps are defined in the ELPROP card. The material properties for the cable and straps are described in Table 3-23 and Table 3-24 respectively.

Figure 4-12 shows the axial stress distribution from a pipelaying simulation for a pipeline-DEH-configuration. It can be observed that all axial tension is constrained to the pipeline, leaving the DEH cable, straps and pipelaying vessel stress-free. This stress distribution is favourable as the mechanical capacity of the pipeline is a major limiting factor in a pipelaying operation.

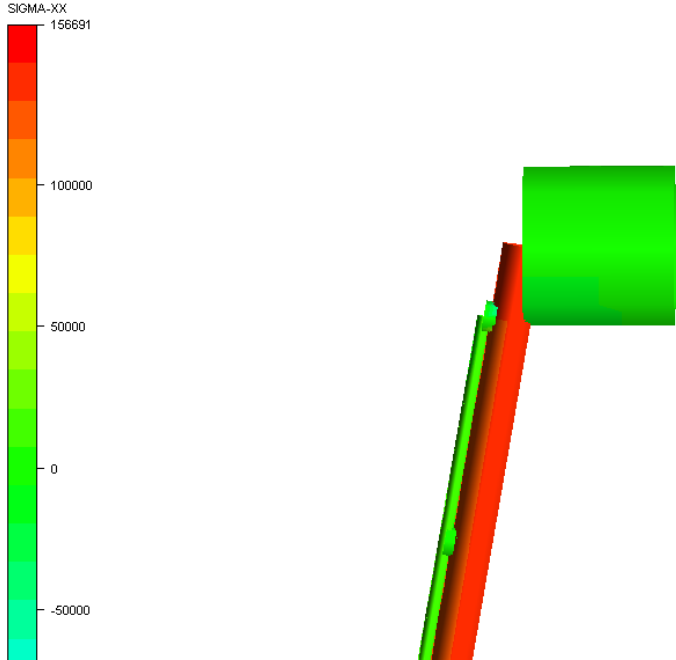


Figure 4-12. Stress distribution on pipeline-DEH-vessel-configuration

4.4 Implementation of Drag Coefficients for Pipelaying

Simulation of a pipeline with piggyback is challenging when implementing drag forces from current induced loads. Two main parameters must be accounted for to obtain reliable results.

1. Pipeline inclination relative to the seabed. The pipeline will have a zero-degree inclination when the pipeline is resting at the seabed but will gradually get to an angle equivalent to the departure angle. The normal component of the current loading will increase as the inclination angle increases. It is the normal component of the current load that defines the drag and lift forces on the pipeline; at an inclination angle of 90 degrees, all current loads will act normal to the pipeline and the highest drag- and lift forces will be experienced. Flow parallel to the pipeline is assumed not induce drag or lift forces on the pipeline.
2. Current heading relative to pipeline geometry. The pipeline geometry consists of the main pipeline with coating, and a DEH cable. As can be seen in Figure 4-13 and Figure 4-14,

the project area of the geometry will change with the current heading, the effect of projected area on current induced loads will be further discussed in Section 5.1.

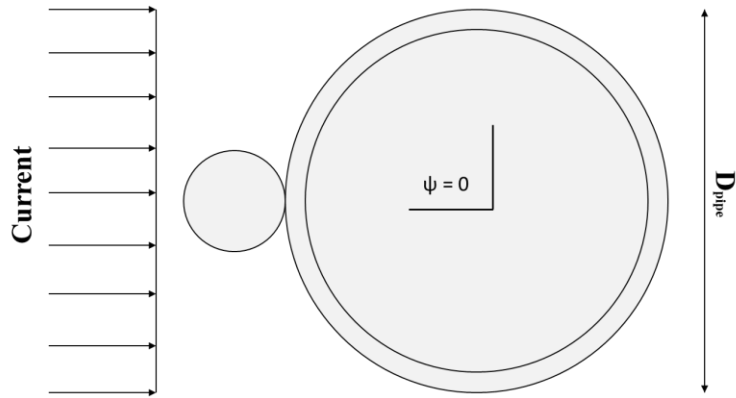


Figure 4-13. Pipeline-DEH-configuration with current flow at $\psi = 0^\circ$

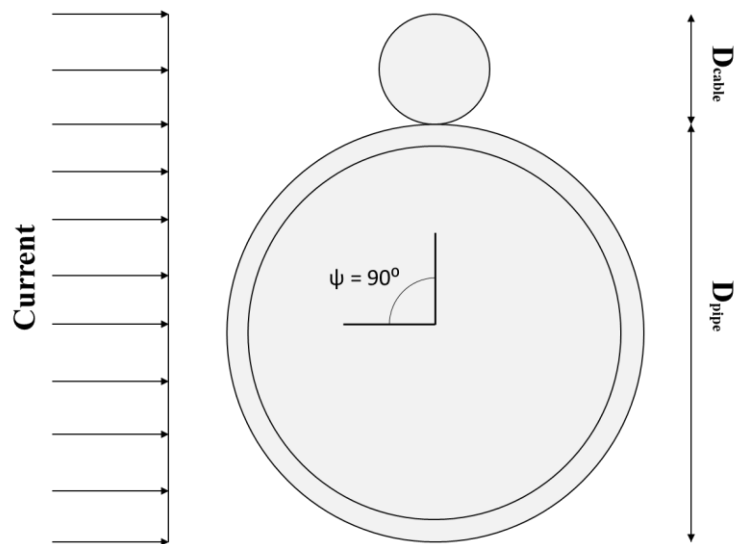


Figure 4-14 Pipeline-DEH-configuration with current flow at $\psi = 90^\circ$

SIMLA has an integrated function called HYDROPRO. HYDROPRO has been used previously for trawl boards to account for drag forces in trawling operations. The SIMLA Theory Manual states that the current angle of attack is based on local velocity components, shown in Figure 4-15 [27]. Thus, the load vector will also be defined in the local system. Drag coefficients are scaled, with the sum of squares of the relative velocity vector, including all components in x, y, and z-direction. It consists of contributions from body-, wave-, and current velocities, shown in Equation 4.1 to Equation 4.3.

$$\dot{v}_x = \dot{v}_x^{body} - \dot{v}_x^{wave} - \dot{v}_x^{current} \quad (4.1)$$

$$\dot{v}_y = \dot{v}_y^{body} - \dot{v}_y^{wave} - \dot{v}_y^{current} \quad (4.2)$$

$$\dot{v}_z = \dot{v}_z^{body} - \dot{v}_z^{wave} - \dot{v}_z^{current} \quad (4.3)$$

When calculating the external drag forces, the following equation is used.

$$F_{drag,ext} = \frac{1}{2} \rho \begin{bmatrix} \tilde{C}_{11} \\ \tilde{C}_{22} \\ \tilde{C}_{33} \\ \tilde{C}_{44} + y_D \tilde{C}_{33} - z_D \tilde{C}_{22} \\ \tilde{C}_{55} + z_D \tilde{C}_{11} - x_D \tilde{C}_{33} \\ \tilde{C}_{66} + x_D \tilde{C}_{22} - y_D \tilde{C}_{11} \end{bmatrix} v_R^2 \quad (4.4)$$

Where:

$\tilde{C}_{11} - \tilde{C}_{66}$ = Coefficients from drag-files in the directions shown in Figure 4-15. They are interpolated with respect to gap and angle of attack of the current in XY-plane

v_R = 3-dimensional resultant velocity vector eq. (4.5)

$$v_R = \begin{bmatrix} v_x \\ v_y \\ v_z \end{bmatrix} \quad (4.5)$$

In this case it does not matter whether the relative velocity vector is defined in a local or global system as the square sums will be equal in both systems.

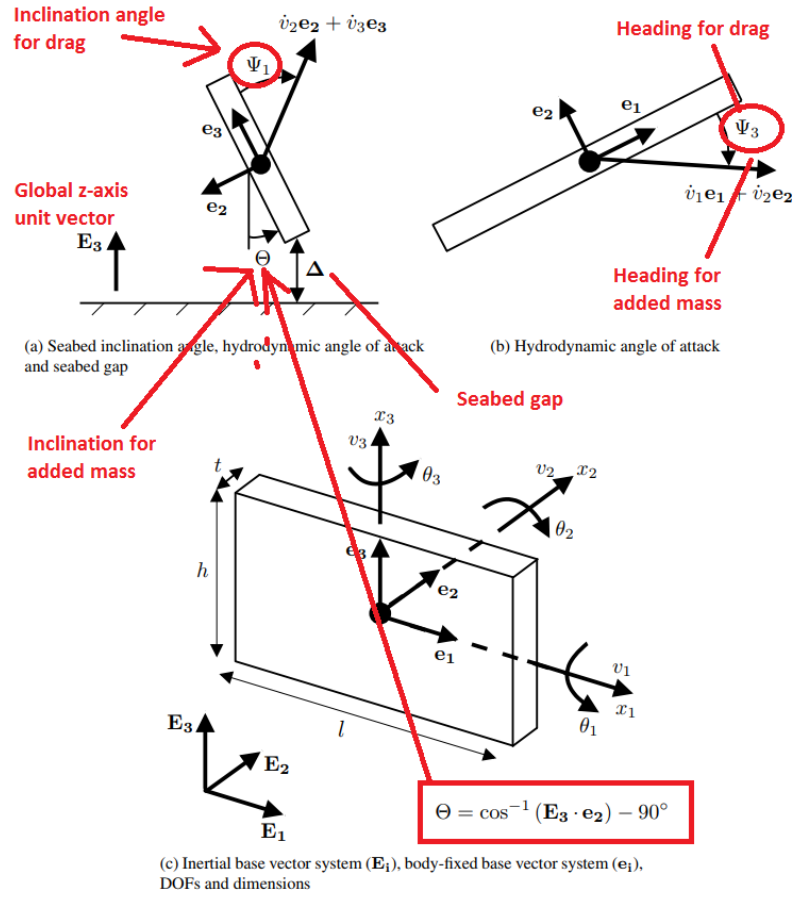


Figure 4-15. Local coordinate systems relative to the global coordinate system [29]

Drag force is characteristically defined by Equation 4.6.

$$F_{Drag} = \frac{1}{2} \rho V^2 C_D A \quad (4.6)$$

In the simulation scenario, there will only be velocities in the global XY- plane and the geometry is assumed to be non-rotational. The drag force equation is modified to:

$$F_{Drag} = \frac{1}{2} \rho V^2 \tilde{C} \quad (4.7)$$

All non-translational components are negligible, resulting in added drag coefficients in pure translational terms.

$$\tilde{C} = \begin{bmatrix} \tilde{C}_{11} \\ \tilde{C}_{22} \\ \tilde{C}_{33} \end{bmatrix} \quad (4.8)$$

As can be seen from Equation 4.8, the added drag coefficient is given as the effective area in which the current is acting multiplied by the drag coefficient. The effective area will be defined by the effective diameter of the pipeline/DEH cable geometry multiplied by the segment length. In the SIMLA model, the body elements which are used to calculate drag/lift forces are set to have an element length of 1m. Drag forces will then be calculated for each individual element.

Calculation of the Drag Coefficient, \tilde{C}

Equation 4.9, Equation 4.10, and Equation 4.11 shows how the drag forces are calculated in SIMLA using the HYDROPRO card. A geometry comprised of a pipeline with piggyback will have varying drag coefficients. To account for the variation in drag coefficients, CFD simulations were performed to identify drag coefficients for different angles of attack. In addition to the varying drag coefficients, the pipeline inclination will affect the induced drag forces due to current only acting in the global horizontal plane. Furthermore, the drag coefficient is defined in the local coordinate system for each element comprising the pipeline, where each drag coefficient is defined either in surge, sway or heave direction. These parameters are accounted for when calculating the different drag coefficients and shown in Equations 4.9 - 4.11.

$$\tilde{C}_{surge} = C_D \cdot D_{pipe} \cdot \cos(\Psi) \cdot \sin(\theta) \cdot L_{element} \quad (4.9)$$

$$\tilde{C}_{sway} = C_D \cdot D_{pipe} \cdot \sin(\Psi) \cdot \sin(\theta) \cdot L_{element} \quad (4.10)$$

$$\tilde{C}_{heave} = 0 \quad (4.11)$$

Where:

ψ = Current angle of attack in the global YZ-plane

θ = Pipeline inclination relative to seabed

Note: At a current heading, $\psi = 0^\circ$ the flow is parallel with the global x-axis, and at $\psi = 90^\circ$ the flow is parallel with the global y-axis.

To show how the local coordinate systems relative to the global coordinate system, and the pipeline-DEH-configuration in the present study, two figures are listed below. Figure 4-16 shows the cross-section of the pipeline-DEH-configuration at $\theta = 90^\circ$, while Figure 4-17 shows the

pipeline-DEH-configuration at a given pipeline inclination, θ and current heading, $\psi = 180^\circ$. Note that the local pipeline-coordinate system is planar with the global coordinate system at $\theta = 0^\circ$, given no heading is applied to the pipelaying vessel.

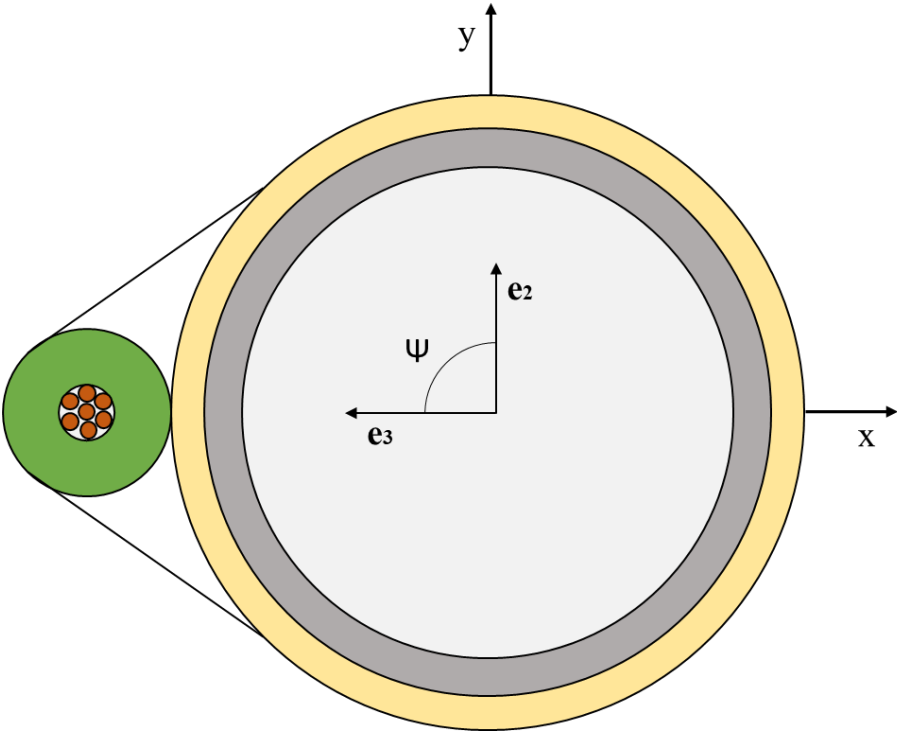


Figure 4-16. Cross section of pipeline-DEH-configuration.

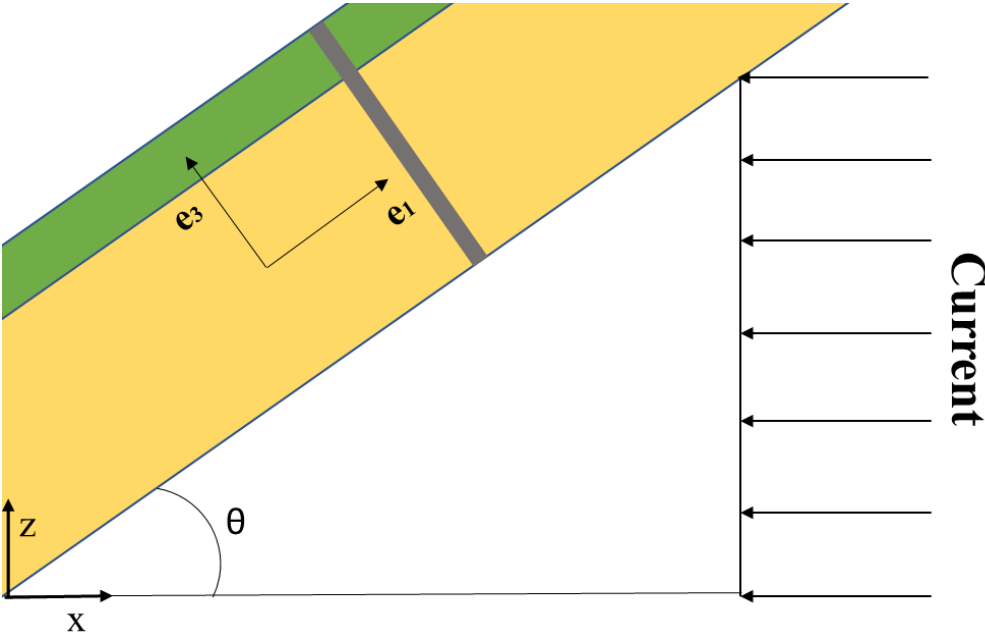


Figure 4-17. Pipeline-DEH-configuration inclination relative to current heading

4.5 Computational Fluid Dynamics (CFD)

CFD has become a key-tool for computational analysis of fluid flows both for academic and industrial purposes. It functions as a bridge between mathematical theory and experimental values. Due to its low cost and accuracy, it has become a common tool to utilize when predicting flow properties. CFD simulations are usually performed by solving the Navier-Stokes equations numerically through the Finite Volume Method (FVM).

4.5.1 OpenFOAM

OpenFOAM is an open source software tool utilizing a C++ framework to solve continuum problems through FVM. The software is free to use and is organized as a set of individual applications with no graphical user interface (GUI). Simulations are performed by applying the proper terminal commands and text files. Information concerning the fluid flow such as model mesh and boundary conditions are stored in various directories as shown in Figure 4-18.

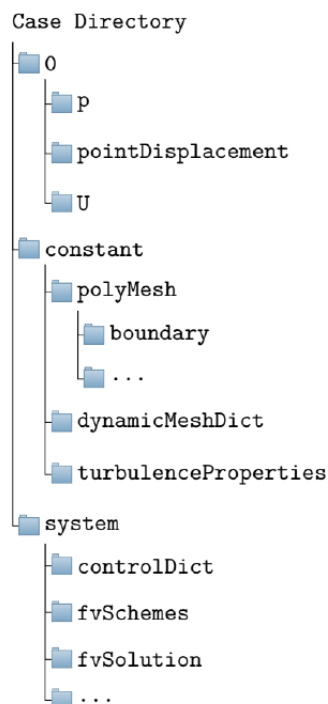


Figure 4-18. Structure of simulation case directory

4.5.2 Governing Equations

The simulated sea water is characterized as an incompressible, viscous, isothermal, 3D flow and is defined by the continuity and momentum equations.

- Continuity equation:

$$\frac{\partial u}{\partial x} + \frac{\partial v}{\partial y} + \frac{\partial w}{\partial z} = 0 \quad (4.12)$$

The continuity equation states that the mass flow into a system is equal to the mass flow out control volume (CV).

- Momentum equation, x-component

$$\frac{Du}{Dt} = -\frac{1}{\rho} \frac{\partial \rho}{\partial x} + \nu \nabla^2 u + f_x \quad (4.13)$$

- Momentum equation, y-component

$$\frac{Dv}{Dt} = -\frac{1}{\rho} \frac{\partial \rho}{\partial y} + \nu \nabla^2 v + f_y \quad (4.14)$$

- Momentum equation, z-component

$$\frac{Dw}{Dt} = -\frac{1}{\rho} \frac{\partial \rho}{\partial z} + \nu \nabla^2 w + f_z \quad (4.15)$$

Where the material derivative is defined by:

$$\frac{D}{Dt} = \frac{\partial}{\partial t} + u \frac{\partial}{\partial x} + v \frac{\partial}{\partial y} + w \frac{\partial}{\partial z} = \frac{\partial}{\partial t} + u \cdot \nabla \quad (4.16)$$

The CFD simulations use the Navier-Stokes equations through the Finite Volume Method (FVM) by discretizing the integral forms of the conservation equations. The generic solution of this integral equation is given in Equation 4.17 [8].

$$\frac{\partial}{\partial t} \iiint_V \varphi dV + \iint_S \vec{F} \cdot d\vec{S} = \iiint_V V_V dV + \iint_S V_S dS \quad (4.17)$$

V expresses the control volume, and S expresses the control surface. ϕ defines the unknown variable to be solved for, where V_V is the potential sources of ϕ within CV and V_S is the potential sources of ϕ within the control surface (CS). \vec{F} is defined as the in/out-flow of ϕ . The distinctive cells account for mass and momentum conservation at the discrete level when the equation is applied to a physical environment.

4.5.3 Finite Volume Method

It is stated that OpenFOAM uses FVM to solve continuum mechanics problems. FVM applies the conservation laws directly through the integral formulation shown in Equation 4.17. The fundament of FVM is discretizing the governing equations from the physical domain to discrete control volumes. This is done by transforming the partial differential equations to several algebraic equations. The divergence theorem is applied to convert the volumetric integral of the divergence to a surface integral at the cell boundaries. This alters the integration terms from integrating inside the cells to integrate over the cell boundary surface. It is then applicable for the iterative solvers to calculate the respective flow domain.

4.5.4 $k - \omega$ SST Turbulence Model

An appropriate model had to be assigned the simulation to ensure a reliable description of the turbulent boundary layer. The shear stress transport (SST) $k - \omega$ turbulence model created by Menter (1994) was selected [30]. Several studies have proven that the $k - \omega$ SST model is predictable and viable for simulations of flows with adverse pressure gradients [31][32]. It combines the $k - \omega$ model and the $k - \epsilon$ model for the “near wall”-region and “outer wake”-region respectively. Further, the $k - \epsilon$ model is also used in the shear-free layers. The following equations give the transport equations for k (kinetic energy) and ω (specific dissipation rate), with the standard coefficients given in Table 4-1 [8]:

$$\frac{Dk}{Dt} = \tau_{ij} \frac{\partial u_i}{\partial x_j} - \beta^* k \omega + \frac{\partial}{\partial x_j} \left[(v + \sigma_k \nu_t) \frac{\partial k}{\partial x_j} \right] \quad (4.18)$$

$$\frac{D\omega}{Dt} = \tau_{ij} \frac{\partial u_i}{\partial x_j} - \beta^* k \omega + \frac{\partial}{\partial x_j} \left[(v + \sigma_k \nu_t) \frac{\partial k}{\partial x_j} \right] + 2(1 - F_1) \frac{\sigma_{\omega 2}}{\omega} \frac{\partial k}{\partial x_j} \frac{\partial \omega}{\partial x_j} \quad (4.19)$$

Table 4-1 Standard coefficients

φ	σ_k	σ_ω	β	β^*	γ
φ_1	0.85	0.5	0.075	0.09	$\beta/\beta^* - \sigma_k k^2/(\sqrt{\beta^*})$
φ_2	1.0	0.856	0.0828	0.09	

Where:

$$v_t = \text{Turbulent viscosity eq. (4.20)}$$

$$v_t = \frac{a_1 k}{\max(a_1 \omega, \Omega F_2)} \quad (4.20)$$

$$a_1 = 0.31 \quad (4.21)$$

$$\Omega = \sqrt{2W_{ij}W_{ij}} \quad (4.22)$$

$$W_{ij} = \frac{1}{2} \left(\frac{\partial u_i}{\partial x_j} - \frac{\partial u_j}{\partial x_i} \right) \quad (4.23)$$

$$F_1 = \tanh(\text{arg}_1^4) \quad (4.24)$$

$$F_2 = \tanh(\text{arg}_2^2) \quad (4.25)$$

$$\text{arg}_1 = \min \left[\max \left(\frac{\sqrt{k}}{\beta^* \omega d_\omega}, \frac{500\nu}{d_\omega^2 \omega} \right), \frac{4\rho\sigma_{\omega 2} k}{CD_{k\omega} d_\omega^2} \right] \quad (4.26)$$

$$\text{arg}_2 = \max \left(2 \frac{\sqrt{k}}{\beta^* \omega d_\omega}, \frac{500\nu}{d_\omega^2 \omega} \right) \quad (4.27)$$

$$CD_{k\omega} = \max \left(2\rho\sigma_{\omega 2} \frac{1}{\omega} \frac{\partial k}{\partial x_j} \frac{\partial \omega}{\partial x_j}, 10^{-20} \right) \quad (4.28)$$

Where:

- W_{ij} = Vorticity magnitude
- F_1 and F_2 = Blend functions which ensures a smooth transition between the two models ($k - \omega$ and $k - \epsilon$)
- arg_1 = “first argument”, the ratio between the turbulent length scale and distance to the closest wall
- arg_2 = “second argument”, makes F_1 be equal to 1 in the viscous sub-layer.
- $CD_{k\omega}$ = Cross-diffusion (the positive value)

All arguments vanish when the flow is far away from a wall. The arguments result in F_1 equal to 1 for both the logarithmic and viscous layers. Ensuring when the flow is close to the wall; $k - \omega$ is used. As the distance to the wall increases, F_1 will decrease resulting in a transformation over to $k - \epsilon$ as F_1 goes toward 0.

4.5.5 Problem definition

Problem definition schematic is presented in Figure 4-19. In the present study, a rectangular computational domain is established with dimensions of $30D$ by $20D$, where D is the diameter of the pipeline. The pipeline centre is located at a distance of $10D$ from the inlet and $20D$ from the outflow. The upper and lower boundaries are located at a distance of $10D$ from the pipeline centre. This ensures that the blockage equals to 5%, and the influence of the domain boundaries proximity on the results is negligible. At the inlet, a uniform horizontal velocity profile is specified, at the outflow a reference pressure $P = 0$ is set. The uniform horizontal velocity in Figure 4-19 is set to 1.0 m/s. This is for a specific simulation. Simulations were performed for inlet velocities at 1.5 m/s, 1.0 m/s and 0.5 m/s.

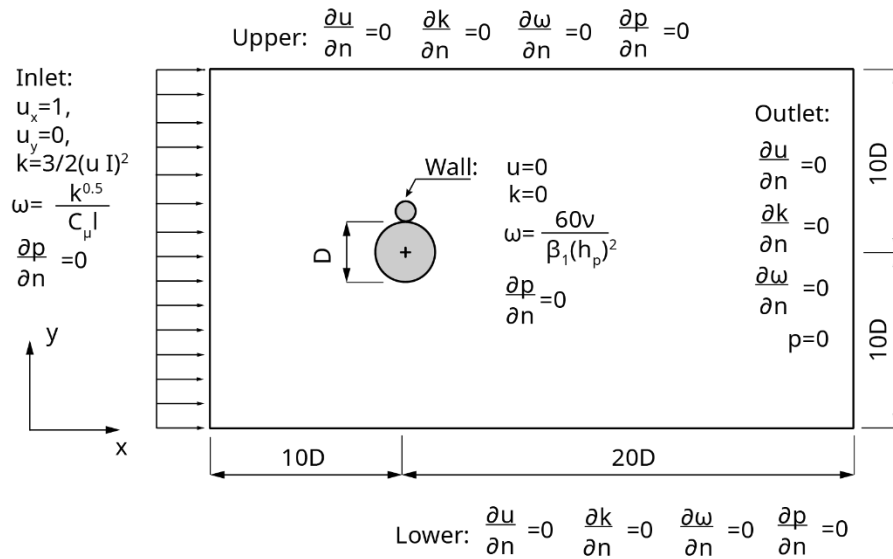


Figure 4-19 Sketch of the computational domain and imposed boundary conditions.

After the geometry of the flow problem is defined, it has to be discretized into a computational mesh. The quality of the mesh is vital for the accuracy of a simulation. The parts of the flow that experience the highest pressure gradients and velocities requires a higher mesh density than areas with low gradients. A convergence study based on three different mesh densities has been performed. The present mesh was selected as the hydrodynamic quantity error relative to a mesh with higher density was only 2%. The total cell count of the applied mesh is 88394.

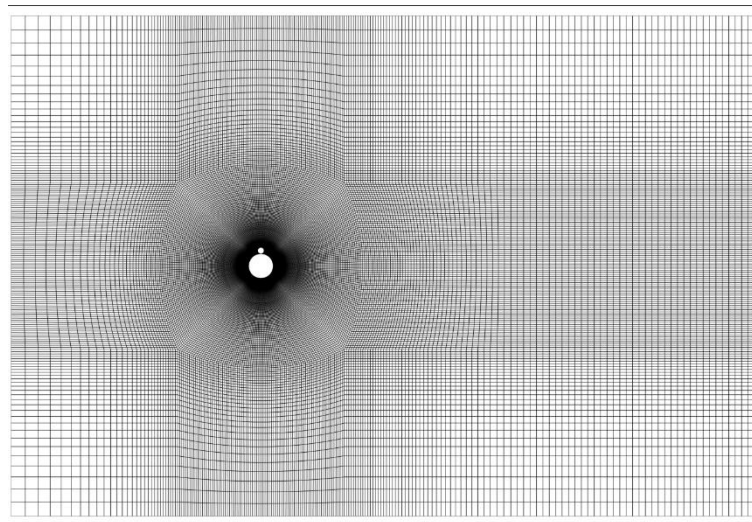


Figure 4-20 Example of the computational mesh used in the simulations. Whole domain view.

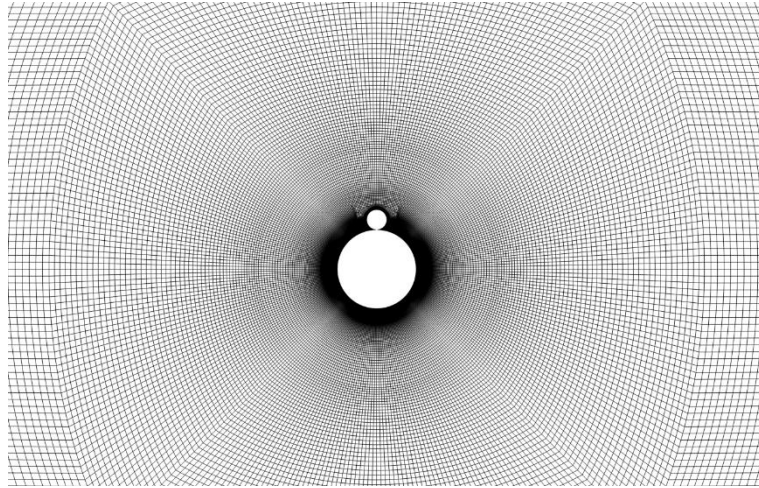


Figure 4-21 Detailed view of mesh close to the pipeline-DEH geometry.

The contact area between pipeline and cable was assumed to be 10 mm. This allows the model to maintain high-quality mesh in the concave area (see Figure 4-22) and avoid highly skewed cells which can affect the stability of the simulations.

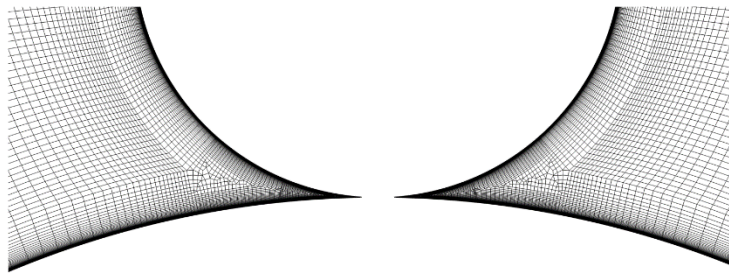


Figure 4-22 Pipeline-DEH interface meshing details

The numerical settings used in the present simulations assure second-order accuracy of the solutions. They are listed below :

- Crank-Nicolson time discretization scheme
- Gauss linear discretization of convective and diffusive terms
- PIMPLE predictor-corrector solution algorithm
 - Algorithm for pressure-velocity coupling merging SIMPLE (Semi-Implicit Method Pressure Linked Equations) and PISO (Pressure Implicit Split Operator) algorithms.
- Geometric agglomerated algebraic multigrid solver for the pressure solution

- Linear Solver. After discretizing the matrix, this solver is used to solve the discretized linear algebra
- Preconditioned bi-conjugate gradient (PBiCG) solver for the U , k and ω solution
 - Linear Solver. After discretizing the matrix, this solver is used to solve the discretized linear algebra

4.6 Assumptions

Some of the main assumptions made to conduct the present study is listed below.

- The seabed is completely flat and does not represent any real seabed topography. Furthermore, it is assumed to be elastic and homogeneous which in real applications would not be the case. Elements of different soil types like rocks could occur which would change the reaction forces.
- The presence of other environmental loads other the current loading are neglected.
- The pipeline is assumed to be empty during installation due to top tension limitations.
- The coating on the pipeline does not contribute to the axial- or bending stiffness. Its only contribution to the simulation is an increase in current-exposed diameter, and total pipeline weight.
- Coating thickness is constant at $t = 30\text{mm}$ assuming the results shown by Morten B. Langhelle (2011) are valid [16].
- DEH-piggyback-cable is not a representation of any real configurations. However, it is assumed that it is a realistic representation of a simple conductor it terms of weight and stiffness. The main contribution of stiffness is from the HDPE-material.
- The pipeline-DEH ratio is maintained equal for all pipeline dimensions. This would not occur in real applications but is done in order to utilize the same drag coefficients for all configurations.
- There is only supplied a static simulation of the different scenarios. This is a general study where pipeline properties are to be investigated during several defined scenarios. For real applications, a dynamic analysis should be included to ensure the operation is within operational limits.

4.7 Analysis Matrix and Main Input Data

Several parameters of the pipeline-DEH-configuration were investigated to perform adequate simulations with comparable data, shown in Table 4-2. Three common subsea pipeline diameters (20", 28" and 30") are applied throughout the simulations. The specific pipeline dimensions are used in two configurations; (1) As a single pipeline and (2) with a piggyback cable. Furthermore, a current is induced on the pipeline configurations at five attack angles: 0, 45, 90, 135, and 180 degrees. Meaning the pipeline-configurations are exposed to 30 comparable conditions. In addition to this, six simulations are performed without environmental loading to identify the functional loading of all pipeline configurations.

Table 4-2. Analysis matrix

<i>Sim. No</i>	<i>Pipe Dia. (inch)</i>	Ψ (deg)	<i>DEH Cable</i>	<i>Current Profile</i> ¹⁾	<i>Depth</i> ²⁾	<i>Mat. Grade</i> ³⁾	<i>Simulation Time (s)</i>
1	20	0	NO	Profile 1	3000	X65	251
2	28	0	NO	Profile 1	3000	X65	251
3	30	0	NO	Profile 1	3000	X65	251
4	20	45	NO	Profile 1	3000	X65	251
5	28	45	NO	Profile 1	3000	X65	251
6	30	45	NO	Profile 1	3000	X65	251
7	20	90	NO	Profile 1	3000	X65	501
8	28	90	NO	Profile 1	3000	X65	501
9	30	90	NO	Profile 1	3000	X65	501
10	20	135	NO	Profile 1	3000	X65	251
11	28	135	NO	Profile 1	3000	X65	251
12	30	135	NO	Profile 1	3000	X65	251
13	20	180	NO	Profile 1	3000	X65	251
14	28	180	NO	Profile 1	3000	X65	251
15	30	180	NO	Profile 1	3000	X65	251
16	20	0	YES	Profile 1	3000	X65	851
17	28	0	YES	Profile 1	3000	X65	501

18	30	0	YES	Profile 1	3000	X65	501
19	20	45	YES	Profile 1	3000	X65	251
20	28	45	YES	Profile 1	3000	X65	251
21	30	45	YES	Profile 1	3000	X65	251
22	20	90	YES	Profile 1	3000	X65	851
23	28	90	YES	Profile 1	3000	X65	851
24	30	90	YES	Profile 1	3000	X65	851
25	20	135	YES	Profile 1	3000	X65	251
26	28	135	YES	Profile 1	3000	X65	251
27	30	135	YES	Profile 1	3000	X65	251
28	20	180	YES	Profile 1	3000	X65	251
29	28	180	YES	Profile 1	3000	X65	251
30	30	180	YES	Profile 1	3000	X65	251
31 ⁴⁾	20	-	NO	NO	3000	X65	251
32 ⁴⁾	28	-	NO	NO	3000	X65	251
33 ⁴⁾	30	-	NO	NO	3000	X65	251
34 ⁴⁾	20	-	YES	NO	3000	X65	251
35 ⁴⁾	28	-	YES	NO	3000	X65	251
36 ⁴⁾	30	-	YES	NO	3000	X65	251
<p>1) Profile 1 is shown in Table 3-25 and Figure 3-8. 2) The seabed is a flat surface with a constant depth of 3000m. 3) Material grades are discussed in Section 3.2.2 4) Simulation 31-36 was performed to obtain the functional loads of the installation (see Section 3.1.1 and Section 5.3.3)</p>							

5 Results and Discussions

5.1 Drag Coefficients

For the calculation of the drag coefficient (C_D), a solid foundation had to be implemented, to ensure reliable simulation values. This section investigates the effects of current heading, pipeline inclination, and pipeline geometry, on C_D .

5.1.1 Projected Area

The current heading is defined by ψ , in the unit degrees. At $\psi = 0^\circ$, the flow acts longitudinally along the pipeline. Furthermore, the flow is in the direction which the pipelaying operation is performed. At $\psi = 90^\circ$, the flow acts perpendicularly to the pipeline; and at $\psi = 180^\circ$ the flow acts head-on the pipeline and the laying operation, shown in Figure 5-1. In the performed pipelaying simulations, only the pipeline experience soil-interaction loads, as the DEH cable is mounted on the top of the pipeline.

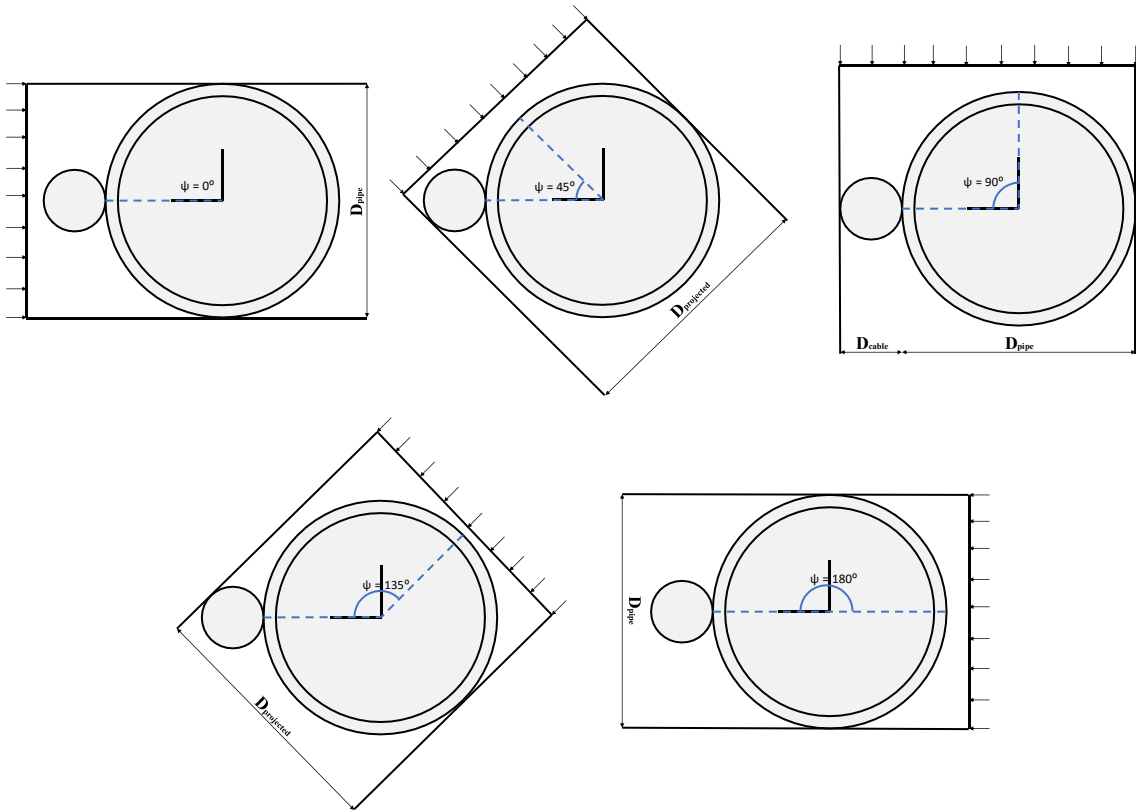


Figure 5-1 Pipeline-DEH-configuration with the projected diameter when exposed to current flows at: $\psi = 0^\circ$, $\psi = 45^\circ$, $\psi = 90^\circ$, $\psi = 135^\circ$, and $\psi = 180^\circ$

The project diameter increases when current heading increases from $\psi = 0^\circ$ to $\psi = 90^\circ$, and then decreases when current heading increases from $\psi = 90^\circ$ to $\psi = 180^\circ$. Traditionally the projected diameter for a given current heading has been applied to a constant drag coefficient. Instead of using this method, the present report performed CFD-simulations to obtain the experienced drag forces on each body. This will be further explained in Section 5.1.2 and Section 5.1.3.

It can be seen that the projected diameter is equal for $\psi = 0^\circ$ and $\psi = 180^\circ$, where the DEH cable location relative to the current is the only difference.

5.1.2 CFD - Results

The DEH cable affects the streamlines and pressure fields around the pipeline-DEH-configuration. This can either increase or decrease the experienced drag coefficient. CFD-simulations were performed for a 20” pipeline-DEH-configuration in the interval $\psi \in [0, 180]$ for every 15° with horizontal velocities at 1.5 m/s, 1.0 m/s and 0.5 m/s. The simulation parameters are summarized in Table 5-1.

Table 5-1 CFD simulation parameters

<i>Pipe Diameter (inches)</i>	<i>Cable Diameter (mm)</i>	<i>Current Headings, ψ (deg)</i>	<i>Horizontal Velocity, u_x (m/s)</i>
20	150	0, 15, ..., 180	0.5
			1.0
			1.5

It is useful to visualize the vorticity and its development, to investigate the impact of the DEH cable relative to the current heading. Eleven iso-contours of vorticity from -2 to 2 are plotted for visualization purposes in Figure 5-2 to Figure 5-4. Figure 5-2 shows the vortex street when the current flow is acting at $\psi = 180^\circ$. It shows a narrow vortex street. The flow behaves like a streamlined body and the vortices do not reattach to the back surface of the pipeline.

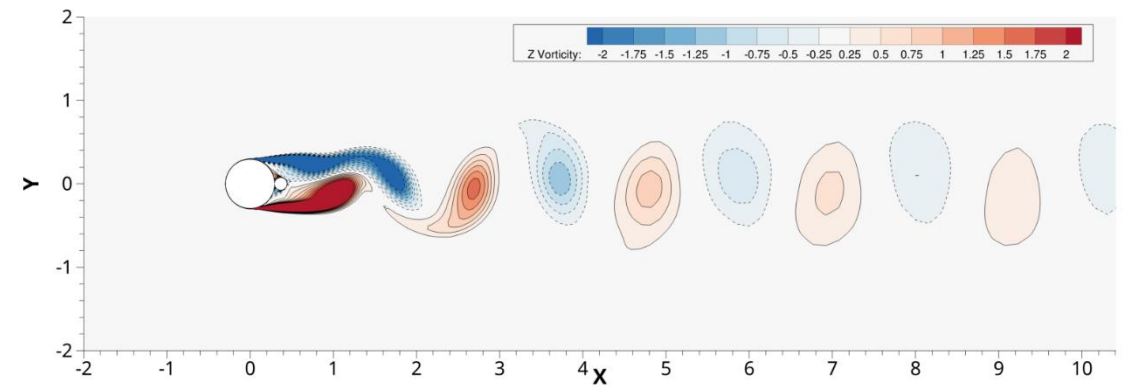


Figure 5-2 Vorticity contours at $\psi = 180^\circ$

When the current heading changes, so do the vortex shedding. At $\psi = 15^\circ$, the vortex shedding is similar to that of $\psi = 180^\circ$, see Figure 5-3. The vortex street remains narrow. The pipeline-DEH system behaves like a streamlined body and the vortices do not reattach to the back surface. However, it shows that the vortices are considerably closer to reattachment compared to Figure 5-2. Furthermore, it can be seen that the vorticity has a greater magnitude for $\psi = 15^\circ$ relative to $\psi = 180^\circ$.

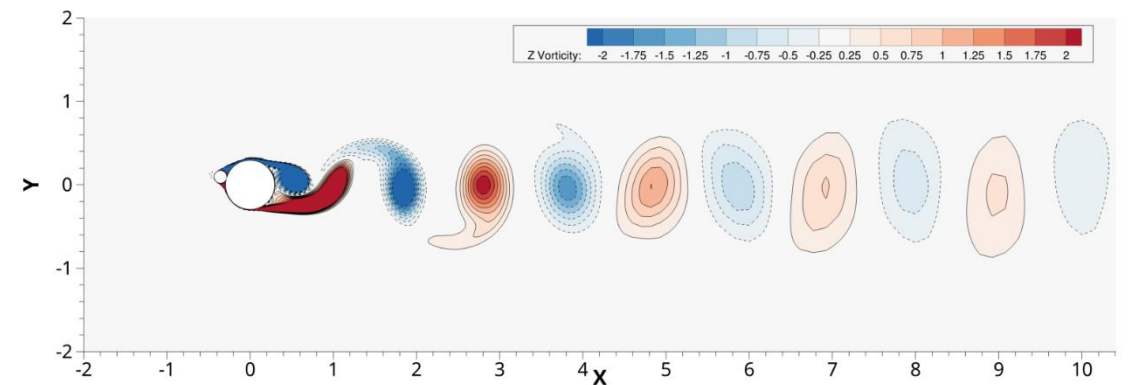


Figure 5-3 Vorticity contours at $\psi = 15^\circ$

When the current heading is changed $\psi = 90^\circ$, dramatic changes occur relative to the previous cases, see Figure 5-4. It shows a much wider vortex street where vortices reattach at the back surface of the pipeline-DEH-configuration, forming large negative pressure regions. It is, in this case, that the projected area will be largest, shown in Figure 5-4.

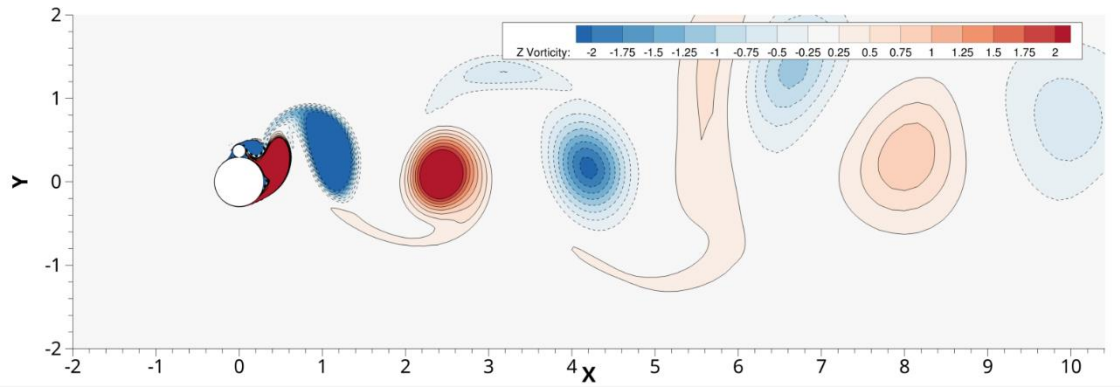


Figure 5-4 Vorticity contours at $\psi = 90^\circ$

From the figures above, it is apparent that the DEH cable configuration has a powerful effect on the vorticity generated by the structure in the flow. To investigate how the streamlines and pressure fields are affected, it is useful to visualize the flow- and pressure fields around the pipeline-DEH-configuration. Figure 5-5 shows the pressure contours in colour-code with the correlated streamlines at $\psi = 90^\circ$. It shows a high-pressure region on the front surface and a recirculation region in the concavity (the contact area of the cylinders), shown by “A”, in Figure 5-5. At the back of the configuration, recirculation bubbles occur, leading to high vorticity, which again results in a significant negative pressure zone development.

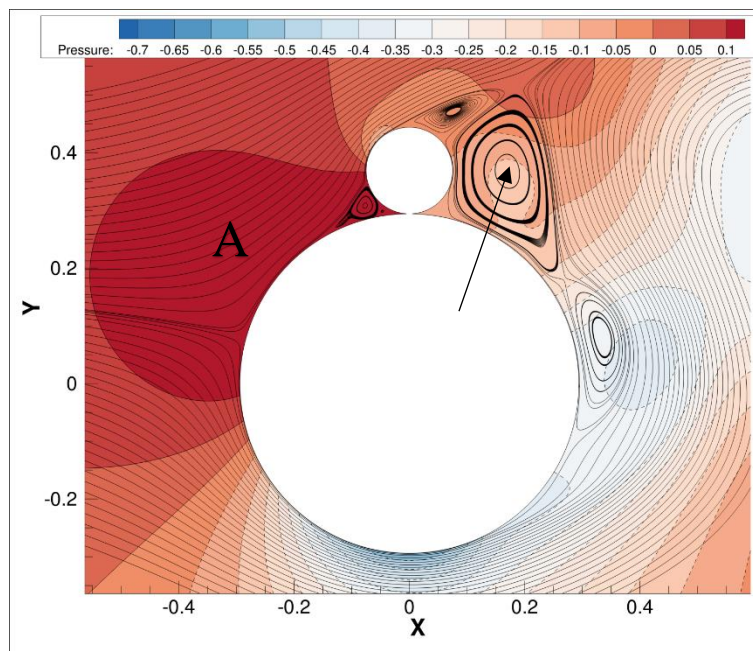


Figure 5-5 Pressure contours and streamlines at $\psi = 90^\circ$

When comparing the pressure contours and streamlines in the $\psi = 90^\circ$ -configuration (Figure 5-5) with those for the $\psi = 180^\circ$ -configuration (Figure 5-6), it is evident that the $\psi = 180^\circ$ -

configuration experiences considerably lower pressure difference between the front and back surfaces. Moreover, the recirculation zones appear further away downstream from the structure. The similarity between the pressure contours and streamlines for $\psi = 15^\circ$ compared to $\psi = 180^\circ$ is shown in Figure 5-7.

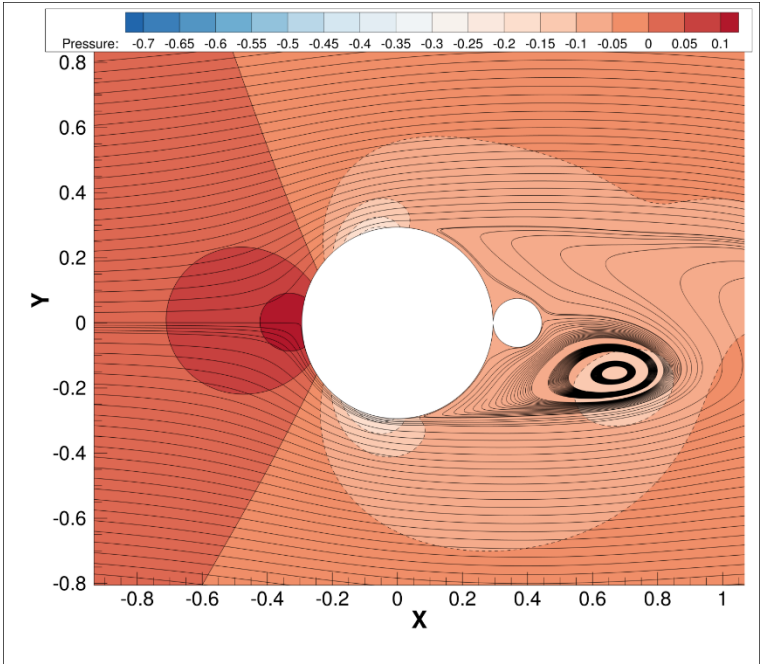


Figure 5-6 Pressure contours and streamlines at $\psi = 180^\circ$

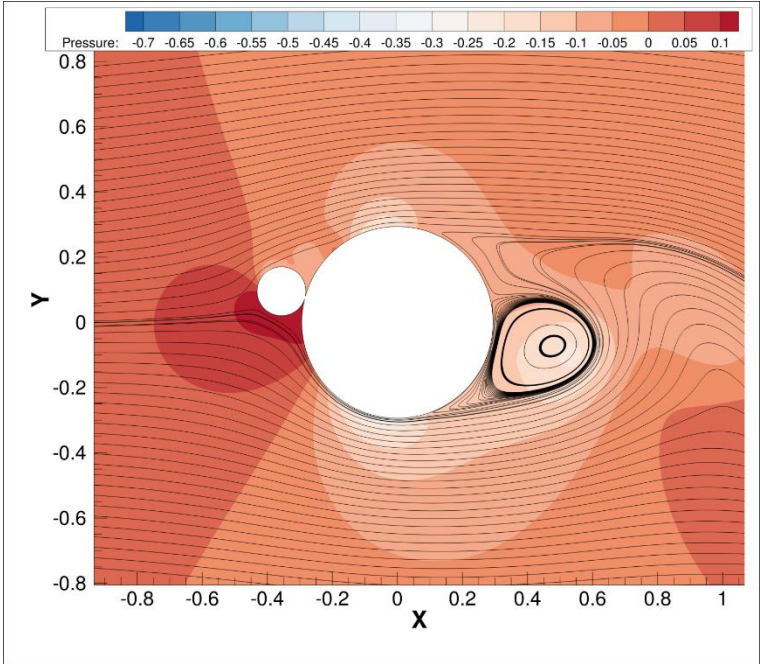


Figure 5-7 Pressure contours and streamlines at $\psi = 15^\circ$

The simulations show for a current heading of $\psi = 90^\circ$; there will be high pressure at the front, with a significant negative pressure at the back. The pressure difference results in the large experienced drag coefficients, as the drag has two components based on viscosity and pressure. This drag build-up is caused mainly by the pressure as can be seen in Figure 5-6 and Figure 5-7.

5.1.3 Applied Drag Coefficients

C_D is defined by the pipeline projected areas and flow velocities for both in-line and cross-flow directions. When investigating the case of a single pipeline, C_D is taken as a constant relative to ψ as the pipeline projected area is always identical. The change of the current velocity has a minor effect on C_D variation. Figure 5-8 shows that C_D has the same value for both current velocities of 1.5 m/s and 1.0 m/s, while an increase of C_D is experienced for a current velocity of 0.5 m/s.

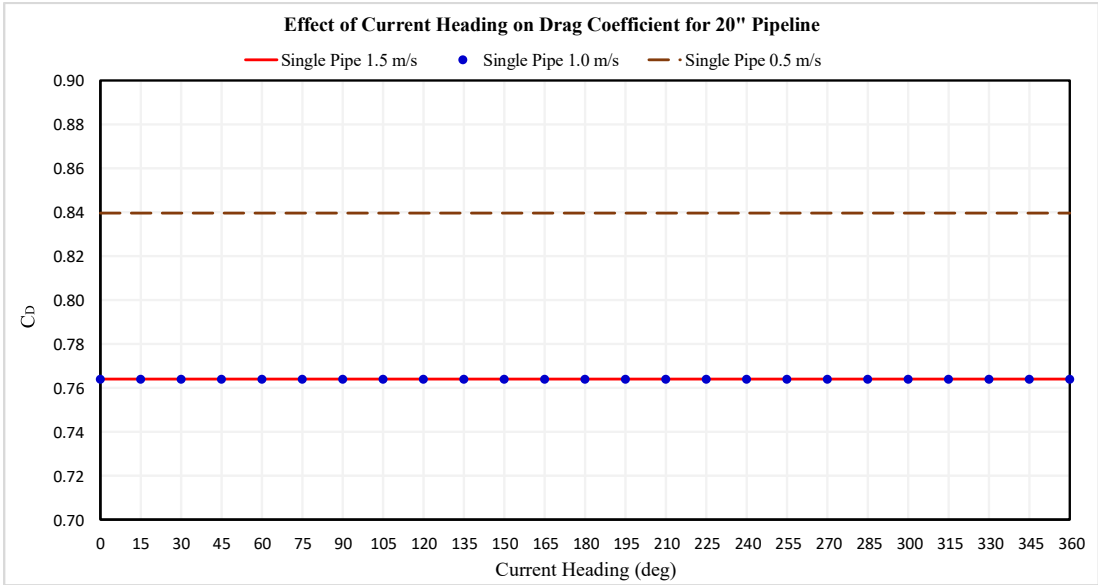


Figure 5-8 Effect of current heading on single pipe C_D

When investigating a pipeline with an attached DEH cable, C_D of the pipeline with piggyback will not be constant relative to current heading ψ . This is due to the variation in the projected area of the configuration. In Section 4.4, it is discussed how the C_D is implemented in the SIMLA-code. The pipeline-DEH-configuration consists of two parts: a singular pipeline with coating and a DEH-piggyback cable. Traditionally, the two parts have been assigned a constant C_D defined by the pipeline/cable diameter and fluid velocity. The C_D has been applied to the projected area to calculate the drag force, see Equation 5.2. All drag force values are in given in force per unit length, as shown in Section 4.4. When $\psi = 0^\circ$, the DEH cable is fully exposed to the current flow.

To calculate the drag force, $C_{D,Cable}$ is multiplied by the DEH cable diameter (projected area). The DEH cable partly covers the pipeline; thus, the $C_{D,Pipe}$ is multiplied with projected diameter shown in Equation 5.1. (Note: $A_{projected} = D_{projected}$, as F_D is given in the unit [N/m]).

$$D_{Pipe,projected} = D_{Pipe} - D_{Cable} \tag{5.1}$$

$$F_D = \frac{1}{2} \cdot \rho \cdot U^2 \cdot A_{projected} \cdot C_D \tag{5.2}$$

Such a procedure is not appropriate, as the DEH cable alters the flow-pattern around the pipeline. In Section 4.5, it is discussed how a CFD-model is built to investigate the response of the pipeline-DEH-configuration at different flow velocities. The drag forces are calculated in the CFD-model by integrating the dynamic pressure over the respective pipe- and cable section surfaces. The drag forces are obtained, equation 5.2 is applied, and solved for the drag coefficient; normalized by the diameter of the pipe or cable.

The CFD simulations are performed in time intervals from 100s to 150s. After the model is stable, C_D is extracted by time-averaging all C_D values from each time step. The time-averaged C_D for the pipeline and DEH cable relative to the current heading is shown in Figure 5-9. It can be seen that C_D for the pipeline and cable is symmetric about $\psi = 180^\circ$.

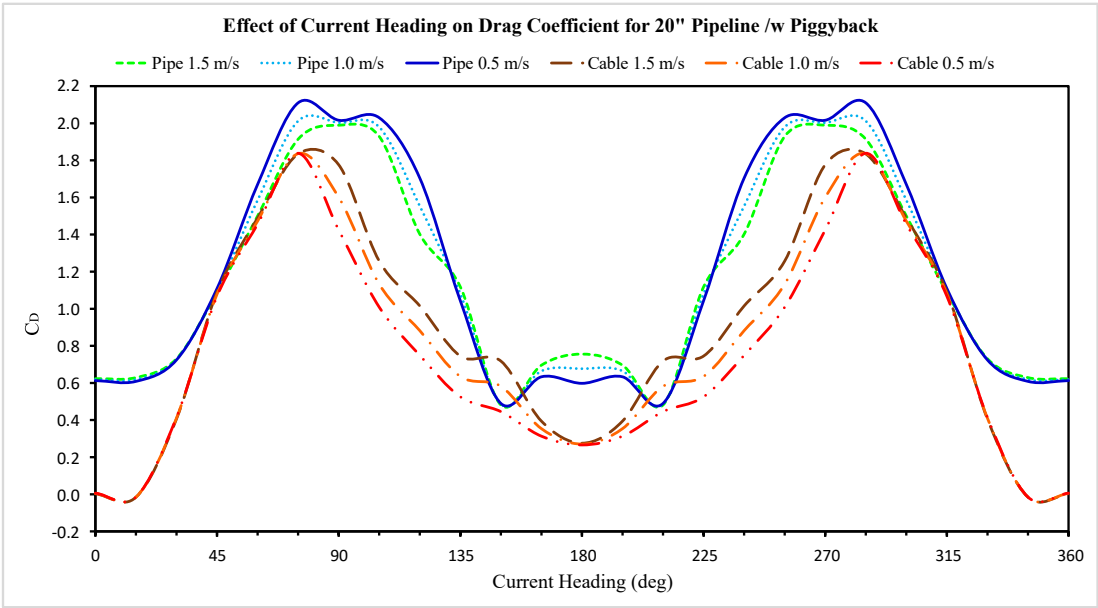


Figure 5-9 Effect of ψ on C_D for 20'' pipeline /w piggyback

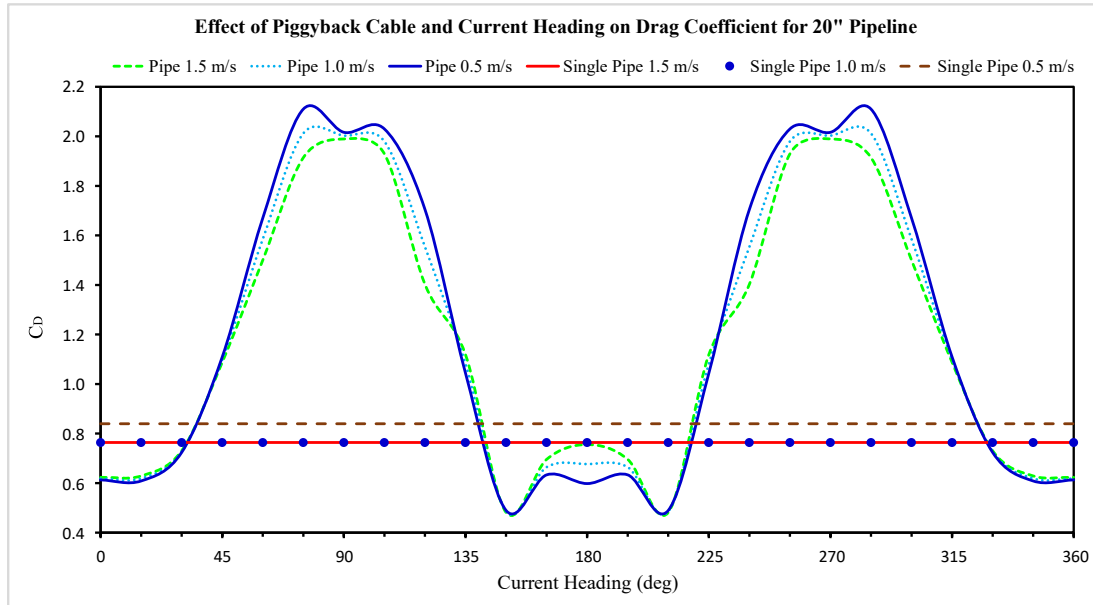


Figure 5-10. Effect of piggyback on pipeline C_D

The effect of the piggyback cable on C_D is shown in Figure 5-10. It can be observed that the variation of C_D is substantial, ranging in values from 0.6 to 2.1, for current headings in the range, $\psi = 60^\circ$ to $\psi = 120^\circ$. The C_D value is considerably larger for a pipeline-DEH-configuration compared to a single pipeline. It can be seen that the drag coefficient experienced by a single pipeline at $\psi = 90^\circ$ and velocity of 1.5 m/s is calculated to be 0.76, while a pipeline-DEH-configuration is calculated to have the drag coefficient of 1.99 under the same conditions. The increase is drastic (162%) and will lead to a corresponding increase in drag forces. Table 5-2 shows the increase/decrease in C_D under given current- heading and velocity.

Table 5-2 Effect of DEH cable on pipe drag coefficients

Current Velocity (m/s)	ψ (deg)	$C_D - \text{Single Pipe}$	$C_D - \text{Pipe /w DEH}$	Increase (%)
1.5	0	0.7640	0.6233	-18.4
	45		1.0879	42.4
	90		1.9893	160.4
	135		1.1183	46.4
	180		0.7555	-1.1

1.0	0	0.7639	0.6181	-19.1
	45		1.0986	43.8
	90		2.0028	162.2
	135		1.0809	41.5
	180		0.6768	-11.4
0.5	0	0.8396	0.6129	-27.
	45		1.1093	32.1
	90		2.0162	140.1
	135		1.0434	24.3
	180		0.5981	-28.8

An increase in the experienced drag forces can affect several key-parameters to the pipeline-DEH-configuration:

- Required top tension
- Pipeline drift from the surface to the seabed (XY-configuration)
- Sagbend stress and strain
- Pipeline-configuration curvature

5.2 Validation of Drag Coefficients Applied Through HYDROPRO

The present section investigates and verifies the applied directions used in the HYDROPRO-card for drag coefficients.

5.2.1 First Parameter Study

A parameter study of a single pipeline was performed to validate the drag coefficients, $C_{D, Pipe}$ and $C_{D, Cable}$. Two cases with different approaches defining the hydrodynamic forces are studied.

Case 1: Singular Pipeline with C_D defined in the ELPROP Card.

ELPROP is a command card that defines the element properties in SIMLA. This is done by defining the element type (PIPE) with its respective geometric features, such as structural- radius and thickness. Furthermore, drag coefficients are defined in both radial and tangential directions, where the added mass coefficients are neglected. Three scenarios are applied for the drag

coefficients: (1) C_D value only applied in the radial direction, (2) C_D value only applied in the tangential direction and (3) C_D values applied in both radial and tangential directions.

Case 2: Singular Pipeline with Body Elements.

By defining extra body elements along the pipeline to take the hydrodynamic force induced by the current, SIMLA opens the possibility with different drag coefficients relative to current heading and pipeline inclination. This is done using the HYDROPRO card. The body elements which are massless have identical geometry as the pipeline elements to ensure that the induced hydrodynamic load will be equal to case 1. The nodes of body elements are fully constrained to the pipeline nodes to transfer the hydrodynamic load from body element to pipeline.

In the ELPROP card, all drag coefficients are set to zero, and the HYDROPRO card is used to define drag coefficients. The drag coefficients are defined in the local in the translational directions surge, sway, and heave, for the respective current heading and inclination angles.

Three scenarios are investigated: (1) C_D value only applied in sway direction, (2) C_D value only applied in heave direction and (3) C_D values applied in both sway and heave directions. Other input parameters, such as pipeline material, wall thickness, and current velocity are kept equal for both cases. The parameters used the simulations are shown in Table 5-3. A comparison of the different case outputs, shows that the results are the same with negligible deviation (0.021%), see Table 5-4. The parameter study verifies the application of body elements to account for hydrodynamic loads is viable to use in SIMLA.

Table 5-3 Pipeline properties

<i>Pipeline radius (m)</i>	<i>Pipeline thickness (m)</i>	<i>Submerged Weight (kg/m)</i>	<i>Current velocity (m/s)</i>
0.254	0.040	253.710	1.000

Table 5-4 First parameter study simulation results

<i>Utilized card command</i>	<i>Current Heading (degrees)</i>	σ_{xx} (MPa)
ELPROP	0	8.50E+03
ELPROP	90	3.74E+05
HYDROPRO	0	8.46E+03
HYDROPRO	90	3.82E+05

5.2.2 Second Parameter Study

A second parameter study for a 20” pipeline without piggyback was performed to verify the current heading direction used in the body element approach. The current velocity profile, material properties and C_D —matrices used in the final simulations are applied in the second parameter study. The results of the simulations are shown in Table 5-5.

- The case with a current heading of 0 degrees has the highest top tension as the current load and lay operation works in the same direction
- The case with a current heading of 180 degrees has the smallest top tension, as the current flow and lay operation work in opposite directions. This is due to the normal component of the hydrodynamic current induced force, which works in a positive upward direction on the pipeline, see Figure 5-17.

Table 5-5 Second parameter study simulation results

<i>Current Heading (degrees)</i>	<i>SIGMA-XX (kN/m²)</i>		<i>Top Tension (kN)</i>	<i>Bending Moment, Sagbend (kN · m)</i>
0	-172462	131498	6930	-561
45	-172155	128206	6747	-559
90	-171923	127332	6698	-558
135	-171686	126462	6650	-557
180	-171475	123166	6466	-555

5.3 The Results for Analysis Matrix

This section will discuss the results of the simulations listed in the analysis matrix.

5.3.1 XY – Configuration

The translational pipeline response is investigated in the XY-plane. Table 5-6 summarizes the translational deviation in y-direction experienced by the pipeline from the surface to the seabed. All “pipeline drift” investigations performed in the present study are the pipeline y-coordinate relative to the global y-axis, where the vessel is located at $y = 0$. It can be seen that the most significant drifting motion for a single-pipeline-configuration is 27.8 meters for the 20” pipeline at $\psi = 90^\circ$. Similarly, the most significant drifting motion for a pipeline-DEH-configuration is

74.7 meters for the 20” pipeline at $\psi = 90^\circ$. It is interesting to note that by attaching a DEH cable with 1/3rd of the diameter compared pipeline diameter, the drifting motion is more than doubled.

Table 5-6 Pipeline drift from surface to seabed

<i>Pipeline Diameter (inch)</i>	<i>Cable Diameter (mm)</i>	ψ (deg)	<i>XY-deviation at 491s (m)</i>	<i>Maximum XY-deviation (m)</i>
20	No DEH	0	0.0	0.0
		45	23.6	24.6
		90	25.1	27.8
		135	23.7	25.7
		180	0.0	0.0
28	No DEH	0	0.0	0.0
		45	14.8	16.7
		90	16.0	18.1
		135	14.8	16.7
		180	0.0	0.0
30	No DEH	0	0.0	0.0
		45	13.9	15.7
		90	15.1	17.1
		135	13.9	15.8
		180	0.0	0.0
20	150	0	0.0	0.0
		45	44.0	50.8
		90	66.5	74.7
		135	51.5	62.0
		180	0.0	0.0
28	210	0	0.0	0.0
		45	34.3	39.0
		90	47.2	52.8
		135	39.1	44.9
		180	0.0	0.0
30	225	0	0.0	0.0
		45	32.9	37.3
		90	44.8	50.1
		135	37.2	42.7
		180	0.0	0.0

A current acting perpendicular to the pipeline will experience the largest projected area. Therefore, the drag force experienced at $\psi = 90^\circ$ and $\psi = 270^\circ$ will be the largest current induced load experienced by the pipeline-configuration, as the pipeline is symmetrical. Due to pipeline symmetry, simulations are performed from $\psi = 0^\circ$ to $\psi = 180^\circ$ with 15 degrees intervals.

Figure 5-11 shows the translational movement in the XY-plane when the installation is exposed to a current load acting at $\psi = 90^\circ$. The plot is extracted at time step 491s for each case; at this stage, the translational movement is stabilized. It can be observed that for a 20" pipeline-DEH-configuration the translation in the y-direction is increased by over 260% when comparing it to the 20" single-pipeline-configuration.

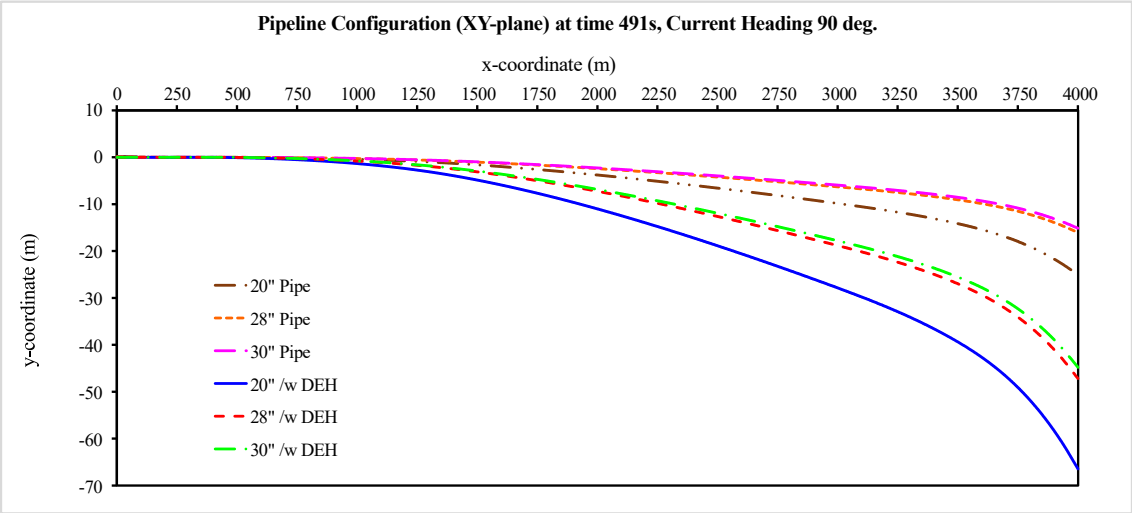


Figure 5-11. XY-configuration at $\psi = 90^\circ$, time = 491s

The maximum drift for the different pipeline configurations did not occur at the same time step. Figure 5-12 shows the highest translational motions for each configuration during the pipelaying simulation.

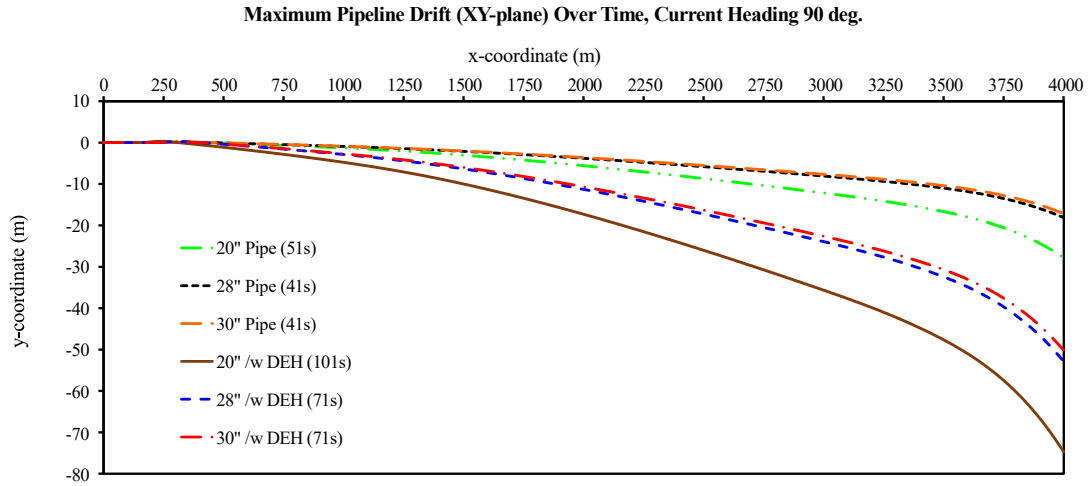


Figure 5-12. Maximum XY-configuration at $\psi = 90^\circ$

It can be observed that the translation in the y-direction for 20" pipeline with DEH cable is 74.5 meters, which is an increase of 8 meters compared to Figure 5-11.

Table 5-7 shows the effect of different current headings for the single-pipeline and pipeline-DEH-configurations. The highest translation is experienced by the 20" pipeline-DEH-configuration. At current headings of $\psi = 0^\circ$ and $\psi = 180^\circ$ the translation in y-direction is negligible. For the pipelines with diameters 28" and 30", the same trend is observed.

It is interesting to note that the translation will be significantly larger at $\psi = 135^\circ$ compared to $\psi = 45^\circ$. These angles will experience the same projected area, but the DEH cable interferes with the flow differently. Figure 5-13 and Figure 5-14 shows the streamlines and pressure fields for the scenarios where $\psi = 45^\circ$ and $\psi = 135^\circ$ respectively. It is interesting to note that for $\psi = 135^\circ$, at the back of the configuration recirculation bubbles occur, leading to high vorticity which again results in a large negative pressure zone. This results in a larger pressure difference for $\psi = 135^\circ$ compared to at $\psi = 45^\circ$. Which leads to the larger top tension for $\psi = 135^\circ$ compared to $\psi = 45^\circ$ observed in Figure 5-23

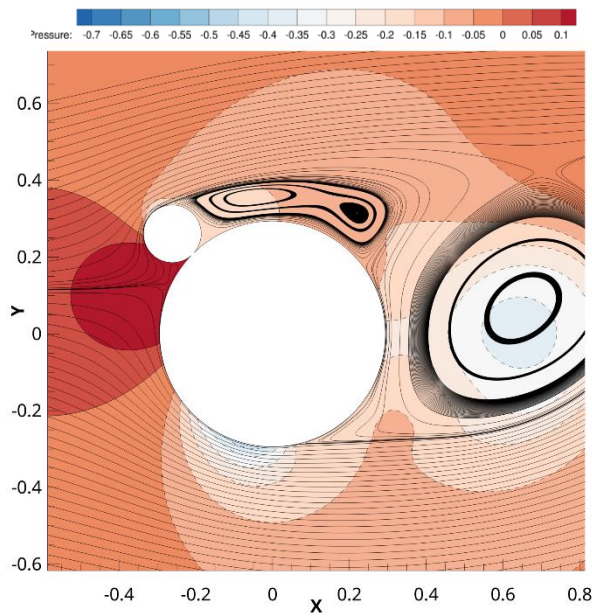


Figure 5-13 Streamlines and pressure fields at $\psi = 45^\circ$

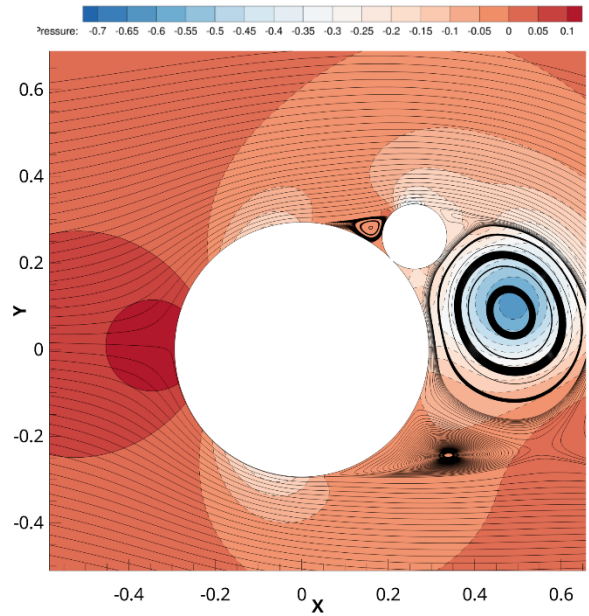


Figure 5-14 Streamlines and pressure fields at $\psi = 135^\circ$

All pipeline-configurations experience the highest translation at $\psi = 90^\circ$, at the same time the translational increase in percent will increase with the pipeline diameter increase, seen in Table 5-7. The large displacements discussed in this section can be critical both in terms of pipeline layability and routing.

Table 5-7. Effect of DEH and ψ on pipeline drift.

Pipeline Diameter (inch)	ψ (deg)	Maximum XY-displacement (m)		Increase (%)
		Single Pipe	Pipeline-DEH-configuration	
20	45	24.6	50.8	106.5
	90	27.8	74.7	168.7
	135	25.7	62.0	141.2
28	45	16.7	39.0	133.5
	90	18.1	52.8	191.7
	135	16.7	44.9	168.9
30	45	15.7	37.3	137.6
	90	17.1	50.1	193.0
	135	15.8	42.7	170.3

5.3.2 Top Tension

Top tension is described to be the most limiting factor in a pipelaying operation and will be determined by the vessel top tension capacity. The present section investigates how the attachment of a DEH cable affects the required top tension.

Table 5-8 shows the time-averaged- and maximum top tension requirements obtained from the SIMLA-simulations. From the table, it can be seen that the maximum top tension for the single-pipeline-configurations are largest at $\psi = 0^\circ$, contrary to the pipeline-DEH-configurations where the maximum top tension is largest at $\psi = 45^\circ$ and $\psi = 90^\circ$. It is interesting to note that the 20''- and 28'' pipeline-DEH-configuration experience the maximum top tension at $\psi = 90^\circ$, while the 30'' pipeline-DEH-configuration experience the highest top tension at $\psi = 45^\circ$. This is due to a combination of dominant body- and current forces, where the 30''-configuration weight is more dominant compared to that of the 20'' and 28''.

Table 5-8. Effect of current heading on required top tension

<i>Pipeline Diameter (inch)</i>	<i>Cable Diameter (mm)</i>	ψ (deg)	<i>Time Averaged Top Tension (kN)</i>	<i>Maximum Top Tension (kN)</i>
20	No DEH	0	6930	6939
		45	6753	6756
		90	6708	6712
		135	6659	6664
		180	6470	6500
28	No DEH	0	14493	14494
		45	14245	14249
		90	14184	14189
		135	14118	14125
		180	14186	14196
30	No DEH	0	16363	16364
		45	16093	16102
		90	16019	16038
		135	15964	15970
		180	16035	16048
20	150	0	7481	7489
		45	7571	7689
		90	7627	7931
		135	7532	7839
		180	7235	7250

28	210	0	15552	15568
		45	15546	15624
		90	15456	15629
		135	15269	15437
		180	15218	15243
30	225	0	17576	17595
		45	17550	17624
		90	17425	17599
		135	17236	17389
		180	17218	17249

The maximum top tension is further investigated in Figure 5-15 for the for different pipeline dimensions in the interval $\psi \in [0, 180]$. It can be observed that the trend-lines of the top tension changes when the DEH cable is introduced. A single pipeline experiences a continuous decline in required top tension from $\psi = 0^\circ$ to $\psi = 180^\circ$. This is due to the current load changes from acting in the same direction as the laying operation, to acting in the opposite direction of the laying operation, from $\psi = 0^\circ$ to $\psi = 180^\circ$ respectively.

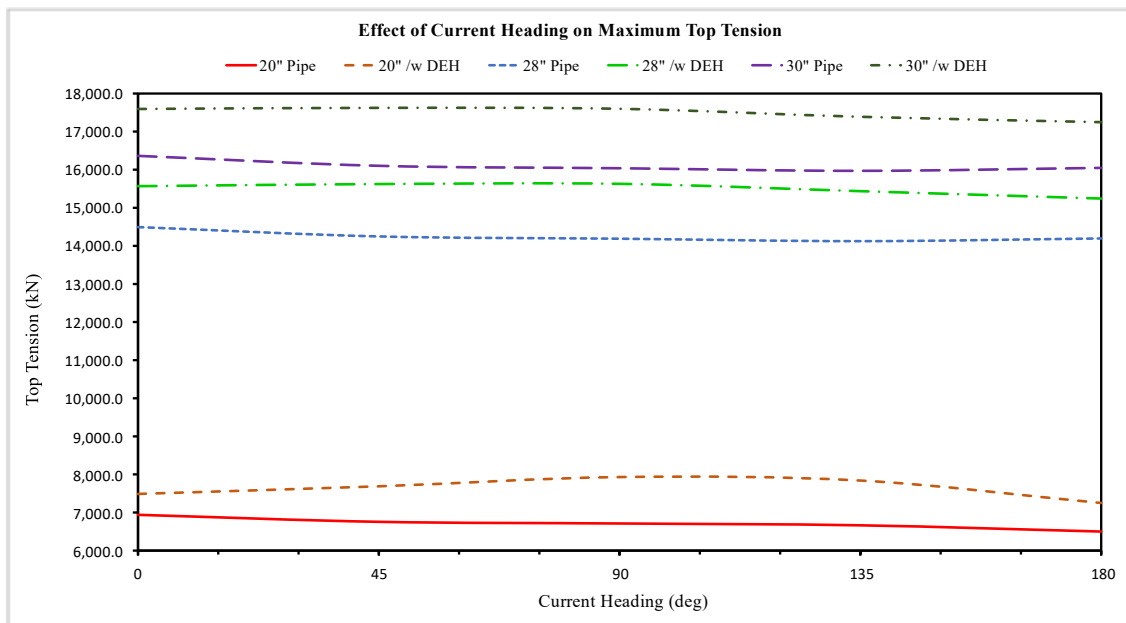


Figure 5-15. Effect of current heading on maximum top tension

The continuous decline in required top tension for the single-pipeline-configurations is explained in Figure 5-16 and Figure 5-17 which shows how the normal component (F_3) of the current force (F_{current}) changes from a downward force to a lifting force, for $\psi = 0^\circ$ and $\psi = 180^\circ$ respectively, on a pipeline-DEH-configuration.

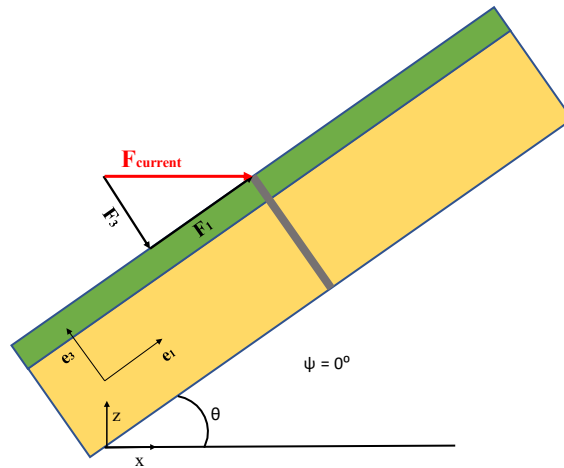


Figure 5-16. Current force components acting on the pipeline-DEH-configuration, at $\psi = 0^\circ$

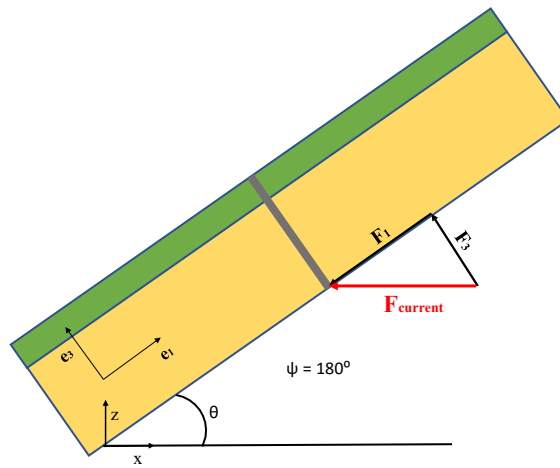


Figure 5-17 Current force components acting on the pipeline-DEH-configuration, at $\psi = 180^\circ$

Furthermore, the effect of current heading on the maximum top tension on the 20" pipeline with and without piggyback is detailed in Figure 5-18. It shows that the single-pipeline-configuration experience a continuous decline in top tension from $\psi = 0^\circ$ to $\psi = 180^\circ$, while the pipeline-DEH-configuration experience an inclination in top tension from $\psi = 0^\circ$ to $\psi = 90^\circ$ and then a reduction to $\psi = 180^\circ$. Some of the top tension increase is due to the DEH cable weight contribution to the overall weight. However, Figure 5-18 proves that the drag force affects the required top tension, as the required top tension is increased when the projected area is increased, from $\psi = 0^\circ$ to $\psi = 90^\circ$.

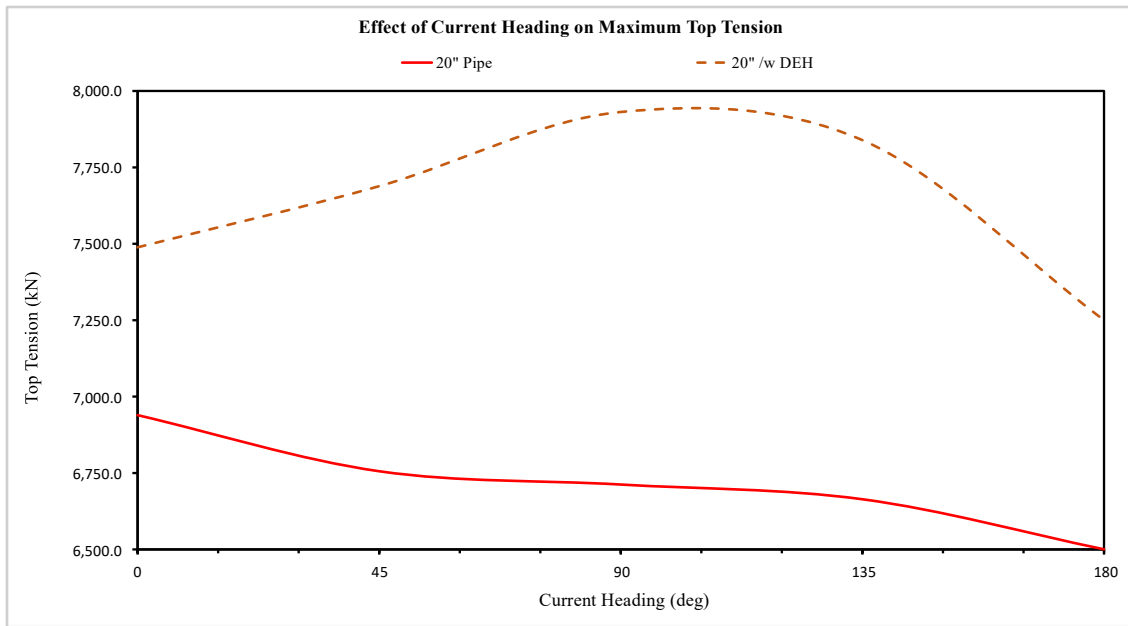


Figure 5-18. Detailed view of the effect of current heading on maximum top tension

Table 5-9 shows the percentage increase in top tension for the single-pipeline-configurations relative to the pipeline-DEH-configurations. It shows that the current induced drag forces affect the 20" pipeline-configurations considerably more than for the 28"- and 30" pipeline-configurations, likely due to the drastic increase in pipeline weight for the larger diameter pipelines. The weight increase results in a more dominant role for the gravitational force compared to the drag force.

Table 5-9 Effect of DEH cable and current heading on top tension

Pipeline Diameter (inch)	Ψ (deg)	Maximum Top Tension (kN)		Increase (%)
		Single Pipe	Pipe-DEH	
20"	0	6939	7488	7.9
	45	6756	7688	13.8
	90	6712	7931	18.2
	135	6664	7839	17.6
	180	6500	7250	11.5
28"	0	14493	15567	7.4
	45	14245	15631	9.7
	90	14184	15629	10.2
	135	14118	15437	9.3
	180	14186	15242	7.4

30''	0	16363	17594	7.5
	45	16093	17623	9.5
	90	16019	17599	9.9
	135	15964	17388	8.9
	180	16035	17249	7.6

Single pipelines experience a stable top tension requirement, while the pipeline-DEH-configurations experience a cyclic top tension requirement. The cyclic nature of the top tension requirement for the pipeline-DEH-configurations is shown in Figure 5-19 to Figure 5-21.

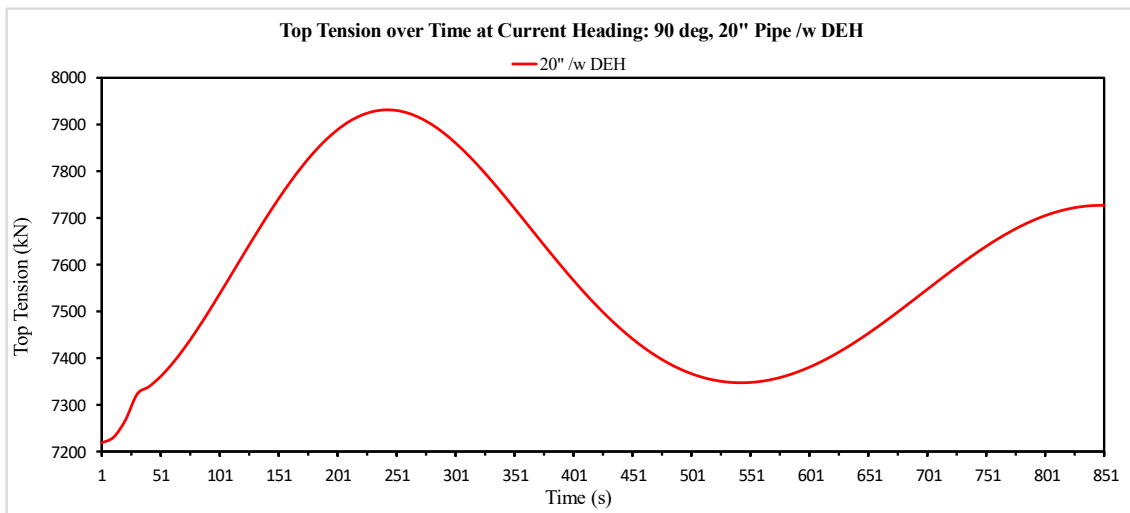


Figure 5-19. Top tension over time at $\psi = 90^\circ$, 20'' /w DEH

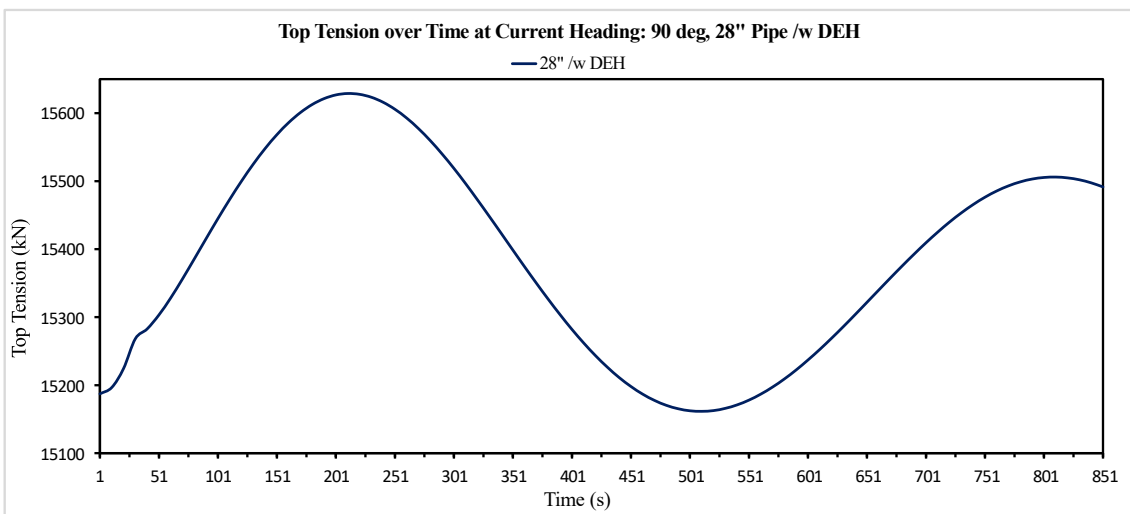


Figure 5-20. Top tension over time at $\psi = 90^\circ$, 28'' /w DEH

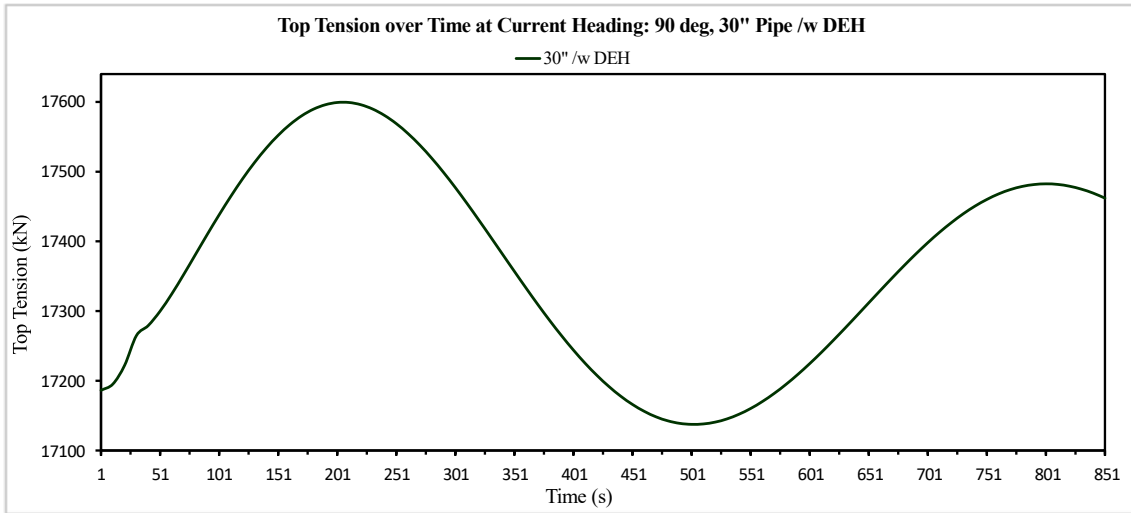


Figure 5-21. Top tension over time at $\psi = 90^\circ$, 30” /w DEH

In Figure 5-22 to Figure 5-27 the time-development of the top tension for 20”, 28” and 30” pipeline both with and without a DEH cable is shown. It is interesting to note how significantly the trend of the top tension requirements are affected by the attachment of a DEH cable.

Figure 5-22 and Figure 5-23 shows the effect of the current heading on the required top tension for a 20” single-pipeline and a 20” pipeline-DEH-configuration respectively. It can be seen how the 20” single-pipeline-configuration experience the largest top tension at $\psi = 0^\circ$ due to the normal component of the current induced drag force, see Figure 5-16. The 20” pipeline-DEH-configuration experience the largest top tension at $\psi = 90^\circ$ as the projected area is largest at this heading.

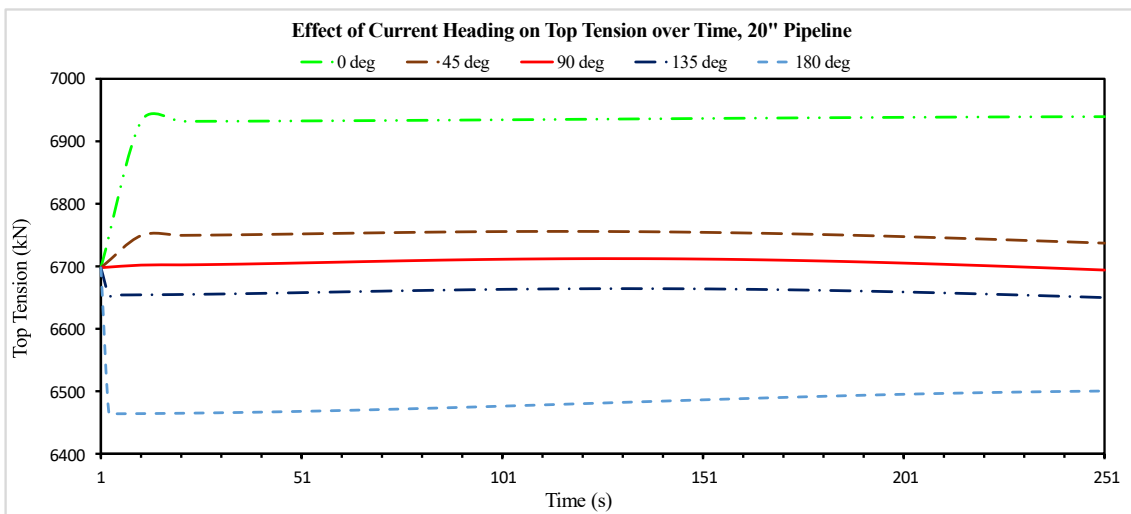


Figure 5-22. Effect of current heading on top tension for a 20” Pipeline

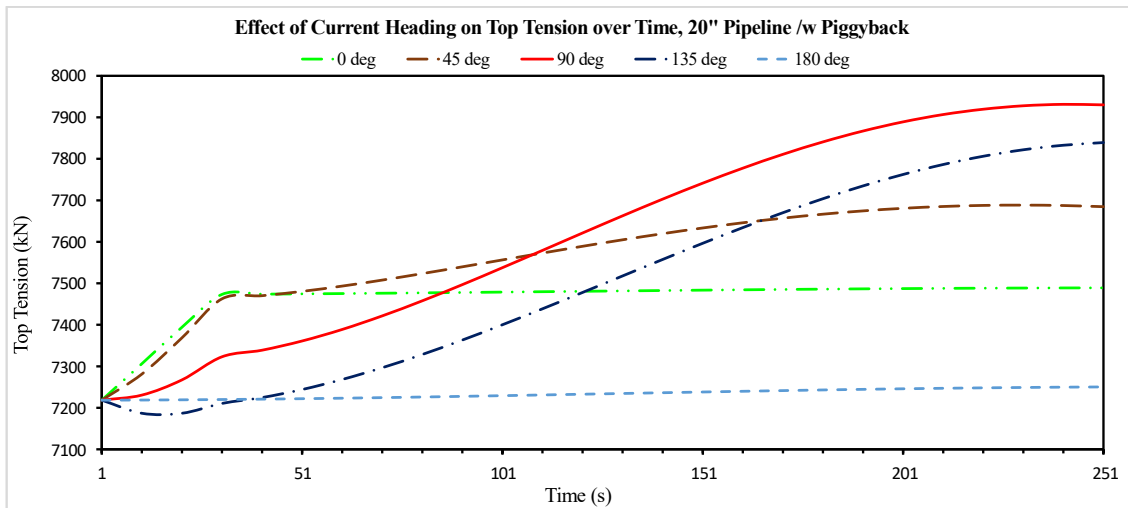


Figure 5-23 Effect of current heading on top tension for a 20'' Pipeline /w DEH

By comparing the two figures above, it can be seen that the top tension trend is the same for $\psi = 0^\circ$ and $\psi = 180^\circ$. However, the trend changes at $\psi = 45^\circ$, $\psi = 90^\circ$ and $\psi = 135^\circ$. This is because of the increased projected area and drag forces discussed in Section 5.1. In addition, it can be seen that the top tension requirement for the 20'' pipeline-DEH-configuration is almost 100 kN (1.32%) larger at $\psi = 135^\circ$ relative to at $\psi = 45^\circ$. The nature of this effect was discussed in Section 5.3.1 and shown in Figure 5-13 and Figure 5-14.

Figure 5-24 and Figure 5-25 shows the effect of current heading on the top tension for a 28'' single-pipeline and 28'' pipeline-DEH-configuration respectively. It can be that the 28'' single-pipeline-configuration experience the most significant top tension at $\psi = 0^\circ$ due to the normal component of the current induced load. The 28'' pipeline-DEH-configuration experience the largest top tension at $\psi = 90^\circ$ as the projected area is largest at this angle, resulting in a more dominating role the drag force. However, the difference is not as evident as in Figure 5-23 and Figure 5-24 due to the drastic increase in pipeline cross-sectional weight.

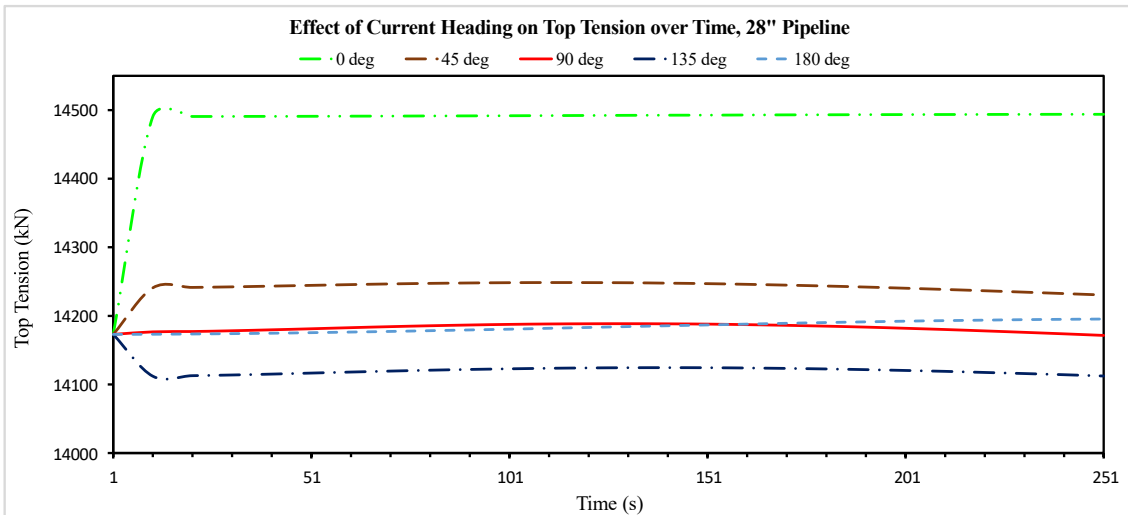


Figure 5-24 Effect of current heading on top tension for a 28'' Pipeline

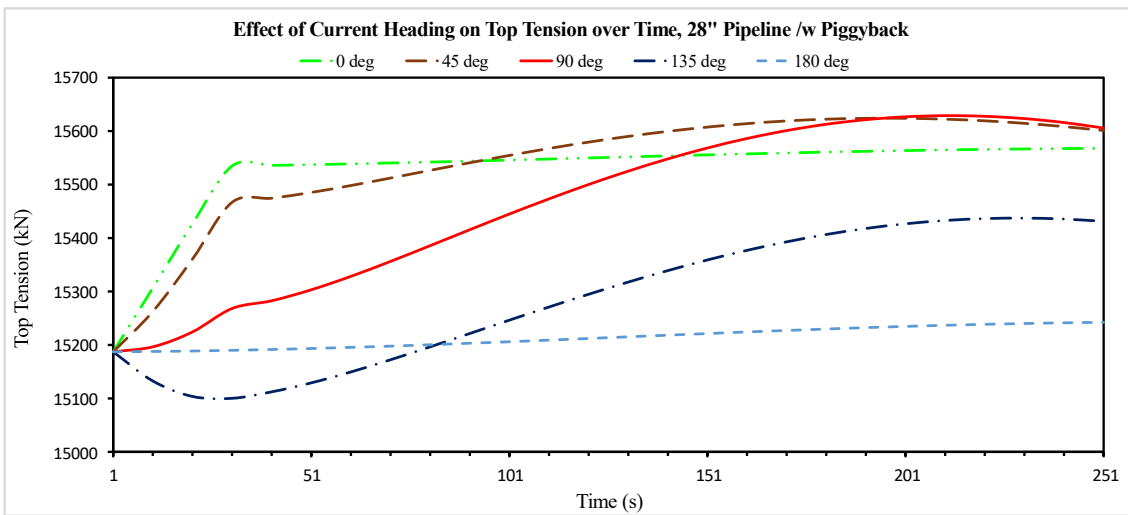


Figure 5-25 Effect of current heading on top tension for a 28'' Pipeline /w DEH

By comparing Figure 5-24 and Figure 5-25, it can be seen that the top tension trend is the same for $\psi = 0^\circ$ and $\psi = 180^\circ$, while the trend changes for $\psi = 45^\circ$, $\psi = 90^\circ$ and $\psi = 135^\circ$. It can be seen that the top tension requirement is almost equal at $\psi = 45^\circ$ and $\psi = 90^\circ$ for the pipeline-DEH-configurations, while at $\psi = 135^\circ$, a lower top tension is required. The reduction in required top tension at $\psi = 135^\circ$ is due to the reduction in magnitude of the normal component of the current load. In addition, the larger diameter will decrease the recirculation zone behind the pipeline-DEH-configuration, as the Reynolds number is increased. This means that the load induced by the pressure difference at the front and back of the pipeline-DEH-configuration is not as significant compared to forces such as the pipeline weight.

Figure 5-26 and Figure 5-27 shows the effect of current heading on the top tension for a 30” single-pipeline and 30” pipeline-DEH-configuration respectively. It can be seen that the 30” single-pipeline-configuration experiences the largest top tension at $\psi = 0^\circ$. However, the most significant top tension for the pipeline-DEH-configuration is experienced at $\psi = 45^\circ$. This is due to effects discussed for the 28” pipeline-DEH-configuration, where the pipeline weight and the normal component of the current induced force are the dominant loads.

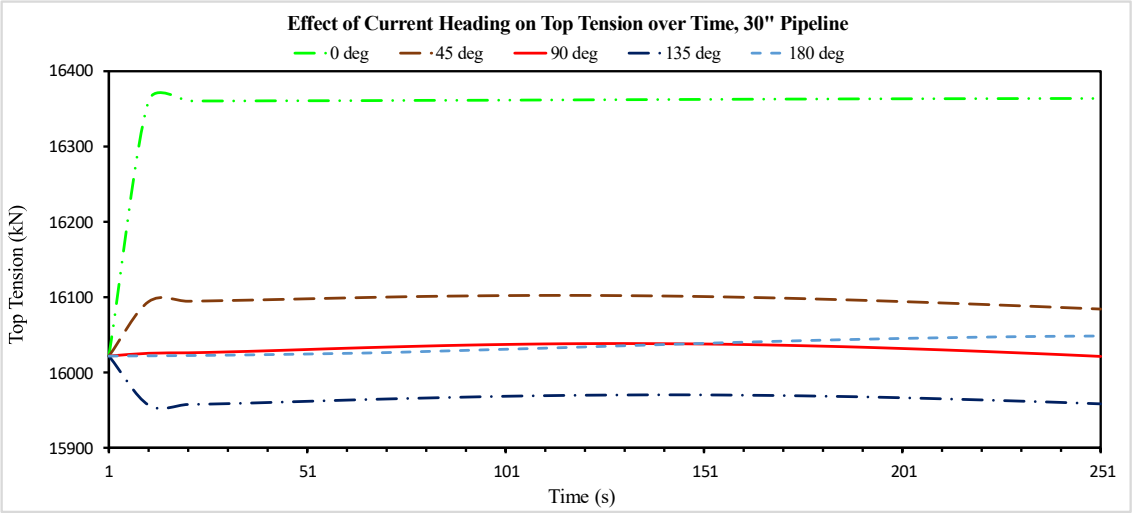


Figure 5-26 Effect of current heading on top tension for a 30” Pipeline

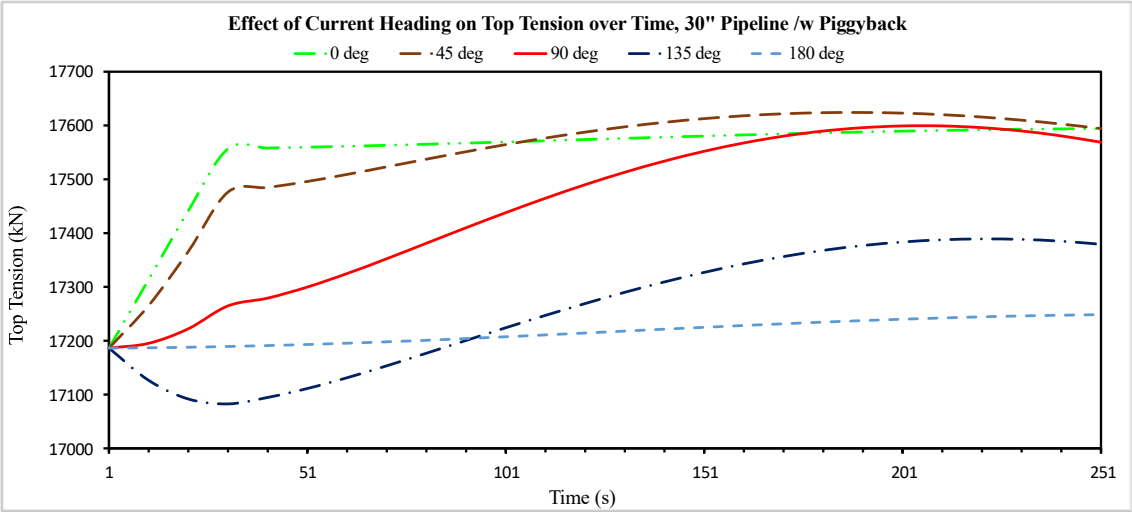


Figure 5-27 Effect of current heading on top tension for a 30” Pipeline /w DEH

The direct impact of the current induced loads is also investigated. The top tension requirements discussed above are compared to the top tension requirements when the effect of current induced loads is neglected, see Table 5-10. It is interesting to note the drastic increase in required top tension for a 20” pipeline-DEH-configuration by introducing current loads.

Table 5-10 Effect of current on top tension requirement

<i>Configuration Specification</i>	ψ (deg)	<i>Maximum Top Tension (kN)</i>		<i>Increase (%)</i>
		<i>No Current</i>	<i>Current</i>	
20”	0	6720	6939.4	3.26
	45		6755.8	0.53
	90		6712.3	-0.12
	135		6664.2	-0.83
	180		6500.4	-3.27
28”	0	14195	14493	2.10
	45		14245	0.35
	90		14184	-0.08
	135		14118	-0.55
	180		14186	-0.07
30”	0	16046	16363	1.98
	45		16093	0.30
	90		16019	-0.17
	135		15964	-0.51
	180		16035	-0.07
20” /w DEH	0	7250	7488.5	3.29
	45		7688.5	6.04
	90		7931.3	9.39
	135		7839.2	8.12
	180		7250.3	0.00
28” /w DEH	0	15242	15567	2.13
	45		15627	2.52
	90		15629	2.54
	135		15437	1.28
	180		15242	0.00

30" /w DEH	0	17247	17594	2.01
	45		17623	2.18
	90		17599	2.04
	135		17388	0.82
	180		17249	0.01

When comparing the required top tension for the different scenarios, it can be seen that the piggyback contribution is more complicated than merely the weight addition. For the 20" pipeline-DEH-configuration the required top tension is increased by almost 10 percent. This trend is reduced for the larger diameter pipelines as the axial- and bending stiffness is increased.

5.3.3 Sagbend Stress and Strain

In Section 3.3 a design moment is defined through "Design Load Effects". The design load effect is defined by DNV-OS-F101 to account for all cross-sectional loads which can arise due to an applied load. The relevant load effects for the simulations are discussed in Section 3.1.1 and are assumed to be environmental (current induced loads) and functional (pipeline weight, soil reaction forces, and hydrostatic pressure). It is crucial to ensure that the designed pipeline-model can withstand all moments induced by the relevant load effects. The design moment is defined by Equation 5.3 and consists of two moments: moment induced by functional loads and moment induced by environmental loads. All applied constant values are summarized in Table 3-17.

$$M_{Sd} = M_F \cdot \gamma_F \cdot \gamma_C + M_E \cdot \gamma_E \quad (5.3)$$

The stress distribution along the pipeline is supplied through SIMLA-simulations, and the equation can be rewritten:

$$M_{Sd}(t) = \frac{\sigma_F(t)}{y_{max}} I_{xx} \cdot \gamma_F \cdot \gamma_C + \frac{\sigma_E(t)}{y_{max}} I_{xx} \cdot \gamma_E \quad (5.4)$$

$$M_{Sd}(t) = \frac{I_{xx}}{y_{max}} (\sigma_F(t) \cdot \gamma_F \cdot \gamma_C + \sigma_E(t) \cdot \gamma_E) \quad (5.5)$$

Six extra simulations were performed for the different dimensional parameters for a single pipeline and a pipeline-DEH-configuration. The current load was neglected, making all loads functional.

Table 5-11 lists the largest compressional stress and strain experienced in the sagbend region for both a single pipeline and pipeline-DEH-configuration at different dimensions.

Table 5-11. Stress and strain in sagbend, no current

<i>Pipeline Configuration</i>	<i>Compressional Stress in Sagbend (MPa)</i>	<i>Compression Strain, Sagbend (Pipe)</i>	<i>Compression Strain Sagbend (Cable)</i>
20" Pipe	-170.12	-0.00082	-
28" Pipe	-197.14	-0.00095	-
30" Pipe	-205.90	-0.00100	-
20" /w DEH	-167.20	-0.00082	-0.00343
28" /w DEH	-191.44	-0.00093	-0.00356
30" /w DEH	-199.68	-0.00097	-0.00360

From these values, the functional moment can be calculated. The environmental moment is extracted by evaluating the compressional stress for the pipeline and pipeline-DEH-configuration at different current headings, ψ . The difference in the total load effect relative to the functional load effect is the environmental load effect. Table 5-12 lists the largest compressional stress and strain experienced in the sagbend region for both a single pipeline and pipeline-DEH-configuration at different dimensions exposed to a current load at heading ψ .

Table 5-12. Effect of current on stress and strain in sagbend

<i>Pipeline Configuration</i>	<i>Current Heading (deg)</i>	<i>Compression Stress, Sagbend (MPa)</i>	<i>Compression Strain, Sagbend (Pipe)</i>	<i>Compression Strain, Sagbend (Cable)</i>
20" Pipe	0	-172.24	-0.00084	-
	45	-171.75	-0.00083	-
	90	-171.29	-0.00083	-
	135	-170.62	-0.00083	-
	180	-171.10	-0.00083	-
28" Pipe	0	-198.63	-0.00096	-
	45	-198.15	-0.00096	-
	90	-197.79	-0.00096	-
	135	-197.62	-0.00096	-
	180	-197.96	-0.00096	-

30" Pipe	0	-207.36	-0.00101	-
	45	-206.89	-0.00100	-
	90	-206.54	-0.00100	-
	135	-206.36	-0.00100	-
	180	-206.32	-0.00100	-
20" /w DEH	0	-168.92	-0.00082	-0.00353
	45	-163.35	-0.00079	-0.00327
	90	-153.58	-0.00075	-0.00300
	135	-153.69	-0.00075	-0.00301
	180	-168.87	-0.00082	-0.00352
28" /w DEH	0	-194.12	-0.00094	-0.00361
	45	-190.44	-0.00094	-0.00352
	90	-187.17	-0.00091	-0.00342
	135	-187.53	-0.00091	-0.00344
	180	-193.41	-0.00094	-0.00360
30" /w DEH	0	-202.85	-0.00098	-0.00365
	45	-198.71	-0.00096	-0.00357
	90	-195.91	-0.00095	-0.00349
	135	-196.24	-0.00095	-0.00350
	180	-201.83	-0.00098	-0.00363

From Table 5-11 and Table 5-12 it is evident that the current does not affect the sagbend stress in any significant way. Table 5-13 summarize the percental increase/decrease in sagbend stress by introducing a current to the laying operation. It shows that the largest percental increase in sagbend stress is 1.59 % for a 30" pipeline-DEH-configuration at $\psi = 0^\circ$. It is evident that the design moment will be dominated by the functional loads with a negligible effect of environmental loading. It can also be observed the drastic reduction in sagbend stress for the 20" pipeline-DEH-configuration (-8.15 % and -8.08 % at $\psi = 90^\circ$ and $\psi = 135^\circ$ respectively).

Table 5-13. Effect of current on sagbend stress

<i>Pipeline Configuration</i>	<i>Sea Current</i>	<i>Current Heading (deg)</i>	<i>Stress, Sagbend (MPa)</i>	<i>Stress Increase due to Current (%)</i>
20" Pipe	NO	-	-170.12	-
	YES	0	-172.24	1.25
		45	-171.75	0.96
		90	-171.29	0.68
		135	-170.62	0.29
		180	-171.10	0.57
28" Pipe	NO	-	-197.14	-
	YES	0	-198.63	0.75
		45	-198.15	0.51
		90	-197.79	0.33
		135	-197.62	0.24
		180	-197.96	0.42
30" Pipe	NO	-	-205.90	-
	YES	0	-207.36	0.71
		45	-206.89	0.48
		90	-206.54	0.31
		135	-206.36	0.22
		180	-206.32	0.20
20" /w DEH	NO	-	-167.20	-
	YES	0	-168.92	1.03
		45	-163.35	-2.30
		90	-153.58	-8.15
		135	-153.69	-8.08
		180	-168.87	1.00
28" /w DEH	NO	-	-191.44	-
	YES	0	-194.12	1.40
		45	-190.44	-0.52
		90	-187.17	-2.23
		135	-187.53	-2.04
		180	-193.41	1.03

30" /w DEH	NO	-	-199.68	-
	YES	0	-202.85	1.59
		45	-198.71	-0.49
		90	-195.91	-1.89
		135	-196.24	-1.72
		180	-201.83	1.07

The environmental loading component of Equation 5.3 is neglected to simplify the design moment criteria. Table 5-11 shows that the pipeline-DEH-configuration functional loading is decreased compared to that of the single-pipeline-configuration. This is due to the contribution of bending stiffness from the DEH cable.

This results in a design moment for each pipeline-configuration independent of the current heading based on Equation 5.6 and given in Table 5-14.

$$M_{sd} = M_F \cdot \gamma_F \cdot \gamma_C + M_E \cdot \gamma_E \quad (5.6)$$

Table 5-14. Pipeline configuration and design moment

<i>Pipeline Configuration</i>	<i>Design Moment (kN·m)</i>
20" Single Pipeline	1229.1
28" Single Pipeline	3999.2
30" Single Pipeline	5098.7
20" Pipeline /w DEH	1208.0
28" Pipeline /w DEH	3883.6
30" Pipeline /w DEH	4944.7

In Appendix A it is shown how the pipeline thickness was calculated to ensure pipeline integrity for a combined loading scenario, where one of the key-parameters was the design moment. The wall thicknesses for all pipeline dimensions are confirmed through the Load Controlled Condition and solved with the same procedure as shown in Appendix A.

5.3.4 Pipeline-Configuration in XZ plane

Subsea pipelines can be split into two major groups; flexible pipelines often used as risers to floating structures, and rigid pipelines used between fixed structures. During pipelaying

operations, rigid pipelines are stable for curvatures over 1000m and greater [33]. For curvatures below 1000m, measures such as turn points may be necessary.

The pipeline curvature is investigated for all pipeline and pipeline-DEH-configurations. Figure 5-28 to Figure 5-30 shows the effect of current heading on a single-pipeline-configuration relative to the global XZ-plane. It can be seen that the current had a negligible impact on the pipeline curvature as the curvature remains constant in the interval $\psi \in [0, 180]$.

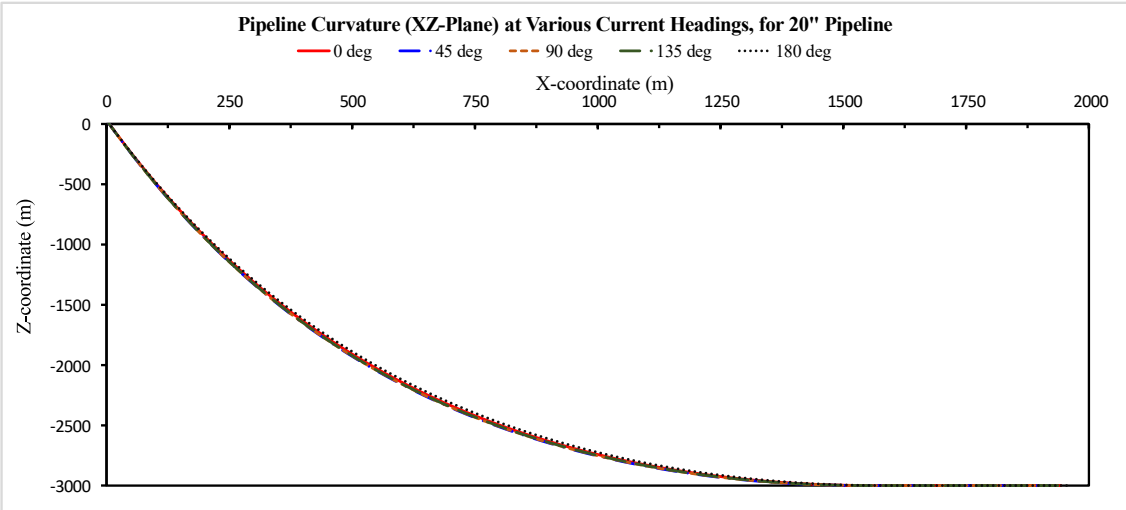


Figure 5-28 Effect of current on 20” pipeline configuration in the XZ-plane

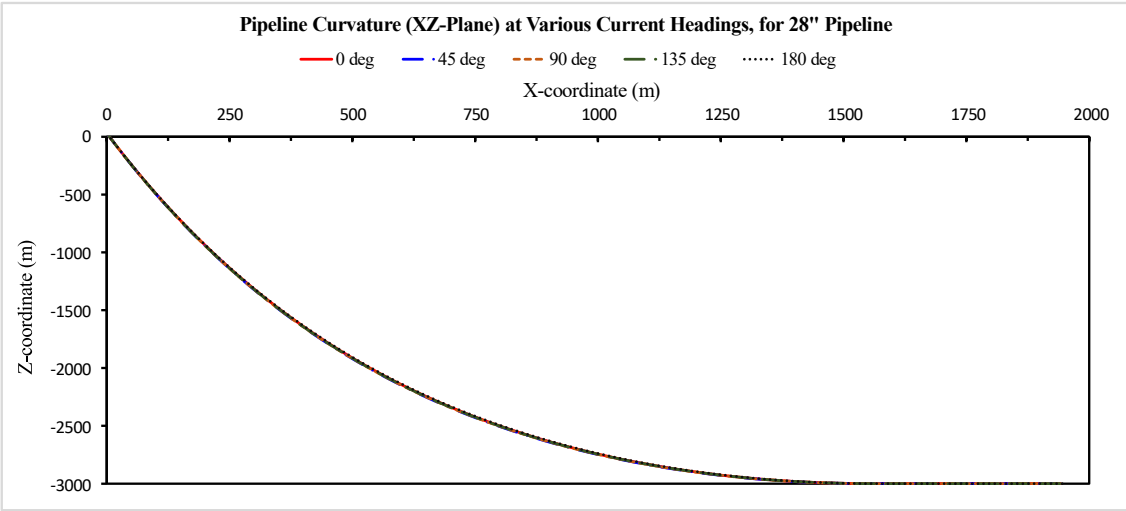


Figure 5-29. Effect of current on 28” pipeline configuration in the XZ-plane

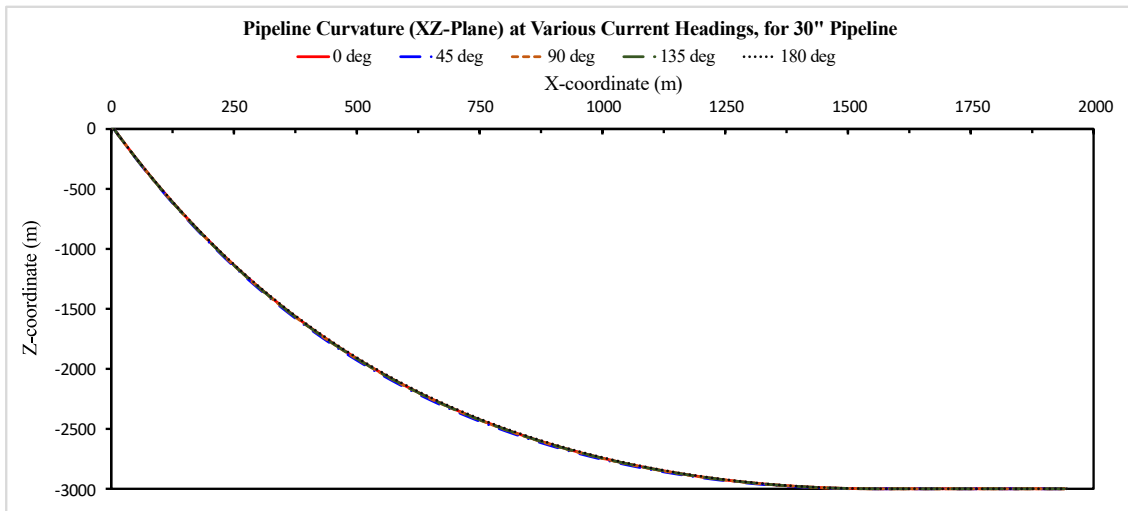


Figure 5-30. Effect of current on 30'' pipeline configuration in the XZ-plane

When introducing a DEH cable to the pipeline-configuration, the interaction between the pipeline and current becomes more dominant. Figure 5-31 to Figure 5-33 shows the pipeline-DEH-configuration relative to the global XZ-plane in the interval $\psi \in [0, 180]$.

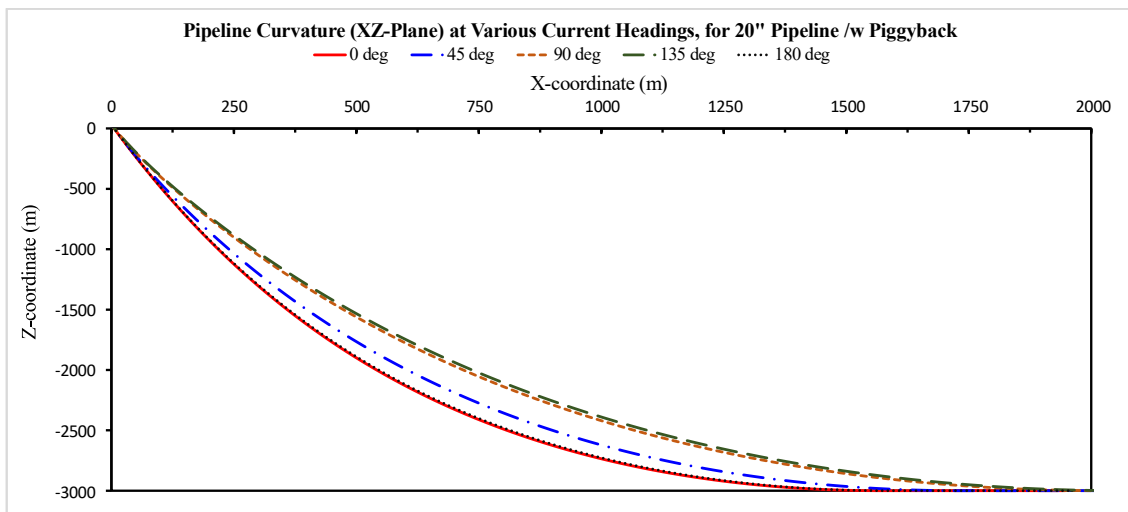


Figure 5-31. Effect of current on 20'' pipeline-DEH-configuration in the XZ-plane

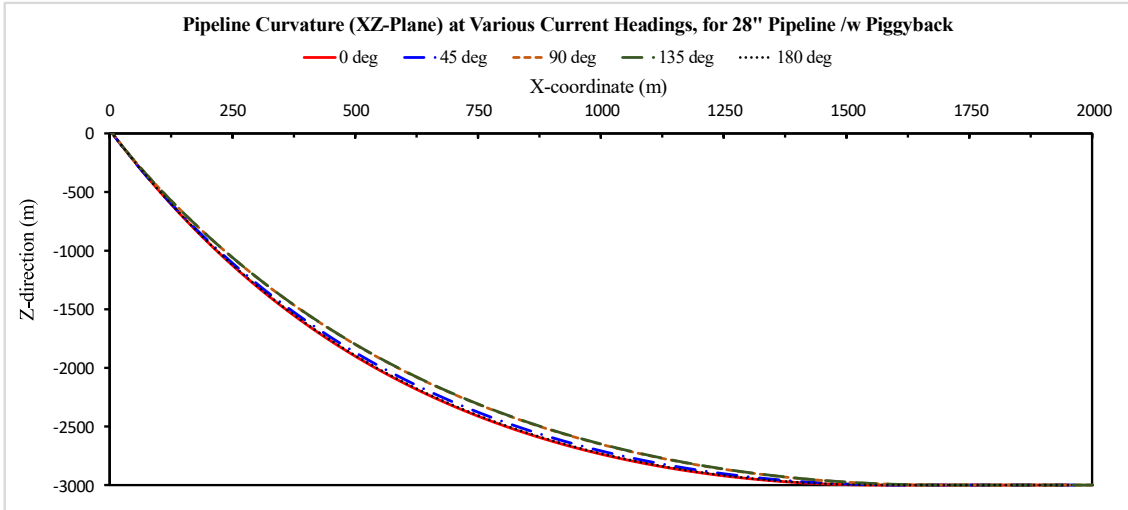


Figure 5-32. Effect of current on 28” pipeline-DEH-configuration in the XZ-plane

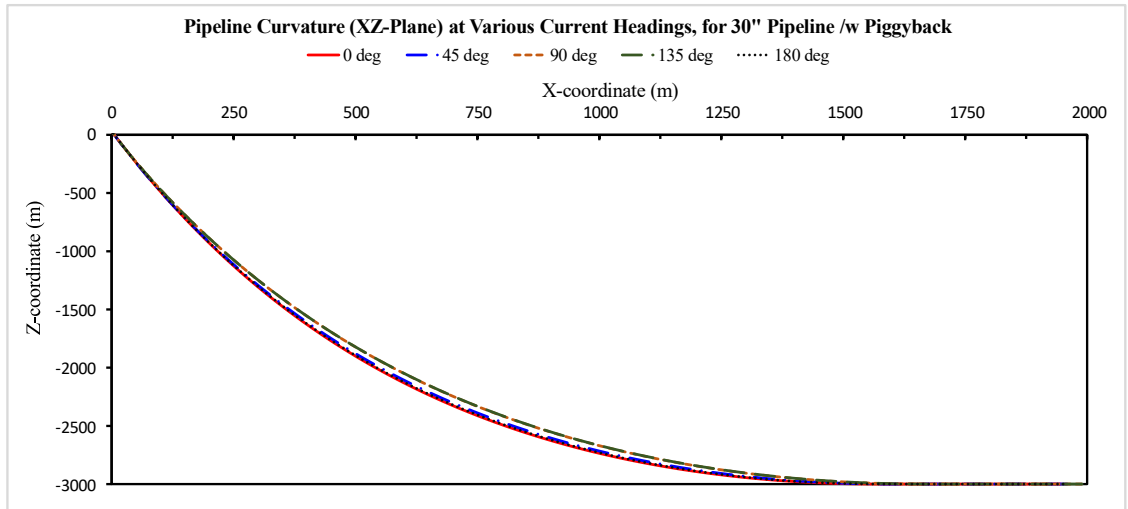


Figure 5-33. Effect of current on 30” pipeline-DEH-configuration in the XZ-plane

Figure 5-31, Figure 5-32, and Figure 5-33 shows that the impact of ψ is most dominant for the 20”-configuration and decrease drastically for the 28” and 30”-configurations. Reduction in pipeline curvature increases the top tension requirement, shown in Table 5-13. Furthermore, the impact is not large enough to generate any complications in terms of pipeline on-bottom stability. All curvatures have a radius far greater than the limit of 1000 meters due to the great depths of the pipelaying operation.

6 Conclusions and Future Work

Summary and Conclusions

The present study presents 36 simulations performed using the J-Lay method. Three pipelines with diameters of 20", 28" and 30" are considered. The effects of current- velocity and headings are investigated. The pipelines are configured in either single pipeline or in piggyback solutions with scenarios listed in Table 4 2. Simulation results are discussed in Section 5, and the following conclusions can be drawn:

- High hydrostatic pressures in ultra-deep waters pose several threats concerning collapse and propagation buckling. In particular, this affects the pipeline wall thickness design, which further influences the top tension requirement.
- A new modelling technique is proposed to account for the effect of current loading. Body elements are employed in the pipeline-piggyback-configuration to account for current induced loads. Drag coefficients are defined in surge, sway and heave direction in the HYDROPRO-card, accounting for the angle of attack of the current. It has been applied in the numerical simulation successfully.
- CFD simulations are used to obtain valid drag coefficients for the investigated pipeline-piggyback-configurations. The CFD results provide good insight into the pipe-cable-flow interaction. It is necessary to use CFD in combination with SIMLA to obtain realistic pipelaying simulations.
- Drag coefficients for piggyback-solutions are highly dependent on the angle of attack of the current and the current velocity. The drag forces experienced by the piggyback-configurations are significantly larger than those experienced by the single pipeline configurations.
- Horizontal displacement experienced by the piggyback-configuration from the surface to the seabed is considerably larger than that experienced by the single pipeline. In addition, the horizontal displacement has a parabolic correlation with the current heading.
- The pipelines are designed to contain functional load induced moments in the sagbend region. It is shown that the current load effect on the sagbend stress is negligible, as the departure angle is kept constant. In addition, it is observed that the top tension increases to maintain the constant departure angle.

- The top tension experienced by the piggyback-configuration is significantly larger than that experienced by the single pipeline configuration. It is shown that the increase in top tension requirement is a combination of larger current loads and increased weight due to the mounting of the piggyback cable.
- Due to the large water depths, there are not any limiting conditions for the pipeline curvature.

Recommendation for Future Work

The following list describes the recommended future research to obtain a better understanding of pipelaying operations.

- The present study neglects the effect of wave loading and vessel response, which will affect the load induced moments on the pipeline and affecting the lay-ability. Furthermore, wave-induced loads result in drag forces on the pipeline, which could also affect the lay-ability. Vessel response loads are not accounted for in any of the results and should be investigated in future studies.
- In the present study, the relationship between coating compression and strap-functionality is not investigated. However, the industry is faced with complications due to this relationship and it should be investigated in future works.
- Only one current velocity profile is investigated in the present study. Future studies on field measurements should be carried out to investigate the effect of different current velocities.
- Only the J-Lay method is considered in the present study. As the S-Lay method is used in ultra-deep pipelaying operations, it would be interesting to investigate and compare the J-Lay and S-Lay methods.
- DEH cable is assumed to be strapped directly to the pipeline. Solutions exist where the piggyback cable is elevated by clamps, which will result in different drag coefficients as compared to the present study. Furthermore, solutions exist where the piggyback-cable embodies the pipeline in a helical configuration. It would be essential to investigate the impact of changing the mounting procedure.
- The coating is assumed to have a constant thickness at $t = 30\text{mm}$. The effect of different coating diameters would be of interest, as they will affect critical parameters such as on-bottom stability, required top tension, and induced current loads.

- The piggyback-cable in the present study is a theoretical DEH cable. The effects of applying a more elaborate model of a DEH cable would be interesting to investigate in future works.
- Water depth is kept constant at 3000 meters. It would be of interest in future studies to compare the impact of increasing/decreasing the depth.
- A seabed representing a real topography should be used to get more representable data.
- The addition of piggyback cables can result in pipeline rotation, leading to torsional moments and should be investigated further.
- The obtained top tension requirements are not compared to lay-vessel capacities. This should be done in future studies to fit the configurations to real-life applications.

7 References

- [1] A. C. Palmer and R. A. King, “Subsea Pipeline Engineering”, 1st ed, PennWell Corporation, 2004.
- [2] Subsea7, *Electrical Heating Technologies*, 2016. Available: https://www.subsea7.com/content/dam/subsea7/documents/technologyandassets/4023_EHT_dataark_JustertSats_2016_05_03_lv_screen.pdf. Accessed on: 08.06.2019.
- [3] Allseas, *Williams Perdido Norte*, 2019. Available: <https://allseas.com/project/williams-perdido-norte/>. Accessed on: 10.06.2019.
- [4] Shell, *Our Major Projects: Stones*, 2019. Available: <https://www.shell.com/about-us/major-projects/stones.html>. Accessed on: 11.06.2019.
- [5] Nexans, *Åsgard. First in the world*, 2019. Available: https://www.nexans.no/eservice/Norway-en/navigate_270045_-3977_20_9029/_sgard.html. Accessed on: 04.06.2019.
- [6] SINTEF Energy, *Direct Electric Heating of pipelines (DEH)*, 2019. Available: <https://www.sintef.no/en/direct-electric-heating-of-pipelines-deh/>. Accessed on: 11.06.2019.
- [7] M. Zhao, “Influence of the position angle of the small pipeline on vortex shedding flow around a sub-sea piggyback pipeline”, *Coastal Engineering Journal*, Vol. 54, No. 3, 2012. doi: 10.1142/S0578563412500179., [Online].
- [8] M. Janocha, “CFD Simulations of Vortex-Induced Vibrations of a Subsea Pipeline Near a Horizontal Plane Wall”, *Marine and Offshore Technology*, University of Stavanger, Stavanger, 2018. Available: <https://uis.brage.unit.no/uis-xmlui/handle/11250/2562273>.
- [9] S. Ussetaiwan, *Pipeline installation methods (lay methods)*, 2014. Available on: <https://anakkelauntan.wordpress.com/2014/01/31/pipeline-installation-methods-lay-methods/>. Accessed on: 10.06.2019.
- [10] D. Karunakaran, *Lecture Notes in OFF520*, “Pipeline Installation”, 2018.
- [11] J. Herdiyanti, “Comparisons Study of S-Lay and J-Lay Methods for Pipeline Installation in Ultra Deep Water”, Graduate thesis, *Offshore Technology – Marine and Subsea Technology*, University of Stavanger, 2013. Available on: <https://uis.brage.unit.no/uis-xmlui/handle/11250/183162>.
- [12] DNV GL, *Submarine Pipeline Systems; Recommended Practice*, DNV-OS-F101, 2013.
- [13] Y. Bai and Q. Bai, “Hydrates”, in *Subsea Engineering Handbook*, 2nd ed. Gulf Professional Publishing, pp. 409-434, 2018. doi: 10.1016/B978-0-12-812622-6.00015-4, [Online].
- [14] API, *Specification for Line Pipe; Recommended Practice*, API-5L, 2004.

- [15] O. Fatoba, “Uniaxial cyclic elasto-plastic deformation and fatigue failure of API-5L X65 steel under various loading conditions”, *Theoretical and Applied Fracture Mechanics*, pp. 1-4, 2018. doi: 10.1016/B978-0-12-812622-6.00015-4, [Online].
- [16] M. B. Langhelle, “Pipelines for Development at Deep Water Fields”, Master Thesis, Marine Technology – Marine and Subsea Technology, University of Stavanger, Stavanger, 2011. Available: <https://uis.brage.unit.no/uis-xmlui/handle/11250/182812>.
- [17] Steel&Tube, *Prduct Technical Statement: High Tensile Steel – AISI 4140*, 2019. Available: <http://stainless.steelandtube.co.nz/wp-content/uploads/2014/06/HighTensileSteel4140.pdf>. Accessed on: 13.06.2019.
- [18] K. Nordland, personal communication, January, 2019.
- [19] International Organization of Standardization, *Petroleum and natural gas industries – Specific requirements for offshore structures – Part 1: Metocean design and operating considerations*. ISO 19901-1:2015, 01.10.2015.
- [20] DNV GL, *Environmental Conditions and Environmental Loads; Recommended Practice*, DNV-RP-C205, 2014.
- [21] NORSOK STANDARD, *Actions and action effects*, N-003, 2007.
- [22] Lebedev et al. *Velocity data assessed from trajectories of Argo floats at parking level and at the sea surface*. IPRC and APDRC, Tech. Note No.4(2), 2007, Available: doi: 10.13140/RG.2.2.12820.71041.
- [23] T. J. Sherwin, “Observations of the velocity profile of a fast and deep oceanic density current constrained in a gully”, *Journal of Geophysical Research*, vol. 115, pp. 1-14, 2010, doi:10.1029/2009JC005557.
- [24] G. C. Johnson, “Deep water properties, velocities, and dynamics over ocean trenches”, *Journal of Marine Research*, vol. 56, pp. 329-347, 1998. doi: 10.1357/002224098321822339 [Online].
- [25] E. Giertsen and J. Taby, *Marintec, Fact Sheet, SIMLA*. SINTEF Ocean, 2012.
- [26] S. Sævik, O. D. Økland, G. S Baarholm, J. K. Ø. Gjøsteen. *Simla Version 3.16.0 User Manual*. SINTEF Ocean, 2019.
- [27] E. Giertsen, J. Taby and O.D. Økland, *SIMLA Quick Start User Guide*. SINTEF Ocean, 2017.
- [28] S. Sævik, *SIMLA Theory Manual*, SINTEF Ocean, 2017.
- [29] V. Longva, personal communication, February, 2019.
- [30] F. Menter, “Two-Equation Eddy-Viscosity Transport Turbulence Model for Engineering Applications, *AIAA Journal*, vol. 32, no. 8, pp. 1598-1605, Sep. 1994. doi: 10.2514/3.12149 [Online].
- [31] D. Zhang, “Comparison of various turbulence models for unsteady flow around a finite circular cylinder at $Re = 20000$ ”. *Journal of Physics: Conference Series*, vol 910, no. 1, pp. 12-27, Oct. 2017. doi: 10.1088/1742-6596/910/1/012027 [Online].

- [32] E. Robertson, V. Choudhury, S. Bhusan, and D. K. Walters, “Validation of OpenFOAM numerical methods and turbulence models for incompressible bluff body flows”. *Computers & Fluids*, vol. 123, pp. 122-145, Oct. 2015. doi: 10.1016/j.compfluid.2015.09.010 [Online].
- [33] C. Andersson, “Rigid Papelay Curve Stability”, Master Thesis, Department of Marine Technology, Norwegian University of Science and Technology, Trondheim, 2014. Available on: <https://ntnuopen.ntnu.no/ntnu-xmlui/handle/11250/238943>.

I. Appendix A

Calculation of pipe thickness

Calculation of 20" pipeline wall thickness is performed with the given parameters in Table I-1.

Values are in accordance with DNV (2007) and given material properties for inspected pipeline.

Table I-1. Input parameters for calculation of pipeline wall thickness.

Parameter	Unit	Value
Pipe Diameter	m	0.508
SMYS – X65	Pa	4.48E+08
SMTS – X65	Pa	5.30E+08
Young's Modulus	Pa	2.06E+08
Poisson's ratio	-	0.300
Sea Density, ρ_{sea}	kg/m ³	1026
Gravity, g	m/s ²	9.810
Sea depth, h	m	3000
Material Strength factor, α_U	-	0.960
Maximum fabrication factor, α_{fab}	-	0.850
Material resistance factor, γ_m	-	1.150
Safety class resistance factor, γ_{SC}	-	1.046
Condition load effect factor, γ_C	-	1.070
Functional load effect factor, γ_F	-	1.200
Environmental load effect factor, γ_E	-	0.700
Fabrication thickness, t_{fab}	m	0.001
Corrosion thickness, t_{corr}	m	0.003
Nominal thickness, t	m	0.034
Initial ovality, f_0 (1.5%)	-	0.015

Coating thickness, t_{coat}	m	0.030
SIMLA Output		
Highest longitudinal stress (compression in sagbend), $\sigma_{eq}(t_1)$	N/m ²	1.725E+08
Highest longitudinal stress (compression in sagbend), $\sigma_{eq}(t_2)$	N/m ²	1.686E+08
Highest axial force in sagbend, $S_F(t_1)$	N	1.313E+06
Highest axial force in sagbend, $S_F(t_2)$	N	1.376E+06

Simplified laying criteria

$$\sigma_{eq} < 0.87f_y$$

Where σ_{eq} is retrieved from the SIMLA output.

$$\sigma_{eq}(t_1) = 172.5 \text{ MPa}$$

$$f_y = (SMYS - f_{y,temp}) \cdot \alpha_U = 430.1 \text{ MPa}$$

Resulting in:

$$172.5 \text{ MPa} < 374.2 \text{ MPa}$$

The pipeline wall thickness satisfies the simplified laying criteria.

Collapse criterion

$$P_e - P_{min} \leq \frac{P_c(t_1)}{\gamma_m * \gamma_{SC}}$$

Hydrostatic Pressure

$$P_e = \rho_{sea} \cdot g \cdot h = 3.02E + 07$$

Internal Pressure

$$P_{min} = 0$$

Characteristic resistance for external pressure

$$P_c(t) - P_{el}(t) \cdot (P_c(t)^2 - P_p(t)^2) = P_c(t) \cdot P_{el}(t) \cdot P_p(t) \cdot f_0 \cdot \frac{D}{t}$$

Where:

$$P_{el}(t_1) = \frac{2 \cdot E \cdot \left(\frac{t}{D}\right)^3}{1 - \nu^2} = 116.1 \text{ MPa}$$

$$P_p(t_1) = f_y \cdot \alpha_{fab} \cdot \frac{2 \cdot t}{D} = 475.0 \text{ MPa}$$

Third-degree polynomial:

$$P_c = y - \frac{1}{3}b$$

Where:

$$b = -P_{el}(t_1) = -116.1 \text{ MPa}$$

$$c = -\left(P_p(t_1)^2 + P_p(t_1) \cdot P_{el}(t_1) \cdot f_0 \cdot \frac{D}{t}\right) = -3.529 \cdot 10^{15} \text{ (Pa)}^2$$

$$d = P_{el}(t_1) \cdot P_p(t_1)^2 = 2.618 \cdot 10^{23} \text{ (Pa)}^3$$

$$u = \frac{1}{3} \left(-\frac{1}{3}b^2 + c \right) = -2.673 \cdot 10^{15} \text{ (Pa)}^2$$

$$v = \frac{1}{2} \left(\frac{2}{27} \cdot b^3 - \frac{1}{3} \cdot b \cdot c + d \right) = -4.731 \cdot 10^{21} \text{ (Pa)}^3$$

$$\Phi = \cos^{-1} \left(\frac{-v}{\sqrt{-u^3}} \right) = 1.605$$

$$y = -2 \cdot \sqrt{-u} \cdot \cos \left(\frac{\Phi}{3} + \frac{60 \cdot \pi}{180} \right) = 1.180 \cdot 10^6 \text{ Pa}$$

Resulting in

$$P_c(t_1) = 39.9 \text{ MPa}$$

Collapse criterion

$$P_e - P_{min} \leq \frac{P_c(t_1)}{\gamma_m \cdot \gamma_{SC}}$$

$$30.2 \text{ MPa} \leq 33.1 \text{ MPa}$$

Pipeline thickness satisfies the collapse criterion.

Combined loading criteria (Load Controlled Condition)

$$\gamma_m \cdot \gamma_{SC} \cdot \frac{|M_{sd}|}{\alpha_c \cdot M_p(t_2)} + \left\{ \left(\frac{\gamma_m \cdot \gamma_{SC} \cdot S_{sd}}{\alpha_c \cdot S_p(t_2)} \right)^2 \right\} + \left(\gamma_m \cdot \gamma_{SC} \cdot \frac{P_e - P_{min}}{P_c(t_2)} \right)^2 \leq 1$$

Applicable for:

$$15 \leq \frac{D}{t_2} \leq 45 \quad P_i < P_e \quad \frac{|S_{sd}|}{S_p} < 0.4$$

$$15 \leq 15 \leq 45 \quad 0 \text{ MPa} < 30.2 \text{ MPa} \quad 0.0812 < 0.4$$

Where:

$$M_{Sd} = M_F \cdot \gamma_F \cdot \gamma_C + \cancel{M_E \cdot \gamma_E} + \cancel{M_I \cdot \gamma_F \cdot \gamma_C} + \cancel{M_A \cdot \gamma_A \cdot \gamma_C}$$

$$M_{Sd}(t_2) = M_F(t_2) \cdot \gamma_F \cdot \gamma_C = \frac{\sigma_{eq}(t_2)}{y_{max}} I_{xx} \cdot \gamma_F \cdot \gamma_C = 1229 \text{ kNm}$$

$$S_{Sd} = S_F \cdot \gamma_F \cdot \gamma_C + \cancel{S_E \cdot \gamma_E} + \cancel{S_I \cdot \gamma_F \cdot \gamma_C} + \cancel{S_A \cdot \gamma_A \cdot \gamma_C}$$

$$S_{Sd}(t_2) = S_F(t_2) \cdot \gamma_F \cdot \gamma_C = 1767 \text{ kN}$$

$$S_p(t) = f_y \cdot \pi \cdot (D - t) \cdot t = 21.77 \cdot 10^6 \text{ N}$$

$$M_p(t) = f_y \cdot \pi \cdot (D - t)^2 \cdot t = 3.285 \cdot 10^6 \text{ Nm}$$

$$f_{cb} = \text{MIN} \left[f_y; \frac{f_u}{1.15} \right] = f_y = 430.1 \text{ MPa}$$

$$P_b(t) = \frac{2 \cdot t}{D - t} f_{cb} \frac{2}{\sqrt{3}} = 71.24 \cdot 10^6 \text{ MPa}$$

$$\frac{P_i - P_e}{P_b} = -0.4238$$

$$\alpha_p = \begin{cases} 1 - \beta & \frac{P_i - P_e}{P_b} < \frac{2}{3} \\ 1 - 3\beta \left(1 - \frac{P_i - P_e}{P_b} \right) & \frac{P_i - P_e}{P_b} \geq \frac{2}{3} \end{cases}$$

$$\beta = \frac{60 - \frac{D}{t_2}}{90} = 0.5007$$

$$\alpha_p = 0.4993$$

$$\alpha_c = (1 - \beta) + \beta \cdot \frac{f_u}{f_y} = 1.092$$

Resulting in:

$$1.00 \leq 1$$

Pipeline thickness satisfies the combined loading criteria utilizing LC-condition.

Propagation buckling

$$P_e - P_{min} \leq \frac{P_{pr}}{\gamma_m \cdot \gamma_{SC}}$$

Where

$$15 \leq \frac{D}{t_2} \leq 45$$

$$P_{pr} = 35 \cdot f_y \cdot \alpha_{fab} \left(\frac{t_2}{D} \right)^{2.5} = 14.8 \text{ MPa}$$

Resulting in:

$$3.02 \cdot 10^7 \leq 1.23 \cdot 10^7$$

Pipeline thickness does not satisfy the propagation buckling criterion. Meaning buckle arrestors must be installed on the pipeline.

On-Bottom Stability

$$\gamma_w \cdot \frac{b}{W_{sub} + b} \leq 1.00$$

Where:

γ_w = Safety factor on weight = 1.1

b = buoyancy per unit length

W_{sub} = Submerged weight for waterfilled pipe

$$b = \rho_{sea} \cdot g \cdot \frac{\pi}{4} \cdot D_{coat}^2 = 2550.4 \frac{N}{m}$$

$$D_{coat} = D_{pipe} + 2 \cdot t_{coat}$$

$$W_{sub} = \frac{\pi}{4} \{ \rho_{pipe} [D_{pipe}^2 - D_{inner}^2] + \rho_{coat} [D_{coat}^2 - D_{pipe}^2] - \rho_{sea} [D_{coat}^2 - D_i^2] \}$$

$$D_i = D_{pipe} + 2 \cdot t$$

$$W_{sub} = 340.11 \frac{kg}{m}$$

Resulting in:

$$0.97 \leq 1.00$$

Pipeline thickness satisfies on-bottom stability criteria.

II. Appendix B

SIMLA – Simulation Code

```
# Heading of processed file
HEAD 20" Flowline 150mm DEH cable. 90 degree heading. With Drag Coefficients. 80 degree dep. angle
#-----
#-----
# Control data:
#-----
#-----
#
#          maxit  ndim  isolvr  npoint  ipri    conr    gacc  iproc
CONTROL    300    3     2      8       1     2e-4   9.81  autostart
#          ie1pip ie2pip  incpip  nrolls  icaten  ivsnod
#          1     4000   1       0       2     4001
#          tens0  depang      freeb  rampan  rample  stirad  KP_tdp0
#          0.0   1.396263402  31.27  0       0       0.0    200.0
#          seabedgrp  stingergrp  vesselgrp  ivscog
#          pseabed    none          vessel1    5001
#
#-----
#-----
# Defining visualization parameters:
#-----
#-----
#
#-----
# Visual presentation in X-POST:
#          Longitudinal stress/strain  Hoop Stress (thin walled theory)
VISRES    INTEGRATION 1  sigma-xx  strain-xx  sigma-yy
#
#-----
# HLA-visualization:
# Defines what to be displayed in the SimVis visualization
# and the name of the log file.
#
#          host    port  federation  federate  logfile
HLA "127.0.0.1"  0    "test"    "Flowline"  "J-layT.log"
#
# Name of the lay vessel: in this example no lay vessel is included in the
# visualization but the body is included here to allow the inclusion after
# the analysis.
#          Kind  Type  ID  Name
HLAVIS body  Node  5001 J-Vessel
#
# Pipe: Defines that the pipe is to be visualized.
#          Kind  IPIgrpe  node1  node2
HLAVIS tpipe  pipe1    1  4001
```



```

#
# Cable: Defines that the cable is to be visualized.
#   Kind  IPIgrpe  node1  node2
HLAVIS  tpipe  cable1  20001  24000
#
# Defines a body at the touch down point. This is done so that the touch
# down point can easily be found during visualization. This body is
# visualized as a little box.
#   Kind  Type  Name
HLAVIS  body  TDP  TDP
#
#-----
# HLA-plots:
#Which plots to be available in SimVis
#   Type  Data
HLAPLOT Tension  0.0 0.0
HLAPLOT SoilMob  30.0
HLAPLOT RouteDev 10.0
HLAPLOT SagUtil  stress 450000
HLAPLOT TowerDist
HLAPLOT LayBack
#-----
#-----
# Units used (for correct display in plots)
#-----
#-----
# This analysis is done in Mg, m, s
#   mass  length  time
UNITS  1.0e-3  1.0  1.0
#
#-----
#-----
# Analysis time control:
#-----
#-----
#
# First a step is done using the Autostart routine (defined in the Control
# card), afterwards load steps defined by the SIMLA card is carried out.
# The accuracy for the second load step sequence is also defined here.

#   t  dt  dtvi  dtdy  dt0  type  hla?
TIMECO  1.0  1.0  1.0  1.0  2.0  STATIC  HLA
#   steptype  iterco  itcrit  maxit  maxdiv  conr
      AUTO  NONE  ALL  300  0  1e-5
#   t  dt  dtvi  dtdy  dt0  type  hla?
TIMECO  851.0  1.0  10.0  1.0  10.0  STATIC-SIMLA  HLA
#   steptype  iterco  itcrit  maxit  maxdiv  conr
      AUTO  NONE  ALL  200  2  1e-5

#
#-----

```

```

#-----
# Building up model:
#-----
#      no    x    y    z
# pipe nodes
NOCOOR COORDINATES 1 0.0 0.0 0.0
      4001 4000.0 0.0 0.0
#
# cable nodes
#      (0.568/2)+(0.15/2) = (pipe/w coat radius)+(DEH radius)
NOCOOR COORDINATES 20001 0.0 0.0 0.355
      24000 3999.0 0.0 0.355
#
# vessel nodes
NOCOOR COORDINATES 5001 4000.0 0.0 0.0
      5002 4002.0 0.0 0.0
#
# sea nodes
NOCOOR COORDINATES 6001 150.0 -150.0 0.0
      6002 -150.0 -150.0 0.0
      6003 -150.0 150.0 0.0
      6004 150.0 150.0 0.0
#
#----- Building up non-physical model for drag/lift-----
#
# pipe2 nodes (for pipe-cable contact)
NOCOOR COORDINATES 10002 1.0 0.0 0.0
      13999 3998.0 0.0 0.0
#
# cable2 nodes (for pipe-cable contact)
#
NOCOOR COORDINATES 30002 1.0 0.0 0.355
      33999 3998.0 0.0 0.355
#
#-----
# Element connectivity input:
# Building up the connectivity matrix.
#
# PIPE -----
#
# group elty material no n1 n2
ELCON pipe1 pipe31 pipemat 1 1 2
REPEAT 4000 1 1
#
# CABLE -----
#
# group elty material no n1 n2
ELCON cable1 pipe31 cabmat 20001 20001 20002
# n nelinc nodinc
REPEAT 3999 1 1

```

```

move_group -2 cable1

# PIPE - CABLE STRAPS -----
#
#   group elty   material no  n1  n2
ELCON strap pipe31  strapmat 45001 1 20001
REPEAT 1334 1 3

# DRAG PIPE -----
#
#   drag elements with hydropro:
#   group elty   material no  n1
ELCON pdrag body502  none   35001 10002
REPEAT 3998 1 1
#
# DRAG CABLE -----
#
#   drag elements with hydropro:
#   group elty   material no  n1
ELCON cdrag body502  none   40001 30002
REPEAT 3998 1 1
move_group -2 cdrag

# PIPE - SEABED CONTACT -----
#
#   group elty   material ELID nod1
ELCON pseabed cont125 route1 25001 1
#   n nelinc nodinc
REPEAT 1000 1 1

# CABLE - SEABED CONTACT -----
#
#   group elty   material no  n1
ELCON cseabed cont125 route1 30001 20001
#   n nelinc nodinc
REPEAT 1000 1 1

# VESSEL -----
#
#   group elty   material no  n1  n2
ELCON vessell pipe31  vessell 5001 5001 5002

# SEA -----
#
#   group elty   material no  n1  n2  n3  n4
ELCON mwlse sea150  sea1 6001 6001 6002 6003 6004
#
#
#-----
# Orient input:
# Giving element normals
#-----

```

```

#
# PIPE -----
#
#           no    x    y    z
ELORIENT COORDINATES  1  0.0  1.0  0.0
                       4000  0.0  1.0  0.0

#
# CABLE -----
#
ELORIENT COORDINATES  20001  0.0  1.0  0.355
                       23999  0.0  1.0  0.355

#
# PIPE - CABLE STRAPS -----
#
ELORIENT COORDINATES  45001  0.0  1.0  0.0
                       46334  0.0  1.0  0.0

#
# VESSEL -----
#
ELORIENT COORDINATES  5001  0.0  1.0  0.0

#
# PIPE - SEABED CONTACT -----
#
ELORIENT EULERANGLE  25001  0.0  0.0  0.0
                       26000  0.0  0.0  0.0

#
# CABLE - SEABED CONTACT -----
#
ELORIENT EULERANGLE  30001  0.0  0.0  0.0
                       31000  0.0  0.0  0.0

#
# DRAG PIPE -----
#
ELORIENT EULERANGLE  35001  0.0  0.0  0.0
                       38998  0.0  0.0  0.0

#
# DRAG CABLE -----
#
ELORIENT EULERANGLE  40001  0.0  0.0  0.0
                       43998  0.0  0.0  0.0

#-----
#
#-----
# Element property input:
#
# PIPE -----
#           name    type rad      th   CDr Cdt CMr CMt wd   ws          ODp  ODw  rks
ELPROP      pipe1   pipe 0.2540  0.034 0.0 0.0 0.0 0.0 0.4440808 0.1841034361 0.5680 0.5680 0
#           rad = ID/2 + th/2 only steel pipe wd with coating ODp with coat

# CABLE -----

```

```

#
# DEH cable with Copper core and HDPE coat. Formed into
# name type rad th CDr Cdt CMr CMt wd ws ODp ODw rks
ELPROP cable1 pipe 0.075 0.02 0 0 0 0 0.03238 0.01425 0.150 0.150 0
# PIPE - CABLE STRAPS -----
#
# name type rad th CDr Cdt CMr CMt wd ws ODp ODw rks
ELPROP strap pipe 0.15 0.12 0.0 0.0 2.0 0.2 0.0 0.0 0.01 0.01 0.5
#
# VESSEL -----
# Vessel is defined as a very stiff but light beam.
# name type rad th CDr Cdt CMr CMt wd ws ODp ODw rks
ELPROP vessell pipe 1.0 0.1 0.8 0.1 2.0 0.2 41.4E-6 15.6E-6 0.1783 0.1783 0.5
#
#
# DRAG PIPE -----
#
# name type GEOM WS WD WDTX WDTY WDTZ CDX CDY CDZ CDTHX CDTHY CDTHZ
ELPROP pdrag body geo2 0 0 0 0 0 0.0 0.0 0.0 0.0 0.0 0.0
# CMX CMY CMZ CMTHX CMTHY CMTHZ COGX COGY COGZ
0.0 0.0 0.0 0.0 0.0 0.0 0.0 0.0 0.0
#
# DRAG CABLE -----
#
# name type GEOM WS WD WDTX WDTY WDTZ CDX CDY CDZ CDTHX CDTHY CDTHZ
ELPROP cdrag body geo1 0 0 0 0 0 0.0 0.0 0.0 0.0 0.0 0.0
# CMX CMY CMZ CMTHX CMTHY CMTHZ COGX COGY COGZ
0.0 0.0 0.0 0.0 0.0 0.0 0.0 0.0 0.0

# Substitute the hydrodynamic properties defined in the ELPROP card
# ELGRP TRAWLBOARD CONTSURF REPLACE SCALEFACT MECCX MECCY MECCZ
HYDROPRO pdrag trawlboard route1 1 1.0 0.0 0.0 0.0
# DECCX DECCY DECCZ NNOD NMASS NDRAG NODEI MASSFILEI DRAGFILEI
0.0 0.0 0.0 1 0 3 100 "Cd_1_pipe" "Cd_2_pipe" "Cd_3_pipe"
# ELGRP TRAWLBOARD CONTSURF REPLACE SCALEFACT MECCX MECCY MECCZ
HYDROPRO cdrag trawlboard route1 1 1.0 0.0 0.0 0.0
# DECCX DECCY DECCZ NNOD NMASS NDRAG NODEI MASSFILEI DRAGFILEI
0.0 0.0 0.0 1 0 3 20100 "Cd_1_cable" "Cd_2_cable" "Cd_3_cable"
#

# GEOMETRY OF BODY -----
# name nseg type theta nvis len dia_1st dia_last
GEOM geo1 1 CYLINDER 0.00 6 1. 0.150 0.150
GEOM geo2 1 CYLINDER 0.00 6 1. 0.568 0.568

#-----
#-----
# Defining the bottom properties:
#-----
#-----
#

```

```

#-----
# Contint data (contact interfaces):
#
#      groupn  mname   sname   isl  isn  istx  isty  istz  gt1  gt2
CONTINT pseabed  pipe1   route1  1   2000 10000  0.0  0.0  10   1
CONTINT cseabed  cable1  route1  20001 22000 10000  0.0  0.0  10   1
CONTINT mwlseas  mwlseas  pipe1
CONTINT mwlseas  mwlseas  cable1
CONTINT mwlseas  mwlseas  pdrag
CONTINT mwlseas  mwlseas  cdrag

```

```

#
#-----
# Cosurfpr data (contact surface properties):
#
#      name  data file      nlines KP1   x0  y0  fi  soil id
COSURFPR route1 "seabed_3000_long.txt"  1  0.0  0.0  0.0  0.0  100
#

```

```

# Soil descriptions
#-----
#  id  startkp  stopkp  soil
COSUPR 100  -5000  9000  soil_1
#
#
#-----
#-----

```

```

# Defining the properties of pipe and vessel:
#-----
#-----
#

```

```

#Loads:
#-----

```

```

# Curload input:
#

```

```

# 0 Deg

```

```

CURLOAD 100  global
           0      2.00  0
          -25     1.80  0
          -50     1.60  0
         -100     1.50  0
         -250     1.20  0
         -348     1.00  0
         -500     0.69  0
         -740     0.50  0
        -1000     0.29  0
        -1500     0.28  0
        -2000     0.27  0
        -2500     0.25  0
        -3000     0.10  0

```

```

# 45 Deg

```

```

CURLOAD 200  global

```

0	2.00	0.785398163
-25	1.80	0.785398163
-50	1.60	0.785398163
-100	1.50	0.785398163
-250	1.20	0.785398163
-348	1.00	0.785398163
-500	0.69	0.785398163
-740	0.50	0.785398163
-1000	0.29	0.785398163
-1500	0.28	0.785398163
-2000	0.27	0.785398163
-2500	0.25	0.785398163
-3000	0.10	0.785398163

90 Deg

CURLOAD 300 global

0	2.00	1.570796327
-25	1.80	1.570796327
-50	1.60	1.570796327
-100	1.50	1.570796327
-250	1.20	1.570796327
-348	1.00	1.570796327
-500	0.69	1.570796327
-740	0.50	1.570796327
-1000	0.29	1.570796327
-1500	0.28	1.570796327
-2000	0.27	1.570796327
-2500	0.25	1.570796327
-3000	0.10	1.570796327

135 Deg

CURLOAD 400 global

0	2.00	2.35619449
-25	1.80	2.35619449
-50	1.60	2.35619449
-100	1.50	2.35619449
-250	1.20	2.35619449
-348	1.00	2.35619449
-500	0.69	2.35619449
-740	0.50	2.35619449
-1000	0.29	2.35619449
-1500	0.28	2.35619449
-2000	0.27	2.35619449
-2500	0.25	2.35619449
-3000	0.10	2.35619449

180 Deg

CURLOAD 500 global

0	2.00	3.141592654
-25	1.80	3.141592654
-50	1.60	3.141592654

-100	1.50	3.141592654
-250	1.20	3.141592654
-348	1.00	3.141592654
-500	0.69	3.141592654
-740	0.50	3.141592654
-1000	0.29	3.141592654
-1500	0.28	3.141592654
-2000	0.27	3.141592654
-2500	0.25	3.141592654
-3000	0.10	3.141592654

```

#-----
# Seaload specification:
#
#   name  x1  y1  x2  y2  CurrNo  ihist
SEALO mwlse -100000 -100000 100000 100000 300 300
#
#-----
# External pressure & gravity load
#   phi ghi
PELOAD 100 100
#
#-----
# History data:
#
#   no  istp  fac
# ext press & grav:
THIST 100 0.0 0.0
      1.0 1.0
      2.0 1.00
      1000.0 1.00
# prescr displ
THIST 200 0.0 1.00
      1000.0 1.00
# current
THIST 300 0.0 0.00
      1.0 0.00
      30.0 1.00
      1000.0 1.00

#
#-----
#-----
# Constraint input:
#-----
#-----
#
#-----
# Pipe bottom end:
#   node dof  ampl  thist
CONSTR PDISP GLOBAL 1 1 0.0 200

```



```
CONSTR PDISP GLOBAL 1 2 0.0 200
CONSTR PDISP GLOBAL 1 3 0.0 200
CONSTR PDISP GLOBAL 1 4 0.0 200
```

```
#-----
```

```
# Pipe upper-end connected to vessel node:
```

```
#
#           node dof C0 node dof C1
CONSTR CONEQ GLOBAL 4001 1 0 5002 1 1
CONSTR CONEQ GLOBAL 4001 2 0 5002 2 1
CONSTR CONEQ GLOBAL 4001 3 0 5002 3 1
```

```
# Pipe - pipe2:
```

```
#
#           node dof C0 nod dof C1
CONSTR CONEQ GLOBAL 10002 1 0 2 1 1
REPEAT 3998 1 1
CONSTR CONEQ GLOBAL 10002 2 0 2 2 1
REPEAT 3998 1 1
CONSTR CONEQ GLOBAL 10002 3 0 2 3 1
REPEAT 3998 1 1
CONSTR CONEQ GLOBAL 10002 6 0 2 6 1
REPEAT 3998 1 1
CONSTR CONEQ GLOBAL 10002 5 0 2 5 1
REPEAT 3998 1 1
CONSTR CONEQ GLOBAL 10002 4 0 2 4 1
REPEAT 3998 1 1
```

```
#
#
#-----
```

```
# Cable - cable2:
```

```
#
#           node dof C0 node dof C1
CONSTR CONEQ GLOBAL 30002 1 0 20002 1 1
REPEAT 3998 1 1
CONSTR CONEQ GLOBAL 30002 2 0 20002 2 1
REPEAT 3998 1 1
CONSTR CONEQ GLOBAL 30002 3 0 20002 3 1
REPEAT 3998 1 1
CONSTR CONEQ GLOBAL 30002 6 0 20002 6 1
REPEAT 3998 1 1
CONSTR CONEQ GLOBAL 30002 5 0 20002 5 1
REPEAT 3998 1 1
CONSTR CONEQ GLOBAL 30002 4 0 20002 4 1
REPEAT 3998 1 1
```

```
#-----
```

```
# Vessel COG:
```

```
#
#           node dof ampl thist
CONSTR PDISP GLOBAL 5001 1 0.0 200
CONSTR PDISP GLOBAL 5001 2 0.0 200
```

```

CONSTR PDISP GLOBAL 5001 3 0.0 200
CONSTR PDISP GLOBAL 5001 4 0.0 200
CONSTR PDISP GLOBAL 5001 5 0.0 200
CONSTR PDISP GLOBAL 5001 6 0.0 200
#
#-----
#-----
# Boundary condition data:
#-----
#-----
#
# Sea surface:
BONCON GLOBAL 6001 1
REPEAT 4 1
BONCON GLOBAL 6001 2
REPEAT 4 1
BONCON GLOBAL 6001 3
REPEAT 4 1
#
#
#-----
#-----
# Lay simulation data:
#-----
#-----
#
# VesselID npipe ID_pipe ID_sbd
SIMLA 5001 1 pipe1 pseabed
# file nodes
"supp-lay-static.txt" 5
# Sigf Util Type nelst dep.angle tol
450000 1.0 J 2 1.396263402 0.5
#
#-----
#-----
# Joint property input:
#-----
#-----
#
JOINTPR_APPLY route1 pipe1
#
# Type
JOINTPR_DEFINE route1 pipe
#
# KP1 KP2 rad th CDr Cdt CMr CMt wd ws ODp ODw rks label
-5000 9000 0.2540 0.034 0.0 0.0 0.0 0.0 0.4440808 0.1841034361 0.5680 0.5680 0 "FBE/PP"
#
#
#-----
#-----
# Material data
#-----

```

```

#-----
#
# PIPE -----
#
# name type poiss talfa tecond heatc beta ea eiy eiz git em gm
MATERIAL pipemat linear 0.3 1.17e-5 50 800 0 1.04E+07 1.84E+04 1.84E+04 1.27E+05 206e6
80E+06
#ONLY STEEL PIPE
#
# CABLE -----
#
# name type poiss talfa tecond heatc beta ea eiy eiz git em gm
MATERIAL cabmat linear 0.35 3.58e-5 50 800 0 249363 37.17 37.17 256.55 14.11e6 4e07
#
# PIPE - CABLE STRAPS -----
#
# name type poiss talfa tecond heatc beta ea eiy eiz git em gm
MATERIAL strapmat linear 0.3 1.17e-5 50 800 0 5.6e5 1.0e4 1.0e4 7.8e2 210e6 79.6e6
#
# VESSEL -----
#
# name type poiss talfa tecond heatc beta ea eiy eiz git em gm
MATERIAL vessell linear 0.3 1.17e-5 50 800 0 1.0e8 3.0e8 3.0e8 1.0e8 210e6 80.8e6
#
# SEABED -----
#
MATERIAL soil_1 contact 0.3 0.3 soilx soily soilz
#
MATERIAL soilx epcurve 1 0.000 0.0
0.005 1.0
100.000 10.0
#
MATERIAL soily epcurve 1 0.00 0.0
0.1 1.0
100.00 999.0
#
MATERIAL soilz hycurve -10000 -2000000.0
10000 2000000.0
#
# SEA -----
#
MATERIAL sea1 sea 1026e-3
#

```